

Hayes E. Ross, Jr. MS 925

VEHICLE EXTERIORS AND PEDESTRIAN INJURY PREVENTION

VOLUME IV - DROP TESTS OF DUMMIES ON A
MOCK VEHICLE EXTERIOR

FINAL REPORT ON CONTRACT DOT-HS-065-1-217

Research Report RF 814-1

May 1973

a

report



from the Texas A&M
RESEARCH FOUNDATION

College Station, Texas



Prepared for

U. S. Department of Transportation
National Highway Traffic Safety Administration
Washington, D. C. 20590

Texas A & M Research Foundation
Texas A&M University, College of Engineering
Texas Transportation Institute
College Station, Texas 77843

VEHICLE EXTERIORS AND PEDESTRIAN INJURY PREVENTION

Volume IV - Drop Tests of Dummies on a
Mock Vehicle Exterior

Hayes E. Ross, Jr.
Monroe C. White
Ronald D. Young
and
Wayne F. Lammert

Final Report on Contract DOT-HS-065-1-217

Research Report RF 814-1

May 1973

Prepared for

U. S. Department of Transportation
National Highway Traffic Safety Administration
Washington, D. C. 20590

Texas A & M Research Foundation
Texas A&M University, College of Engineering
Texas Transportation Institute
College Station, Texas 77843

1. Report No.		2. Government Accession No.		3. Recipient's Catalog No.	
4. Title and Subtitle VEHICLE EXTERIORS AND PEDESTRIAN INJURY PREVENTION, Vol. IV - Drop Tests of Dummies on a Mock Vehicle Exterior				5. Report Date July 1973	
				6. Performing Organization Code	
7. Author(s) Hayes E. Ross, Jr., Monroe C. White, Ronald D. Young, Wayne F. Lammert				8. Performing Organization Report No. RF 814-1, Vol. IV	
9. Performing Organization Name and Address Texas A & M Research Foundation Texas A&M University, College of Engineering Texas Transportation Institute College Station, Texas 77843				10. Work Unit No.	
				11. Contract or Grant No. DOT-HS-065-1-217	
12. Sponsoring Agency Name and Address U. S. Department of Transportation National Highway Traffic Safety Administration Washington, D. C. 20590				13. Type of Report and Period Covered Final Report July 1971 - July 1973	
				14. Sponsoring Agency Code	
15. Supplementary Notes					
16. Abstract The final report, entitled "Vehicle Exteriors and Pedestrian Injury Prevention", is presented in five volumes, as follows: <u>Volume I</u> - "Summary Report". Summarizes results of entire study. <u>Volume II</u> - "Analysis of Pedestrian Accident Information". Statistical analysis of 263 pedestrian accident records was conducted in search of injury causation factors. Multivariant analysis and item selection techniques were used to evaluate the data. <u>Volume III</u> - "The Texas A&M University Injury Severity Index". A method was developed to quantify the severity of injuries given (1) medical descriptions from accident records, or, (2) victim kinematics as determined from numerical or physical simulation. <u>Volume IV</u> - "Drop Tests of Dummies on a Mock Vehicle Exterior". A series of drop tests were conducted with instrumented anthropometric dummies for data to validate a numerical simulator. High-speed cameras recorded dummy kinematics and accelerations were recorded on magnetic tape. <u>Volume V</u> - "A 3-D Math Simulation of a Crash Victim-Extension and Validation Study". This volume describes various additions and extensions of an occupant model needed to simulate the pedestrian accident victim and the model's performance in simulating the drop tests of Volume IV. The modifications included changes to the victim-vehicle interaction subroutines, victim geometry, and vehicle geometry.					
17. Key Words Pedestrian Accidents, Injury Causation, Injury Index, Statistics, Math Models, Computer Programs, Drop Tests, Anthro- pometric Dummies			18. Distribution Statement		
19. Security Classif. (of this report)		20. Security Classif. (of this page)		21. No. of Pages 165	22. Price

The contents of this report reflect the views of the Texas A & M Research Foundation, Texas Transportation Institute, Texas A&M University, which is responsible for the facts and the accuracy of the data presented herein. The contents do not necessarily reflect the official views or policy of the Department of Transportation. This report does not constitute a standard, specification or regulation.

PREFACE

The investigation reported in this publication was conducted by the Texas Transportation Institute (TTI), Texas A&M University, under Contract DOT-065-1-217, National Highway Traffic Safety Administration. The program was directed by Dr. H. E. Ross, Jr. of TTI. The Contract Technical Manager was Dr. Lee J. Ovenshire and the Contracting Officer was Mr. Joseph R. Amato, both of NHTSA.

The research was divided into four distinct but related areas and the results are published as follows:

Volume I - "Summary Report". This document summarizes the methods of research, the conclusions and the recommendations of the study.

Volume II - "Analysis of the Pedestrian Accident Information". An extensive statistical analysis of 263 pedestrian accident records was conducted by Dr. Adil M. Mayyasi with assistance from Dr. Udo Pooch, in search of injury causation factors. Multivariate analysis and item selection techniques were used to evaluate the data. This document describes that analysis and its results.

Volume III - "The Texas A&M University Injury Severity Index". Drs. Thomas A. Krouskop and Paul H. Newell, Jr. and Mr. Albert E. Swarts developed a method to quantify the severity of injuries as reported by medical practitioners. Also developed was a method to quantify the severity of pedestrian accidents, given the pedestrian's kinematics, as determined by numerical or physical simulation. Their results are given in this document.

Volume IV - "Drop Tests of Dummies on a Mock Vehicle Exterior". Drs.

H. E. Ross, Jr. and R. D. Young and Messrs Monroe C. White and Wayne F. Lammert conducted a series of drop tests with instrumented male, female and child anthropometric dummies. The objective of these tests was to provide data from which the TTI numerical simulator (described in Volume V) of the pedestrian accident victim could be validated. Volume IV gives the results of those tests.

Volume V - "A 3-D Math Simulation of a Crash Victim--Extension and

Validation Study". A vehicle occupant simulation model, developed by Dr. Ronald D. Young in earlier studies at TTI, was modified for use as a more general crash-victim simulator, one such victim being the pedestrian. The tests described in Volume IV were then simulated by the model and the results were compared. Drs. R. D. Young and H. E. Ross, Jr., and Mr. W. F. Lammert conducted this phase of the study.

TABLE OF CONTENTS

	<u>Page</u>
TECHNICAL REPORT STANDARD TITLE PAGE	ii
DISCLAIMER	iii
PREFACE	iv
LIST OF TABLES	viii
LIST OF FIGURES	ix
I. INTRODUCTION	1
II. MEASUREMENT OF DUMMY PROPERTIES	2
Weight and Center of Gravity Location	2
Geometric Measurements	7
Moments of Inertia	7
Static Surface Force-Deformation Properties	14
III. MOCK VEHICLE EXTERIOR AND ITS SURFACE PROPERTIES	17
Analytical Formulation of Static Force-Deflection Properties of Polyurethane Foam	17
Experimental Determination of Static Force-Deflection Properties of Polyurethane Foam	20
Comparison of Theoretical and Experimental Results	20
Experimental Determination of Static Force-Deflection Properties of a Foam-Plywood Composite	20
Coefficient of Friction	28
IV. PHOTOGRAPHY AND INSTRUMENTATION	29
High-Speed Film Coverage	29
Dummy Accelerometers	32
Electronic Recording Equipment	34
V. DETAILS OF DROP TESTS	37
Test Procedures	37
Determine columb torques	37

	<u>PAGE</u>
Calibrate accelerometers	44
Position dummy and conduct test	44
Impact Conditions	47
Test Results	53
VI. CONCLUSIONS	61
REFERENCES	62
APPENDICES	
A. Derivation of Force-Deformation Relationships for Rigid Spheres Penetrating Polyurethane Foam	A-1
B. Estimation of Mass Distribution and Moments of Inertia of Dummy Torsos	B-1
C. Static Force-Deformation Curves of Dummy Segments	C-1
D. Tabulation of Impact Conditions	D-1
E. Accelerometer Data	E-1

LIST OF TABLES

<u>TABLE NO.</u>	<u>TITLE</u>	<u>PAGE</u>
II-1	Dummy Types	2
II-2	Weights of Dummy Segments	4
II-3	Measurements of Dummy Segments	5
II-4	Exterior Dummy Dimensions	8
II-5	Moments of Inertia for Dummy Segments	11
IV-1	Accelerometer Ranges	32
V-1	Summary of Child Drop Tests	39
V-2	Summary of Female Drop Tests	40
V-3	Summary of Male Drop Tests	41
V-4	Columb Joint Torques	46

LIST OF FIGURES

<u>FIGURE NO.</u>	<u>TITLE</u>	<u>PAGE</u>
II-1	Photos of Dummies	3
II-2	Articulated Body of the TCVS with Coordinate Systems	6
II-3	Moment of Inertia Measurements	12
II-4	Load Tests of Dummy Segments	15
II-5	Force-Deformation Properties of Male Dummy Segments	16
III-1	Mock-up & Background Grid	18
III-2	Mock-up Details	19
III-3	Polyurethane Foam Load Tests	21
III-4	Force-Deformation of 6 Inch Thick Foam	22
III-5	Force-Deformation of 4.5 Inch Thick Foam	23
III-6	Force-Deformation of 3.0 Inch Thick Foam	24
III-7	Force-Deformation of 1.5 Inch Thick Foam	25
III-8	Load-Deflection Curves for Simply Supported Polyurethane and Plywood Composite with Hemispherical	26
IV-1	Camera Locations	30
IV-2	Location of Flash Bulb	31
IV-3	Dummy Accelerometers	33
IV-4	Location of Tri-Axis Accelerometers	35
IV-5	Electronic Recording Equipment	36
V-1	Adult Male Dummy in Position for Drop Test No. 2 (M-2)	38

LIST OF FIGURES (cont'd)

<u>FIGURE NO.</u>	<u>TITLE</u>	<u>PAGE</u>
V-2	Prototype Configurations	42
V-3	Upright & Tilted Mock-up Positions	43
V-4	Measurements of Joint Torques in Adult Female Dummy	45
V-5	Fixed Axis Orientation	49
V-6	Eulerian Angles	50
V-7	Elbow & Knee Constraints	51
V-8	High Speed Film Frames of Test M-3, Camera No. 1	54
V-9	High Speed Film Frames of Test M-3, Camera No. 2	56
V-10	Typical Accelerometer Data	58

I. INTRODUCTION

As discussed in Volume V of this report, a math model of the vehicle occupant (1) was extended to include the pedestrian accident victim. The revised model is denoted herein as the TTICVS (Texas Transportation Institute's Collision Victim Simulator). Of particular interest in this contract was the pedestrian accident victim and the information presented in this volume was obtained to provide data for validating the TTIVCS in the pedestrian mode. The data, however, are not limited to the validation of the TTICVS only, and could be used for similar reasons on other simulators.

The simple, but effective test procedure consisted of dropping instrumented anthropometric dummies on a mock vehicle exterior. High-speed cameras recorded the dummy's kinematics and nine accelerometers, three each in the head, chest, and pelvis, measured accelerations. Tests were conducted on an adult male dummy, an adult female dummy, and a child dummy. A variety of impact positions and impact speeds of the dummies were used to insure a wide range of three-dimensional dummy motions.

Detailed measurements were made of each dummy's mass and inertia properties, geometry, joint properties, and surface force-deformation properties. Static force-deformation measurements were also made on the polyurethane foam which was used to cover the vehicle mock-up.

II. MEASUREMENT OF DUMMY PROPERTIES

The three anthropometric dummies used in the drop tests are listed in Table II-1. Pictures of the dummies are shown in Figure II-1.

TABLE II - 1. DUMMY TYPES

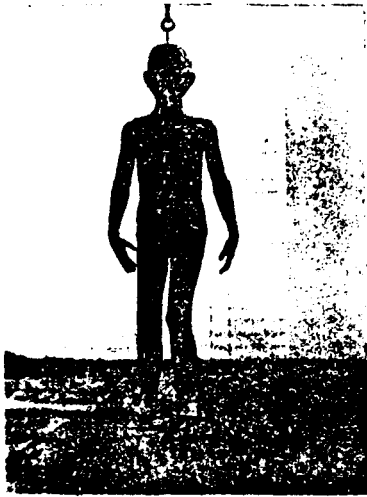
<u>TYPE</u>	<u>NUMBER</u>	<u>DESCRIPTION</u>
6-year	Sierra 492-106	Child
5 Percentile	Sierra 592-805	Adult Female
95 Percentile	Sierra 292-895	Adult Male

Each dummy was disassembled into a series of segments. Measurements were then made on each segment to determine its weight, geometry, inertia properties, and static force-deformation properties. This information was needed for simulation of the drop tests by the TTICVS.

Weight and Center of Gravity Location

Each segment was weighed on an Ohaus balance scale to an accuracy of 0.1 grams. Table II-2 lists the weights of each segment. The center of gravity was found by balancing each segment on the edge of a 1/8 inch thick steel angle-section about three orthogonal axes. The intersection of these axes located the C.G. The centers were located for each axis with an approximate accuracy of ± 0.1 inch. Table II-3 presents the distance from a definable point to the center of gravity of each segment.

Since the dummies did not disassemble into the same number of segments as had the TTICVS refer to Figure II-2, it was necessary to estimate the weights and centers of gravity of some segments. The procedures used in this estimation and the results are given in Appendix B.



6-YEAR CHILD



5 PERCENTILE FEMALE ADULT



95 PERCENTILE MALE ADULT

FIGURE I4-1. PHOTOS OF DUMMIES

21328

TABLE II-2. WEIGHTS OF DUMMY SEGMENTS

SEGMENT	SEGMENT WEIGHTS (LBS)					
	MALE		FEMALE		CHILD	
	<u>RIGHT</u>	<u>LEFT</u>	<u>RIGHT</u>	<u>LEFT</u>	<u>RIGHT</u>	<u>LEFT</u>
Leg & Foot	14.859	14.754	4.824	4.965	3.904	3.729
Thigh	23.503	23.819	13.805	13.278	4.394	4.460
Forearm & Hand	5.742	5.647	2.489	2.467		
Upper Arm	7.707	7.832	3.014	3.444	2.967*	3.005*
Head & Neck	17.718		11.181		27.024**	
Torso	91.6		43.936			

* Upper arm could not be disassembled from forearm for child dummy.

** Torso could not be disassembled from neck and head for child dummy.

TABLE II-3. MEASUREMENTS OF DUMMY SEGMENTS

SEGMENT	DIMENSIONS (IN.)***					
	MALE		FEMALE		CHILD	
	RIGHT	LEFT	RIGHT	LEFT	RIGHT	LEFT
Leg & Foot						
length	21.4	21.4	16.3	16.3	12.3	12.3
knee to ankle	18.3	18.3	13.6	13.6	9.7	9.7
knee to C.G.	10.8	11.4	8.8	8.4	6.7	6.7
Thigh						
length	18.3	18.3	14.3	14.3	9.3	9.3
hip to C.G.	8.9	9.0	6.7	6.6	3.7	3.6
Forearm & Hand						
length (fingers curled)	16.6	17.0	13.0	13.0	11.0	11.1
elbow to wrist	11.0	11.0	8.2	8.2	6.1	6.1
elbow to C.G.	7.8	7.7	3.8	5.6	*	*
Upper Arm						
length	11.6	11.6	10.1	10.1	7.6	7.6
shoulder to C.G.	5.6	5.4	4.7	4.8	6.9*	6.9*
Head						
length (neck to top of head)	12.7		11.7		9.0	
neck to C.G.	6.8		5.9		**	
Torso						
neck to hip	23.0		18.0		15.0	
shoulder width	15.0		11.5		8.5	
hip width	7.5		6.9		4.2	
neck to C.G.	12.0		8.6		3.1** (down)	

* Hand, Forearm, & Upper Arm all one piece on child dummy.

** Head, Neck, & Torso all one piece on child dummy.

*** All dimensions from pivot center to pivot center unless otherwise noted.

Terminal end of segment No. 1,
 chosen as reference point --
 with coordinates $(X'_{T1}, Y'_{T1}, Z'_{T1})$
 relative to space-fixed system

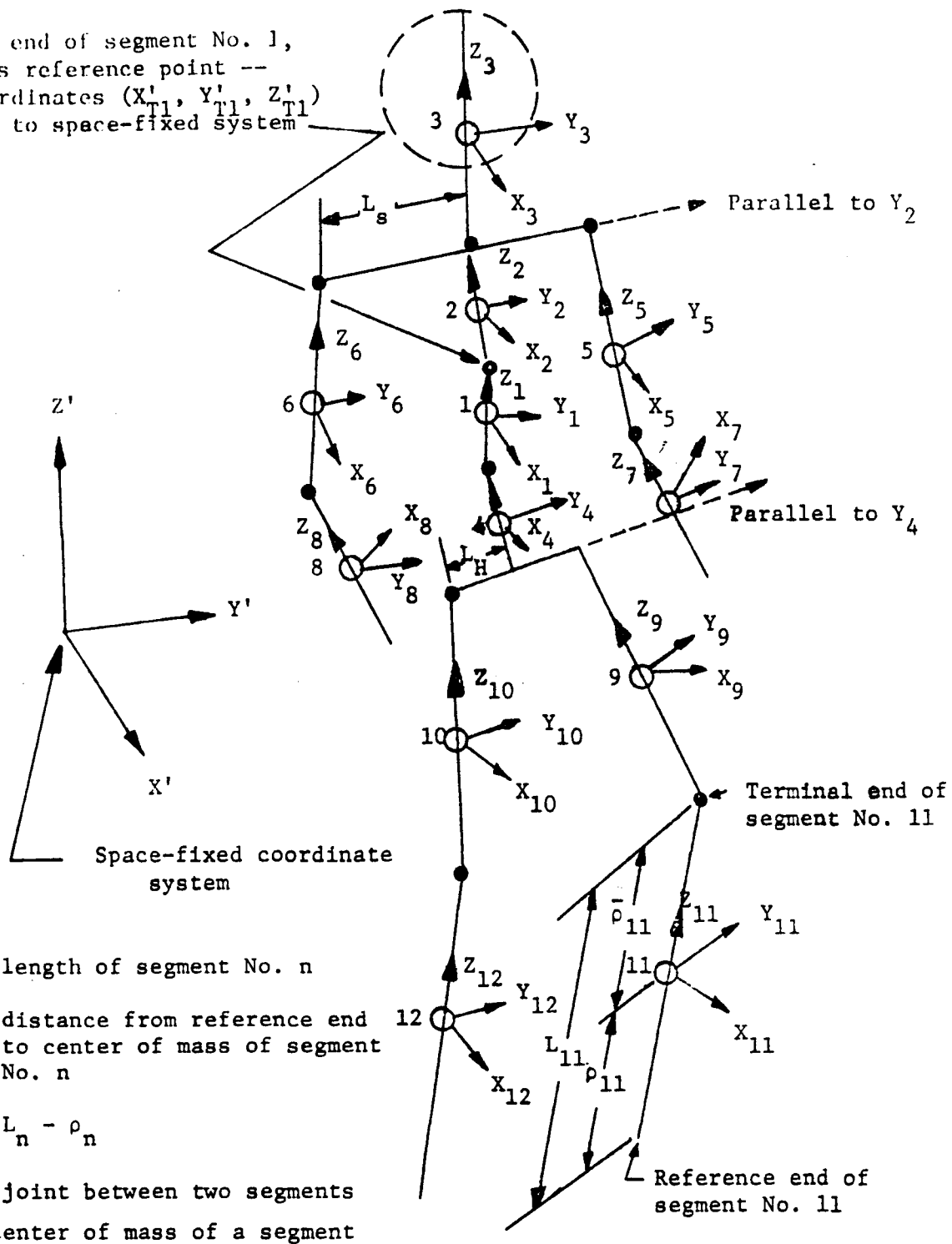


FIGURE II-2 ARTICULATED BODY OF THE TTICVS WITH COORDINATE SYSTEMS

Geometric Measurements

Two basic types of geometric measurements were made, namely, internal pivot center to pivot center measurements and external dimensions. The pivot center to pivot center measurements are given in Table II-3 and the external measurements are given in Table II-4. The dimensions are to an accuracy of ± 0.1 inches.

Moments of Inertia

A simple torsional pendulum device was used to measure each segment's moment of inertia about the three segment axes (see Figure II-2 for segment axes). The procedure consisted of measuring the period of the segment and the device combined, then calculating the segments' moment of inertia knowing the torsional spring constant, K , and the periods of the device alone.

For a free vibrating torsional pendulum the damped frequency of vibration, ω_d , is given by:

$$\omega_d = \omega_n \sqrt{1-\zeta^2} \quad (\text{II-1})$$

where ω_n = natural frequency (undamped), and

ζ = damping ratio.

a solution for ζ can be obtained from the logarithmic decrement, stated below:

$$\ln \frac{x_{n+1}}{x_n} = -2\pi\zeta / \sqrt{1-\zeta^2} \quad (\text{II-2})$$

TABLE II-4. EXTERIOR DUMMY DIMENSIONS

SEGMENT	DIMENSIONS (IN.)*								
	MALE			FEMALE			CHILD		
	Fore-Aft	Lateral	Circumference	Fore-Aft	Lateral	Circumference	Fore-Aft	Lateral	Circumference
Head	9.2	6.9	25.2	7.3	6.0	21.0	7.2	6.0	21.8
Chest	10.5	16.25	44.5	8.25	9.5	31.0	5.0	8.25	23.75
Waist	10.0	13.50	39.0	6.5	7.5	24.0	6.0	7.25	21.0
Hips	11.25	15.50	44.0	7.0	13.0	34.0	4.75	9.0	23.5
Thigh									
upper	8.2	6.3	24.6	6.0	5.75	18.3	4.0	3.9	12.7
lower	4.5	4.9	16.5	3.5	3.8	12.1	2.7	2.8	9.0
Leg									
upper	4.5	5.0	16.1	4.0	3.9	12.1	2.9	3.0	9.9
lower	3.2	3.0	10.2	2.75	2.1	7.6	2.1	1.9	6.9
Upper Arm									
upper	4.75	3.0	13.9	3.75	2.0	10.3	2.2	1.6	6.9
lower	3.75	3.75	12.0	2.5	2.4	7.7	2.0	2.0	6.5
Forearm									
upper	3.30	4.10	12.5	2.4	3.0	8.6	2.1	2.0	6.5
lower	2.75	2.10	8.0	2.0	1.6	6.0	1.5	1.25	4.9
Hand	4.9	3.0	5.0**	3.8	2.3	4.5**	3.0	1.2	5.0**

* These dimensions were taken with the dummies in a standing position with the arms in their normal at-rest position (inside of hands adjacent to dummy's side).

** Up and down

where x_n = a displacement (generally a maxima) and

x_{n+1} = a displacement one cycle from x_n

The amplitude of the torsional pendulum reported on herin decayed from 20° to approximately 2° in 100 cycles. Assuming an average amplitude decrease of 0.18° per cycle,

$$\begin{aligned} \ln \frac{x_2}{x_1} &= \ln \left(\frac{19.82}{20} \right) && \text{(II-2a)} \\ &= -0.00904. \end{aligned}$$

Then $-2\pi\zeta / \sqrt{1-\zeta^2} = -0.00904$

and $\zeta = .0014.$

Thus

$$\omega_d = \omega_n \sqrt{1-.00000196} \approx \omega_n \sqrt{1} \quad \text{(II-1a)}$$

and one can justifiably assume that

$$\omega_d = \omega_n, \quad \text{(II-3)}$$

i.e., viscous and coulomb damping are small enough to be neglected and solving for the moment of inertia will involve the simple equations presented next.

The period for the undamped torsional pendulum is:

$$P_1 = 2\pi \sqrt{I/K}, \quad \text{(II-4)}$$

and the period for the pendulum and the attached segment is:

$$P_2 = 2\pi \sqrt{(I_1+I_2)/K} \quad \text{(II-5)}$$

where P_1 = period of pendulum in seconds,

P_2 = period of pendulum and segment in seconds,

I_1 = moment of inertia of pendulum about axis of rotation, in lb/in/sec^2 ,

I_2 = moment of inertia of segment, and

K = torsional spring constant of pendulum, in in.-lb/rad.

Solving equation (II-4) for I_1 and substituting into equation (II-5) and solving for I_2 , the following is obtained:

$$I_2 = \frac{P_2^2 - P_1^2}{4\pi^2} K . \quad (\text{II-6})$$

Table II-5 presents a summary of the values of the moments of inertia for all the dummy segments for the three orthogonal axes through the center of gravity of each segment as measured by the torsional pendulum.

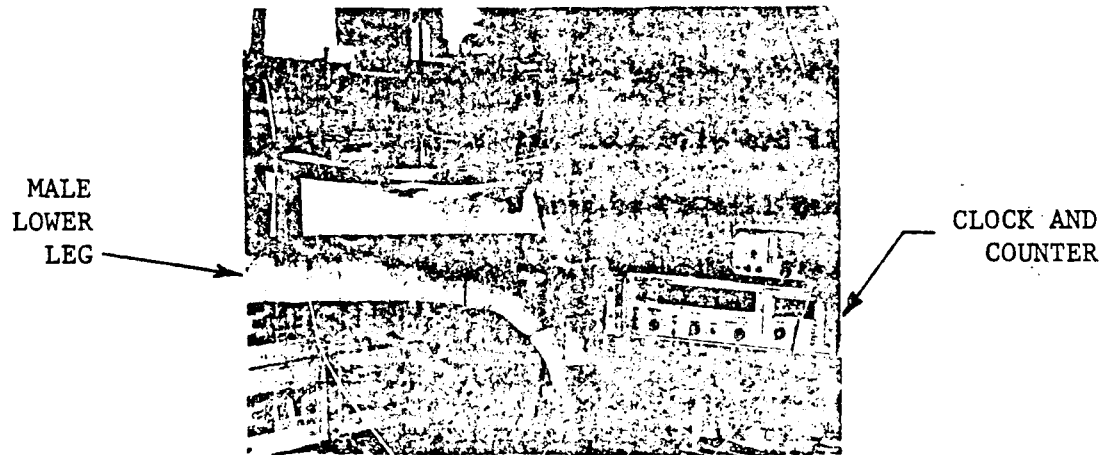
The period measurements were obtained with a Hewlett-Packard Electronic clock/counter, Model No. 5245 L. This device had an optional on-off trigger circuit that would start the clock, count a preselected number of cycles, then shut off the clock within ± 1 msec. The trigger circuit sensing device consisted of a cadmium sulphide photocell and a small 1-volt light bulb that was placed near the rim of the pendulum such that a small aluminum tab glued to the rim would interrupt the light beam impinging on the photocell, thus triggering the on-count-off circuit. Figure II-3 shows photos of the sensor and the clock/counter in action with the male lower leg being rotated about its X-axis. For 100 cycles of the pendulum, the sensor would activate 200 times, or every half cycle. Thus, the counter was set for 200 counts to obtain the period for 100 cycles. The counter was set at 100 counts for 50 cycles for the x and y-axis of the male torso, though, because the amplitude decreased to approximately $\pm 2^\circ$ at about 50 cycles.

TABLE II-5. MOMENTS OF INERTIA* FOR
DUMMY SEGMENTS

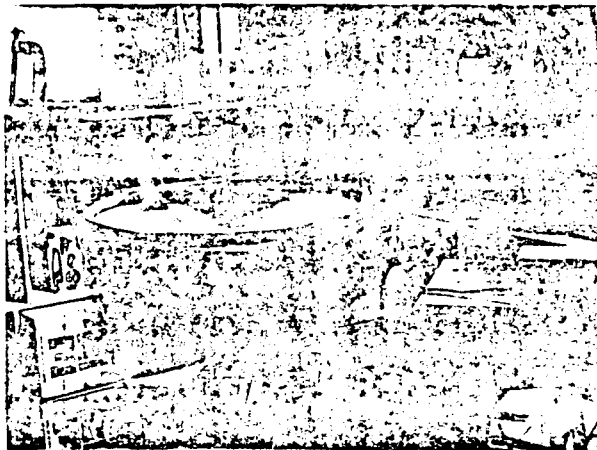
SEGMENT	RIGHT SIDE			LEFT SIDE		
	Long(x) Axis	Lat.(Y) Axis	Vert.(z) Axis	Long(x) Axis	Lat.(Y) Axis	Vert(z) Axis
MALE:						
Foot & Calf	1.880085	1.953360	.139710	1.941865	2.009707	.140128
Thigh	1.473326	1.504586	.218314	1.511191	1.544474	.218154
Hand & Forearm	.368305	.362709	.022173	.387547	.392370	.021960
Upper Arm	.267452	.268697	.030335	.292759	.283275	.032625
Head**	.848981	.937262	.295583			
Torso**	14.233831	13.567673	3.507716			
FEMALE:						
Foot & Calf	.316342	.327747	.032703	.317695	.336504	.035944
Thigh	.666167	.610037	.097945	.586810	.585662	.088346
Hand & Forearm	.096943	.101474	.015897	.090545	.090751	.011882
Upper Arm	.105826	.106799	.014717	.114293	.114034	.009787
Head**	.351415	.370176	.117019			
Torso**	4.876114	4.605181	1.167683			
CHILD:						
Foot & Calf	.156348	.172193	.022976	.157709	.160947	.027165
Thigh	.112909	.112601	.018106	.121968	.121573	.027293
Hand, Forearm & Upper Arm	.184647	.183292	.013327	.184057	.186947	.011942
Head & Torso	3.731806	3.652102	.408504			

* Units are in.-lb-sec²

** The head and torso moments of inertia are listed under the "Right Side" column for convenience only, i.e., they are not to be associated with a right or left side. Refer to Appendix B for Moments of Inertia of dummy segments within the torso.



MEASURING DEVICES



TEST IN PROGRESS

FIGURE II-3. MOMENT OF INERTIA MEASUREMENTS

The variations of the measured periods between the six runs for a particular segment and orientation ranged from a maximum of 0.0653% of the lowest value for the male torso, x-axis, to a minimum of 0.0027% of the lowest value for the male, left forearm and hand, z-axis. This indicates a high degree of repeatability, i.e., small variations in initial angle and hand release of the pendulum introduce a very small error in the measured period.

To check the validity of the measured data, a steel bar 1.000 in. in diameter and 22.00 in. long was attached to the pendulum and cycled. The period was found to be 1.2962715 seconds and, using equation (II-6), the bars' moment of inertia was calculated to be 0.523814 lb/in/sec². The theoretical moment of inertia was calculated using the formula

$$I_{\text{theory}} = \frac{w}{g} \left(\frac{d^2}{16} + \frac{e^2}{12} \right) \quad (\text{II-7})$$

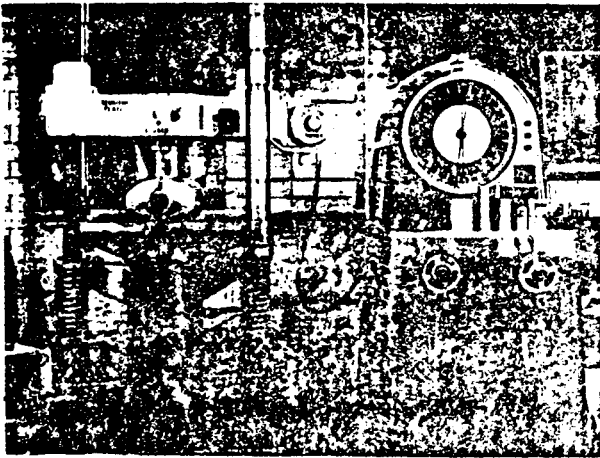
where w = weight of bar, 2291.8 gms or 5.052553 lb,
 g = acceleration of gravity, 32.2 ft/sec,
 d = diameter of bar, 1.000 in., and
 e = length of bar, 22.00 in.

The theoretical moment of inertia was calculated to be 0.528214 lb/in/sec². The measured value, then, was only 0.833% lower than the theoretical.

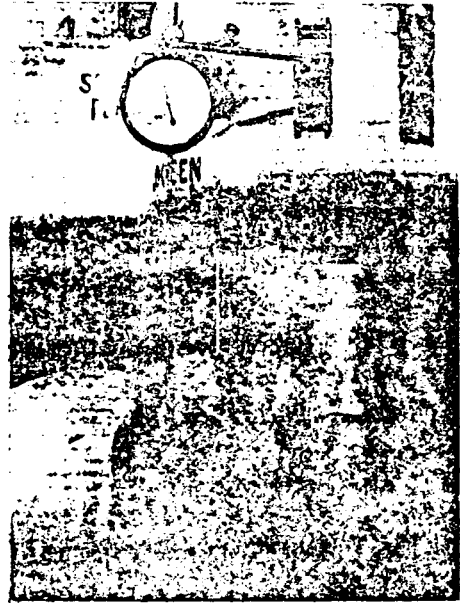
The pendulum shaft consisted of a 1/4 in. steel shaft 132 in. long with a bicycle wheel for a 26 in. x 1.25 in. tire as a flywheel. The segments were attached to the bicycle wheel with 14 ga. iron wire and lightweight plastic tape. The pendulum was similar to one used by Cornell Aeronautical Laboratory (2) for determining moments of inertia of dummy segments.

Static Surface Force-Deformation Properties

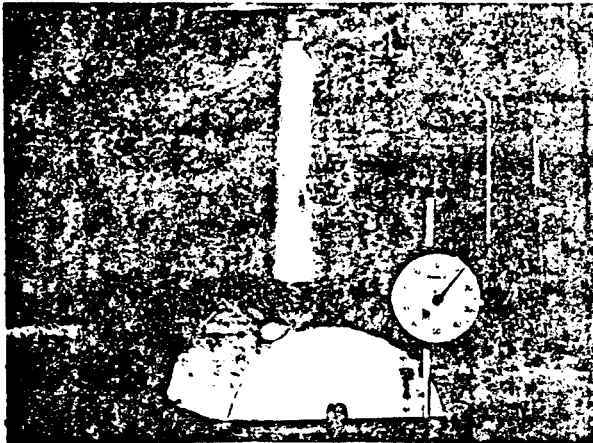
The static surface force-deformation properties of the dummy segments were measured using a Baldwin-Southwark-Emery universal testing machine. Deformations were determined by dial indicator gages. Figure II-4 shows a view of the overall set up and close up views of the female torso abdominal test, male calf test, and child skull cap test. The deformation was measured with respect to a "bone structure" to simulate the deformation due to impact since static testing causes deformation on both sides of a dummy segment. Examples of measuring with respect to a "bone structure" are evident in the photos of the female torso and male calf tests presented in Figure II-4. Right circular cylinders of 1.5, 2.5, 5.0, and 7.0 in. diameters were used to deform the segments flesh with the segments dimension determining the appropriately matching cylinder diameter. Figure II-5 presents a plot of force versus displacement for the male chest under frontal loading and unloading. A complete set of plots is presented in Appendix C.



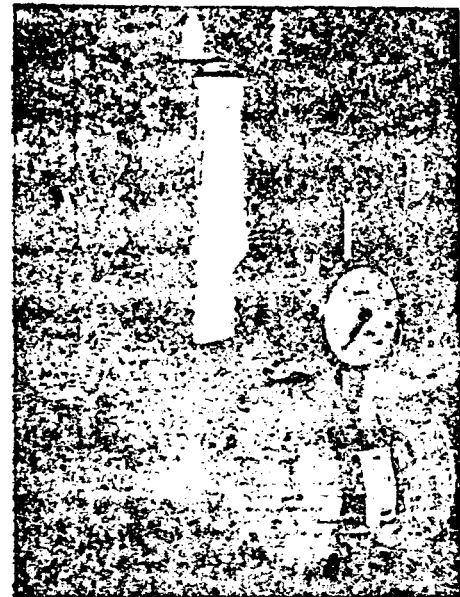
TEST APPARATUS



FEMALE ABDOMEN



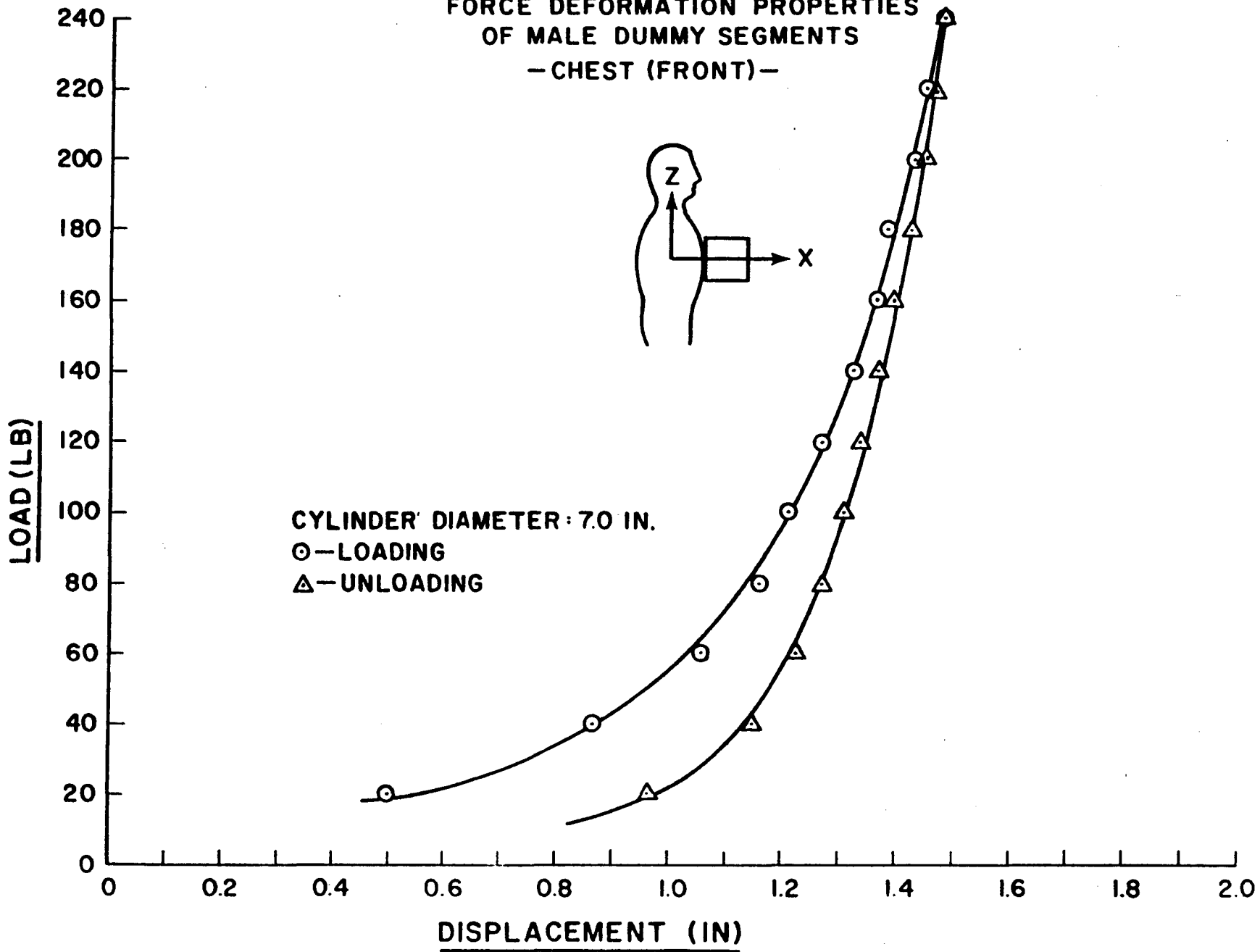
CHILD SKULL CAP



MALE CALF

FIGURE II-4. LOAD TESTS OF DUMMY SEGMENTS

FIGURE II-5
FORCE DEFORMATION PROPERTIES
OF MALE DUMMY SEGMENTS
- CHEST (FRONT) -



III. MOCK VEHICLE EXTERIOR AND ITS SURFACE PROPERTIES

To maintain close control on shape and stiffness, an idealized vehicle exterior was constructed and covered to a uniform thickness with a relatively soft material. Figure III-1 shows a photograph of the mock-up and Figure III-2 shows its details. The dimensions are representative of late model medium weight sedans. Plywood panels with internal ribs were used to form a rigid template type support structure. A 6 inch layer of polyurethane foam, of density 2.72 lb/ft^3 , covered the exterior surfaces where contact was anticipated.

To assess the foam's stiffness characteristics, both analytical and experimental methods were used. A description of these methods and their comparison follows.

Analytical Formulation of Static Force-Deformation Properties of Polyurethane Foam

A formulation was sought which would describe the force-deformation properties of spheres in contact with the foam. The objective of this formulation was a closed form relationship which could be easily incorporated in the TTICVS and one which could be used to approximate the forces caused when the dummy contacted the foam.

Derivations of the equations are given in Appendix A. The results of the equations are shown in the following section in comparison with experimental results.

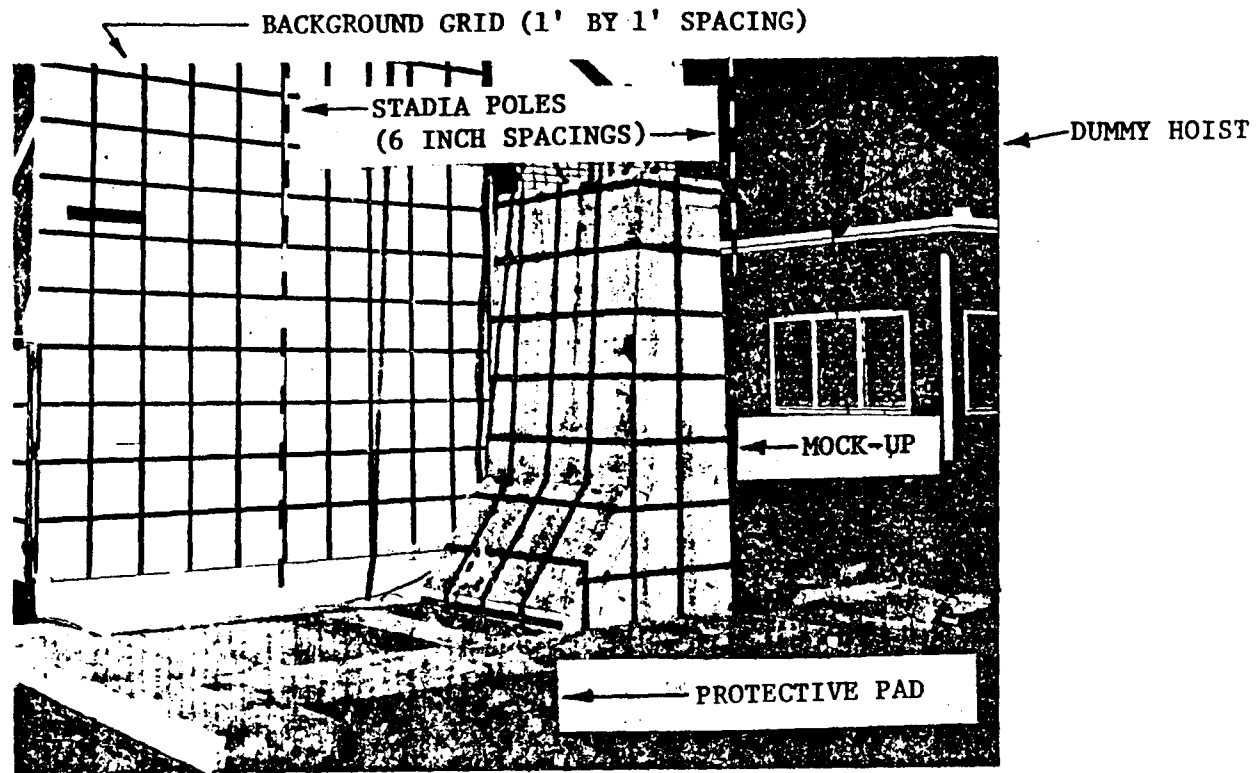
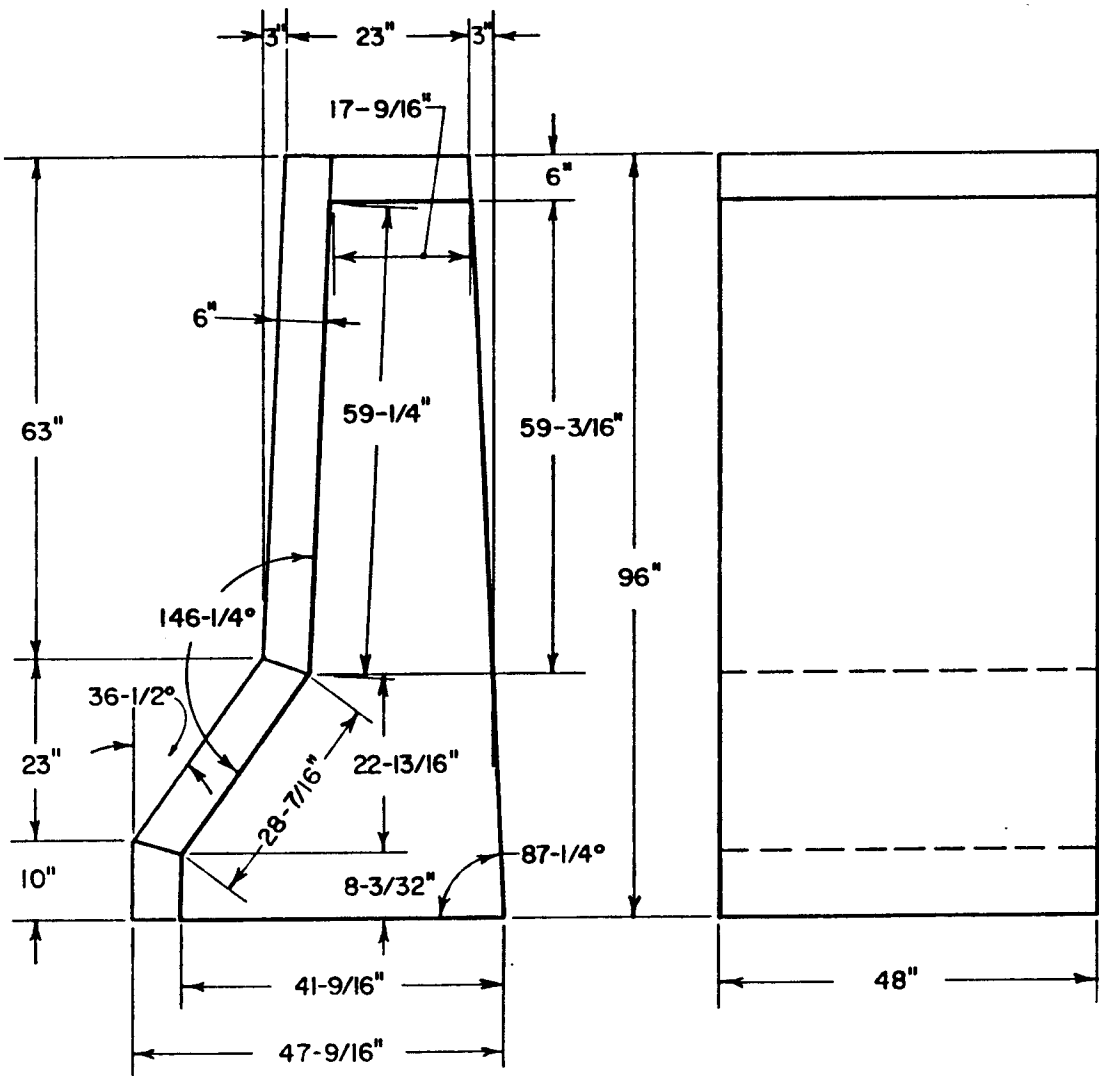


FIGURE III-1. MOCK-UP AND BACKGROUND GRID



POLYURETHANE FOAM

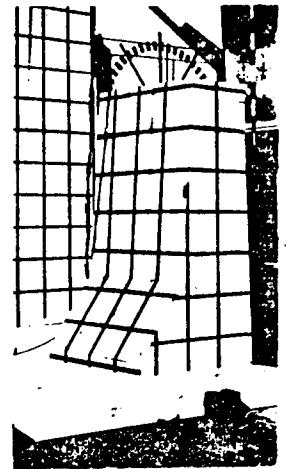
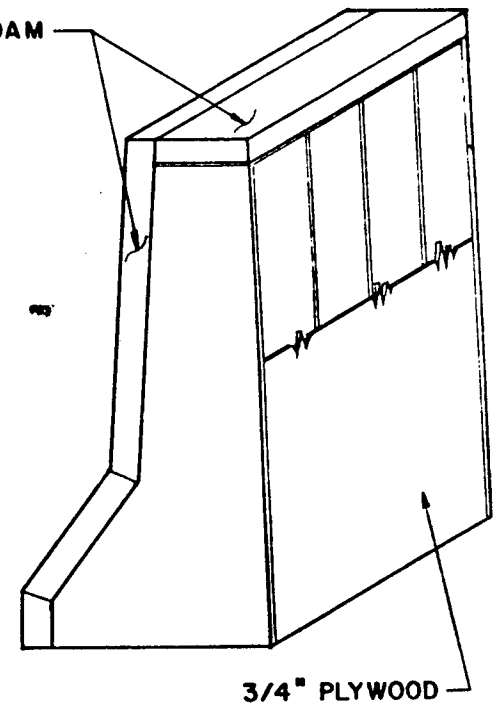


FIGURE III-2. MOCK-UP DETAILS

Experimental Determination of Static Force-Deformation Properties of Polyurethane Foam

Foam samples 24 inches wide by 48 inches long with thicknesses of 6 inches, 4.5 inches, 3 inches, and 1.5 inches were load tested on a Universal testing machine. Hemisphere loading heads, made of hard Northern maple, of 10 inch, 7.5 inch, 5 inch, and 2.5 inch diameters, were used to load the foam. Photographs of the hemispheres and the test operation are shown in Figure III-3. The results are given in the following section.

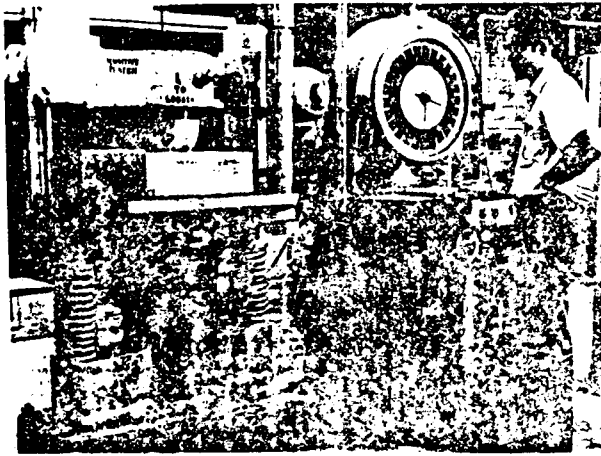
Comparison of Theoretical and Experimental Results

Both experimental and theoretical values are shown plotted in Figures III-4 thru III-7. The parameters used in the theoretical calculations are given in Appendix A.

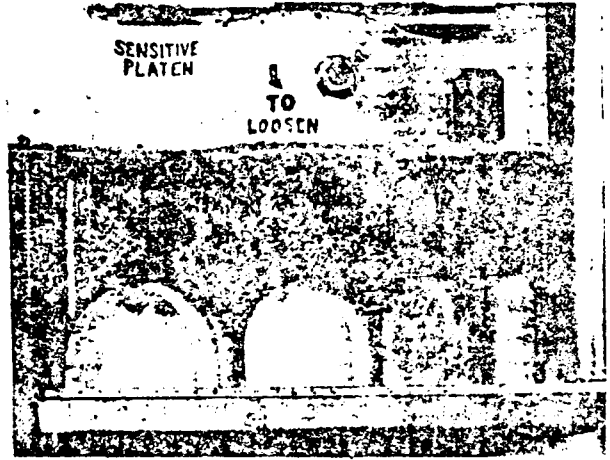
The theoretical results were in reasonable agreement with the experimental values for ratios of deformation to foam depth ($\frac{y}{w}$) less than about 0.75. This was expected since the idealized stress-strain relationship for the foam diverged from experimental values for strains greater than about 75 percent. However, differences at the higher strain values were not considered significant since the dummy penetrations were anticipated to occur at values of $\frac{y}{w}$ less than 0.75.

Experimental Determination of Static Force-Deflection Properties of a Foam-Plywood Composite

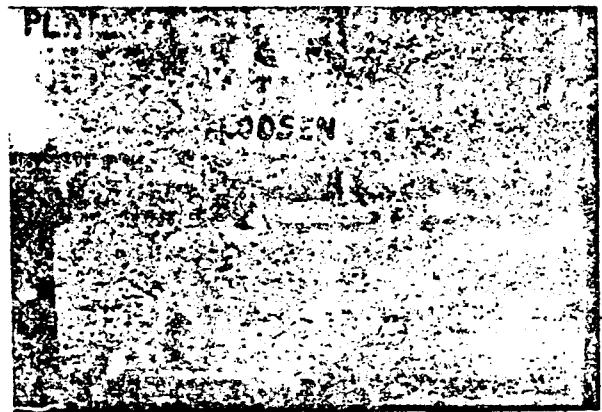
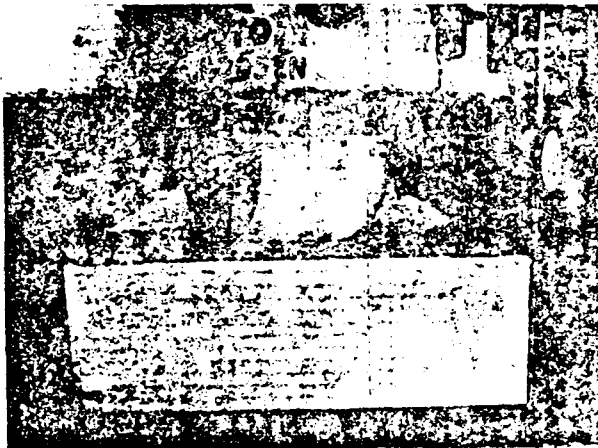
Although the plywood framework for the mock vehicle exterior was designed to be very stiff, a test was conducted to determine a measure of its actual stiffness. Figure III-8 shows a sketch of a foam-plywood composite panel, the



TEST APPARATUS



HEMISPHERE LOADING HEADS



10 INCH HEMISPHERE HEAD DEFORMING 6 INCH THICK FOAM

FIGURE III-3. POLYURETHANE FOAM LOAD TESTS

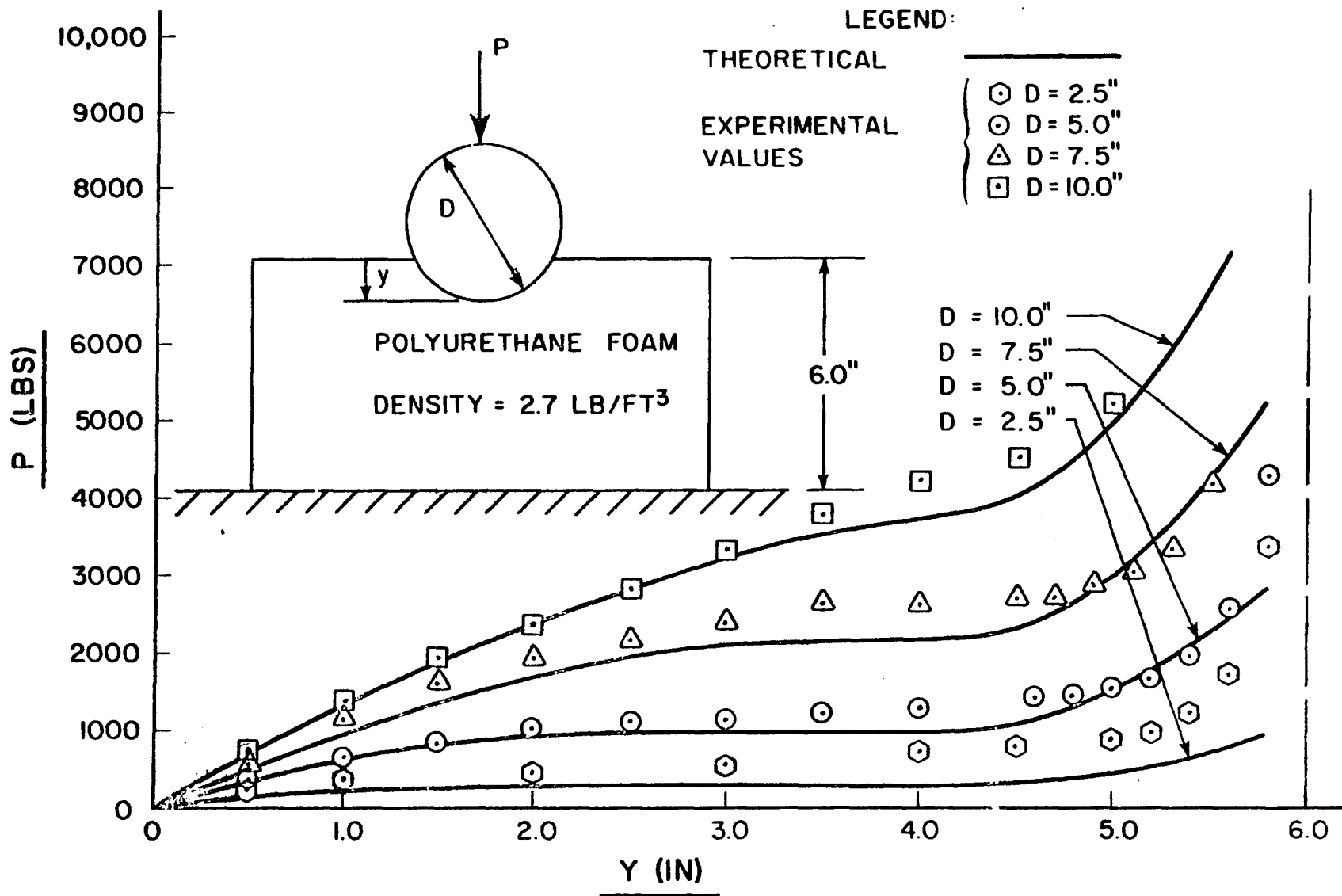


FIGURE III-4. FORCE-DEFORMATION OF 6 INCH THICK FOAM

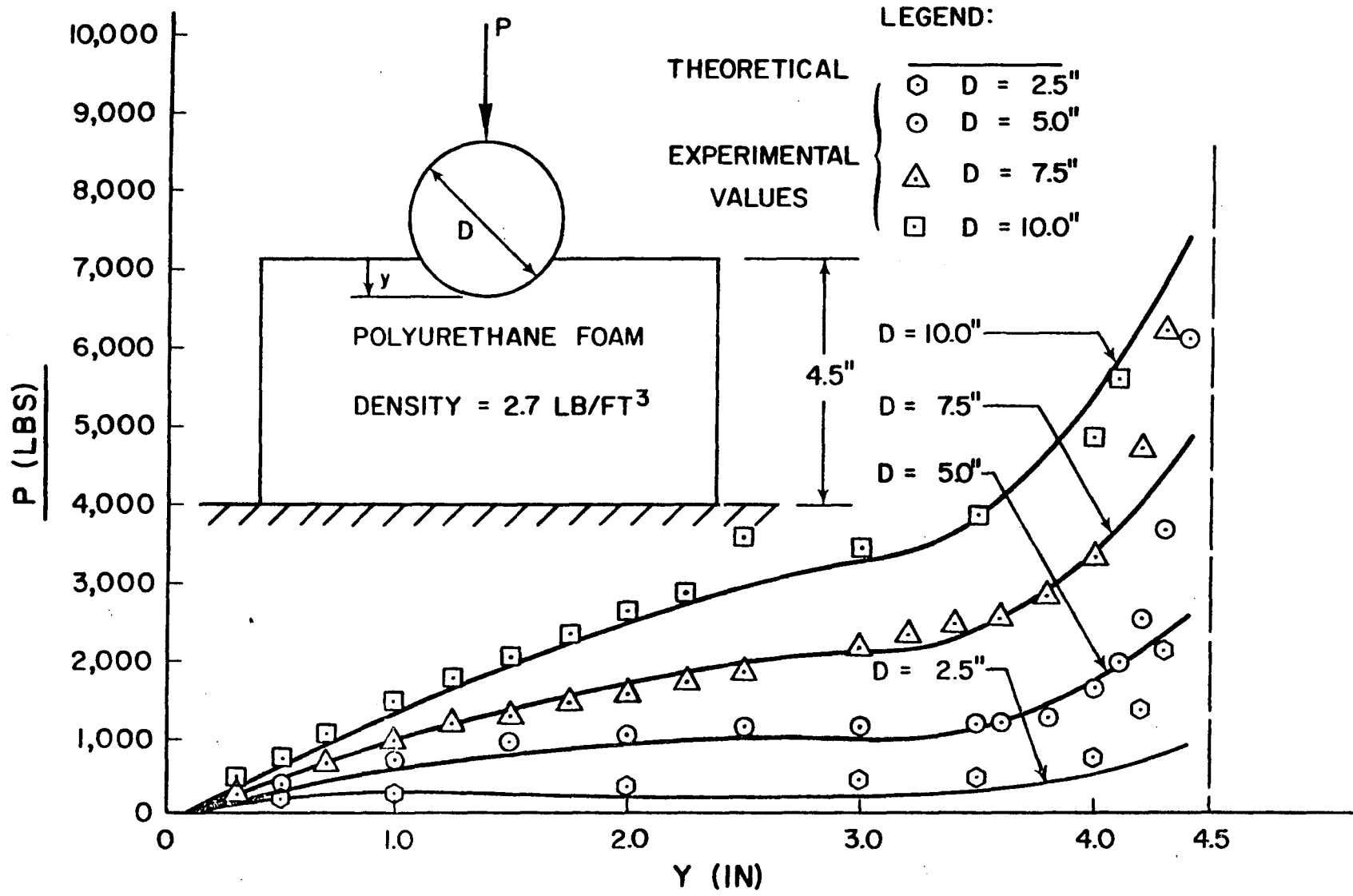


FIGURE III-5. FORCE-DEFORMATION OF 4.5 INCH THICK FOAM

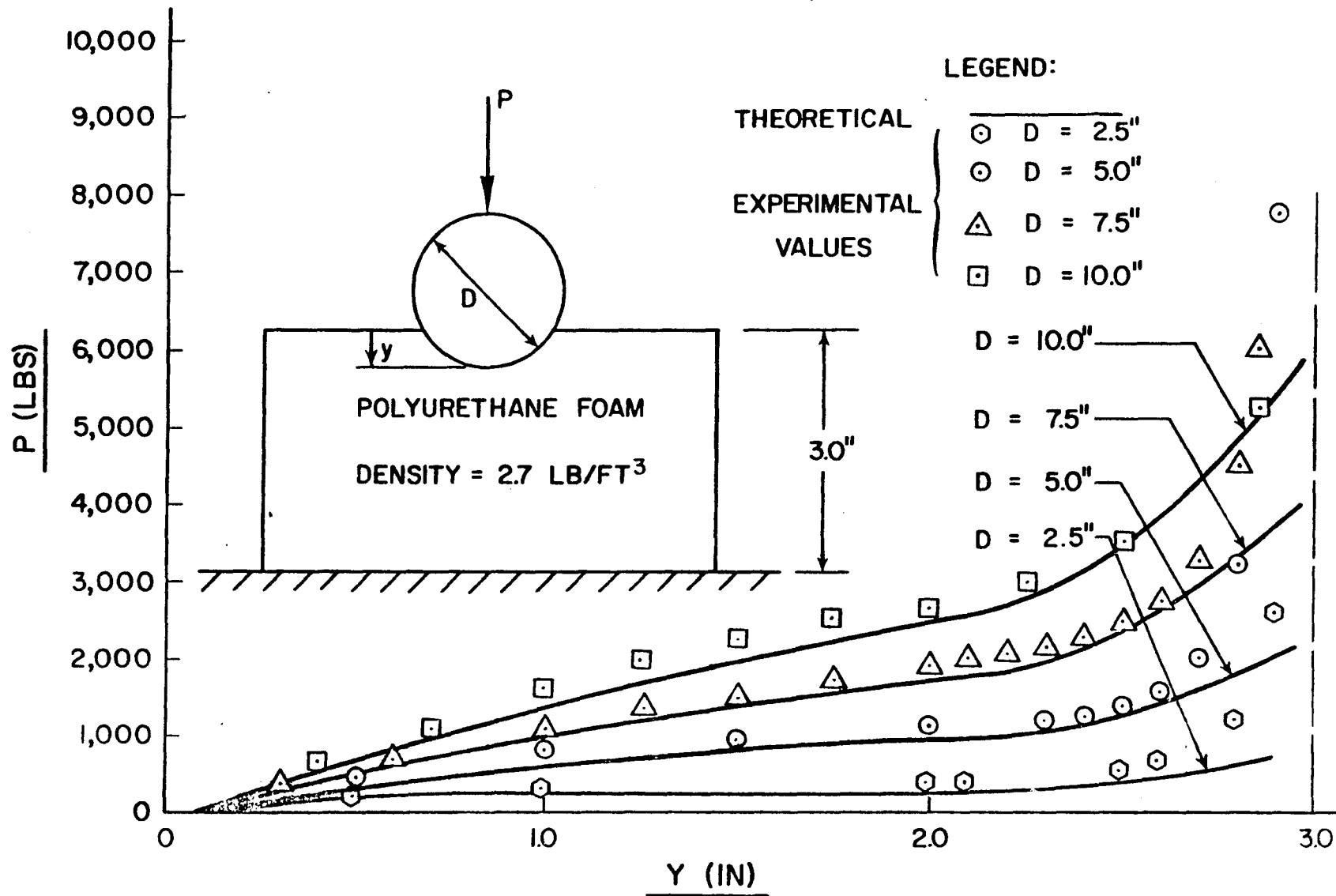


FIGURE III-6. FORCE-DEFORMATION OF 3.0 INCH THICK FOAM

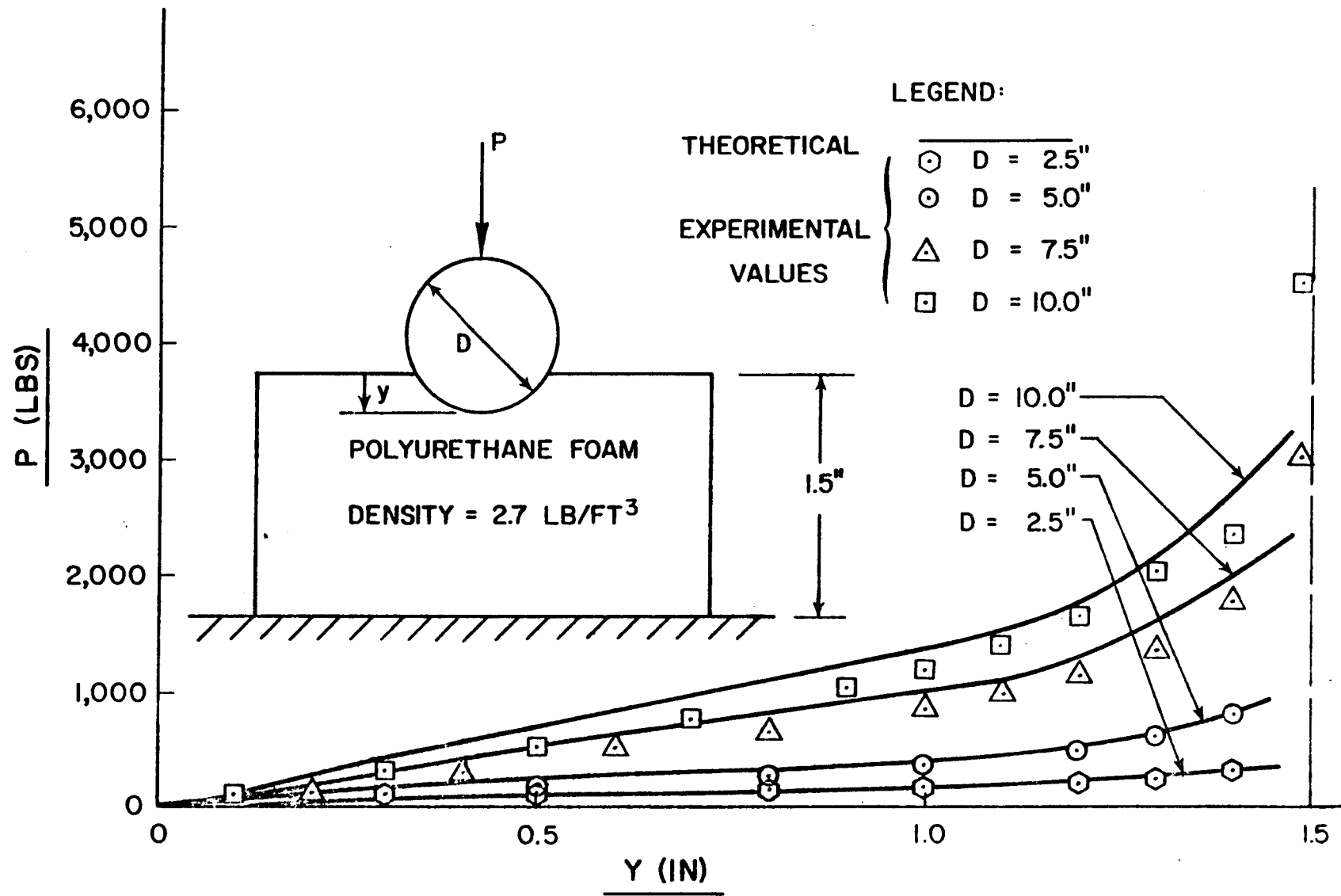


FIGURE III-7. FORCE-DEFORMATION OF 1.5 INCH THICK FOAM

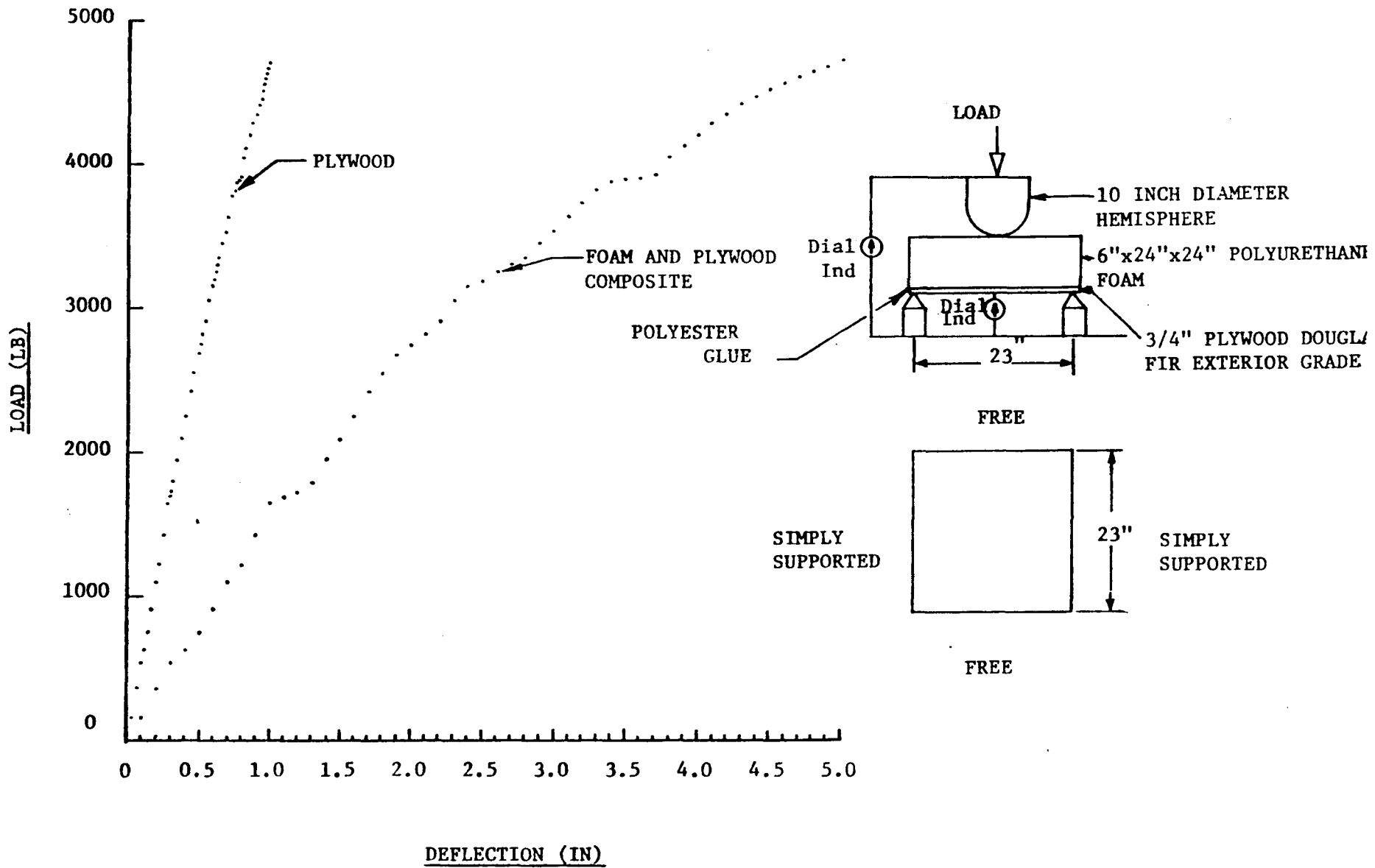


Figure III-8. LOAD-DEFLECTION CURVES FOR SIMPLY SUPPORTED POLYURETHANE AND PLYWOOD COMPOSITE WITH HEMISPHERICAL LOADING BLOCK

method of loading, and the results.

It should be noted that the edge constraints (free-free and simply supported on the other edges) result in larger plywood deflections (and a less stiff composite structure) than would occur in the mock vehicle exterior. The edge constraints of the plywood panels in the mock-up were approximately fixed rather than simply supported. Also, for all possible points of load application the chosen point (midway between supports) results in the largest possible deflection. Hence, the plywood panels in the mock-up will be considerably stiffer than the as-tested configuration. Even so, the as-tested plywood panel is considerably stiffer than the foam and thus the mock-up can be assumed to be composed of a rigid plate covered with foam.

For a 2,000 lb load, which was estimated to be the upper limit on the actual loading occurring during any drop test, the plywood deflects 0.35 inches and the composite deflects 1.45 inches. The stiffness for the composite, K_c , and for the foam on a rigid plate, K_f , would be as follows, assuming a linear force-deflection relationship:

$$K_c = \frac{2000}{1.45} = 1,379 \text{ lb/in.}$$

and

$$K_f = \frac{2000}{1.45-0.35} = 1,818 \text{ lb/in.}$$

Thus, the upper limit on the error would be

$$e = \frac{1818-1379}{1379} \times 100 = 32\%$$

As another example, for a 1,000 lb load the deflection of a 5-inch diameter sphere in the foam is 2.0 inches (see Figure III-4). From Figure III-8, the deflection of the plywood for a 1,000 lb load is 0.17 inches. In this case, assuming a linear force-deflection relationship:

$$K_c = \frac{1000}{2.0 + 0.17} = 461 \text{ lb/in.}$$

and

$$K_f = \frac{1000}{2.0} = 500 \text{ lb/in.}$$

and the error would be

$$e = \frac{500-461}{461} \times 100 = 8\%$$

Coefficient of Friction

To determine the coefficient of friction between the dummy and the foam surface, the dummy was placed in a prone position on a 6 inch layer of foam. The force needed to cause the dummy to start sliding along the foam was then measured. With this force and the known weight of the dummy a coefficient of friction of approximately 1.0 was completed.

It is pointed out that simulations of the drop tests by the TTICVS (described in Volume V) indicated that a coefficient of friction of 1.0 was too high. The "apparent" value was found to be somewhere between 0.3 and 0.5. This seems reasonable since the experimental value of 1.0 was a "static" coefficient and the simulation values include sliding.

IV. PHOTOGRAPHY AND INSTRUMENTATION

High-speed cameras were used to record the dummy's kinematics during each drop test. Accelerations of strategic body segments were measured by highly sensitive accelerometers and recorded on magnetic tape. Details of the measuring devices are given in the following sections.

High-Speed Film Coverage

Two high-speed cameras, positioned as shown in the plan view of Figure IV-1, recorded the dummy's kinematics in two different planes. Both high-speed cameras were Red Lake Hycam's with 50 millimeter lens. Eastman Kodak 4 x reversal 16 millimeter film was used and the cameras recorded at 500 frames per second. In addition to the high-speed cameras, a 16 mm movie camera running at 24 frames per second provided a colored documentary film of each drop test.

Although the high-speed camera film speeds are accurate to within \pm 2% of stated values, a more accurate means of determining film speed is used. A small bulb inside the camera flashes 120 times per second, exposing the edge of the film. The bulb flashes at the positive and negative peaks of a 60 Hz power supply. When the developed film is placed in a motion analyzer, the pulses or flashes are clearly visible.

A common time reference between the two high-speed cameras was obtained by a flash bulb, visible in both camera's field of view, which flashed upon release of the suspended dummy. The flash bulb can be seen in a photo shown in Figure IV-2. The flash appears in the lower left corner of the appropriate frames of the film from Camera No. 1 and the lower right corner of the frames of the film from Camera No. 2.

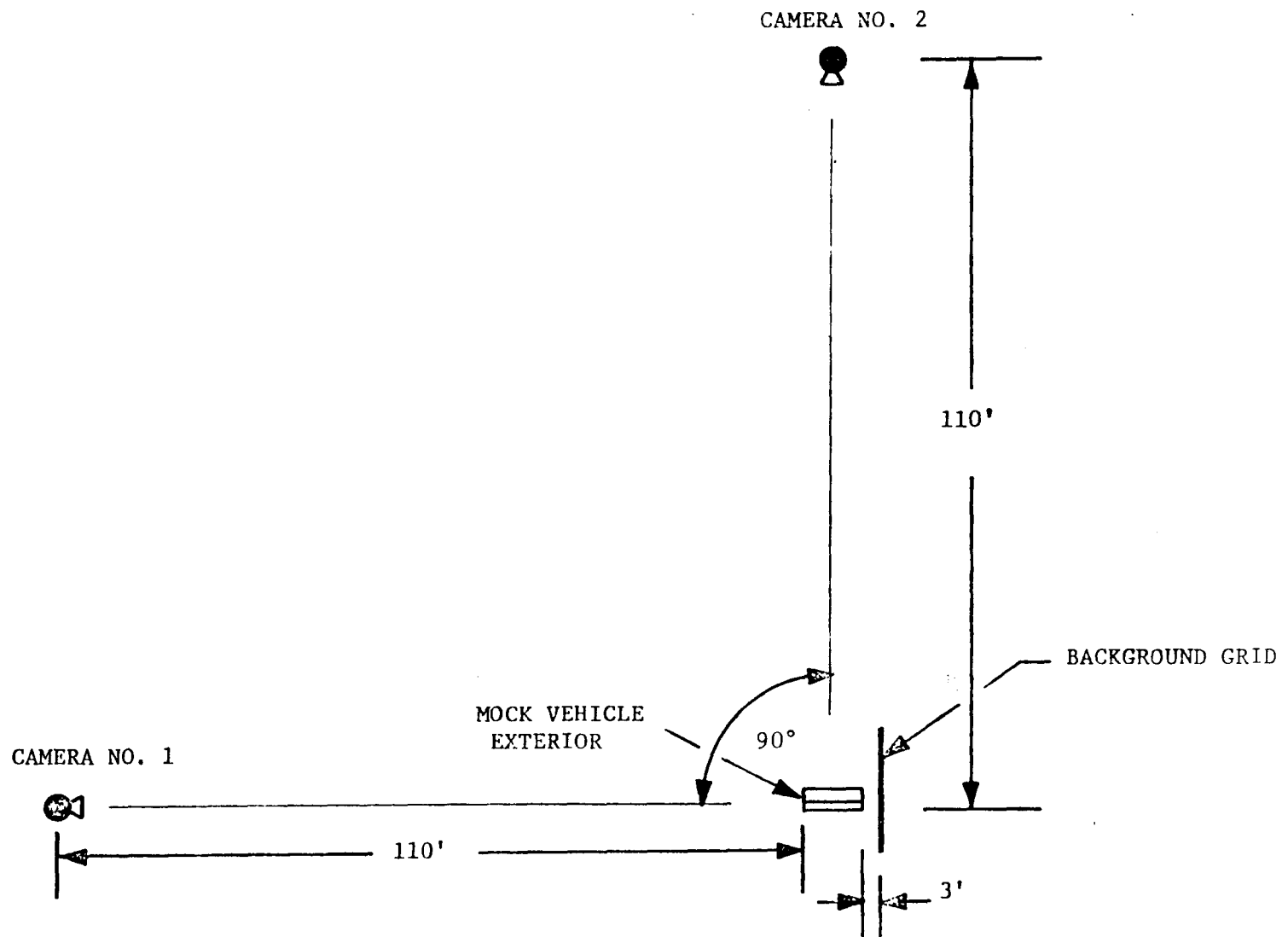
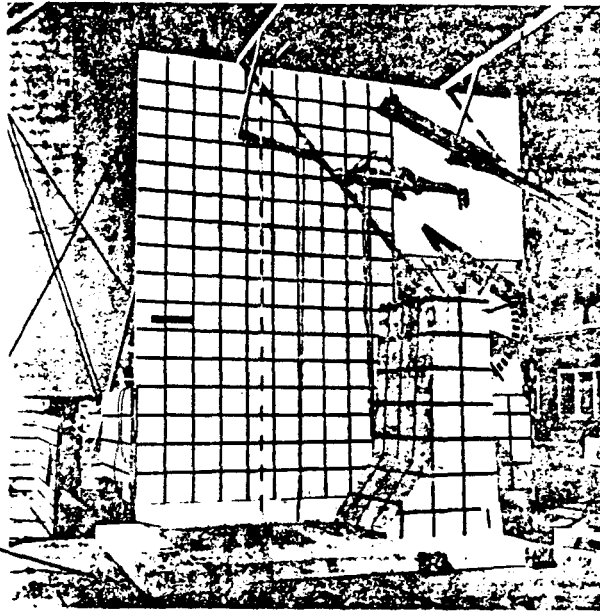
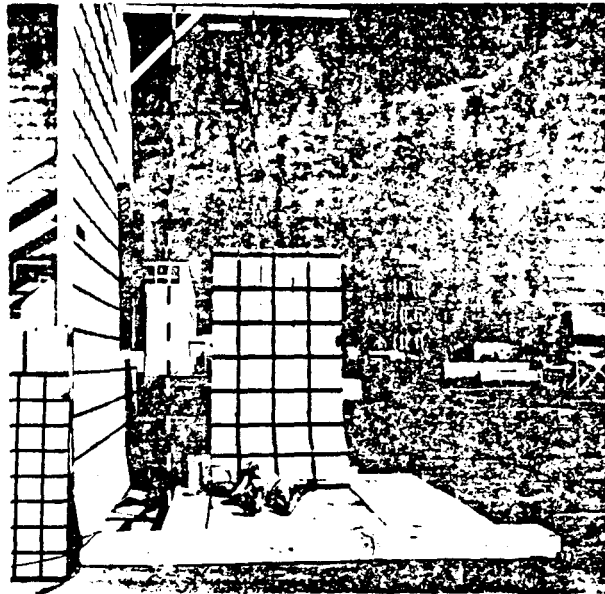


FIGURE IV-1 CAMERA LOCATIONS

FLASH
BULB



CAMERA NO. 1 VIEW



FLASH
BULB

CAMERA NO. 2 VIEW

FIGURE IV-2. LOCATION OF FLASH BULB

Stadia poles with 6 inch graduations and a background grid with one foot graduations provided references for measuring distances and angles from the film. The stadia poles and the background are shown in Figure IV-2. Targets composed of 1 inch strips of white tape were placed on the limbs, torso, and head of each dummy to delineate the dummy's attitude with respect to time.

Dummy Accelerometers

Three triaxial strain gage type accelerometers were mounted in each dummy; one in the head, one in the chest, and one in the pelvis. The rated range of the accelerometers was as given in Table IV-1.

TABLE IV-1 ACCELEROMETER RANGES

<u>LOCATION</u>	<u>Rated Range (g's)*</u>		
	<u>X</u>	<u>Y</u>	<u>Z</u>
Head	+250	+250	+250
Chest	+100	+100	+100
Pelvis	+100	+100	+100

* Axes refer to segment's axis system, as shown in Figure II-2.

The accelerometers, purchased from Consolidated Electroynamics (CEC), were CEC's Type 4-202.

Figure IV-3 shows photographs of the accelerometers placed in the dummies. Mounting brackets were fabricated from a 1/4 inch thick angle section for the male and female chests. A 1/4 inch thick plate was used to mount the accelerometers in the heads of the female and child, whereas a flat spot was

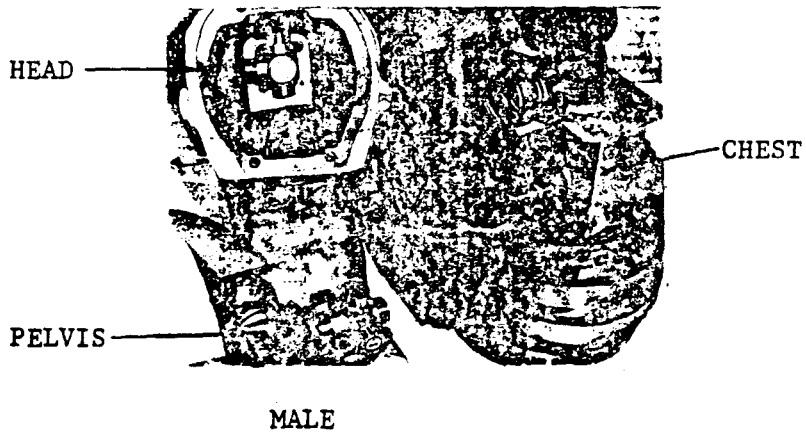
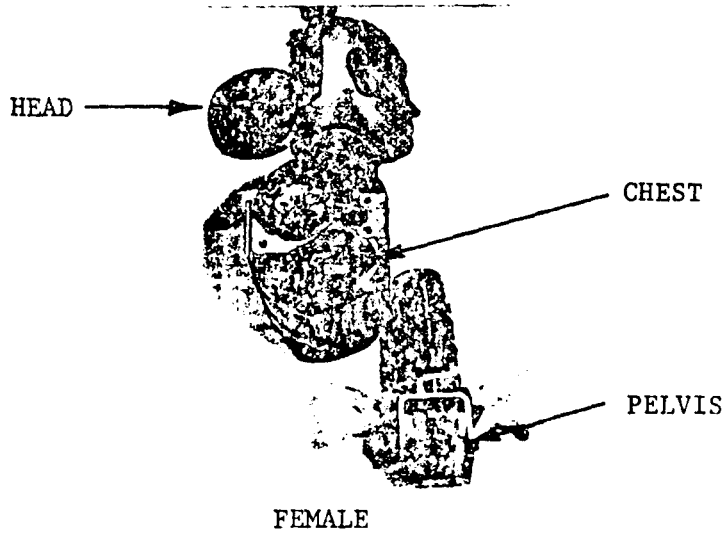
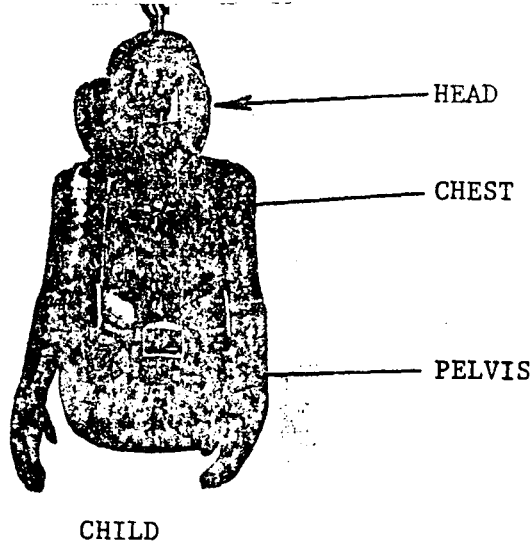


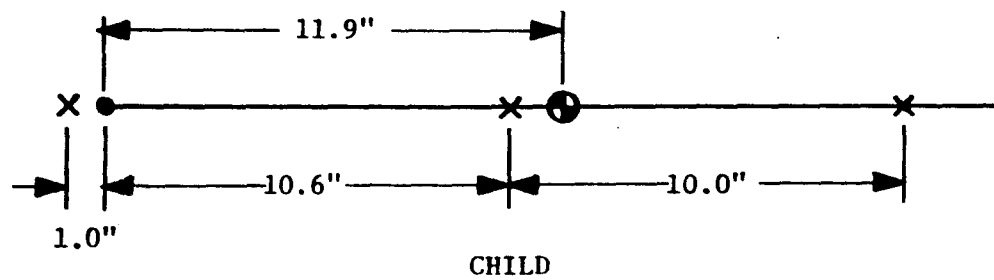
FIGURE IV-3. DUMMY ACCELEROMETERS

milled on the inside of the male head. A 1/4 inch thick plate was used in both the child's chest and the female's pelvis, and existing metal in the male and child pelvis was used for mounting accelerometers.

The location of the triaxial accelerometers in the vertical direction (dummy in standing position) are shown in Figure IV-4. With regard to the fore and aft directions, the pelvis and chest accelerometers were located on the dummy's spinal column and the head accelerometers were located approximately at the geometric center of the dummy's head. With regard to the lateral directions (left or right), the accelerometers were located approximately at the geometric center of the head, chest, and pelvis.

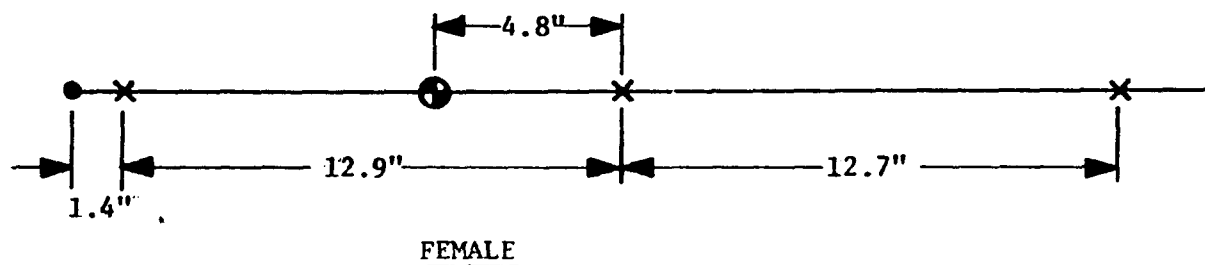
Electronic Recording Equipment

Accelerometer output was fed into signal conditioning amplifiers, one each for the nine accelerometers. All accelerometers were hard wired to the amplifiers. Calibration resistors, simulating 40 g's, were built in each signal conditioning system. After conditioning, the signal was recorded on FM tape. Also, certain channels were monitored during each drop test by use of an oscillograph strip chart recorder. Figure IV-5 shows the recording equipment.

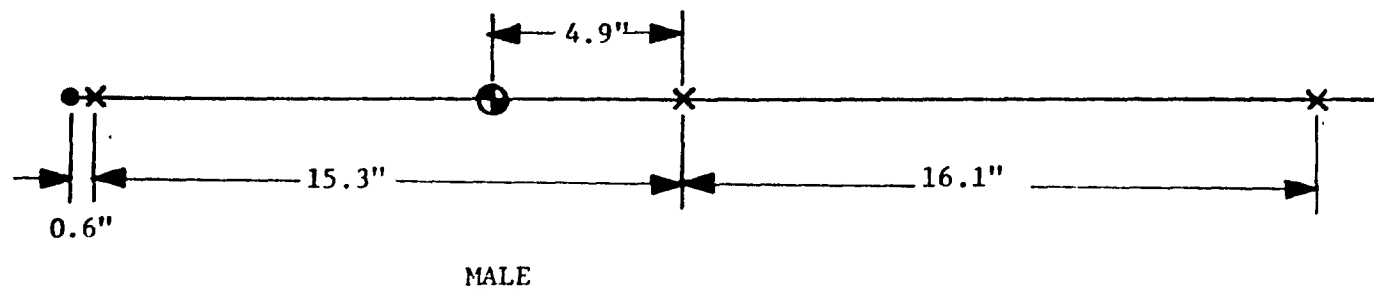


LEGEND:

- X - LOCATION OF TRI-AXIS ACCELEROMETERS
- - HIP PIVOT
- ⊙ - TORSO C.G. (INCLUDES HEAD FOR CHILD)



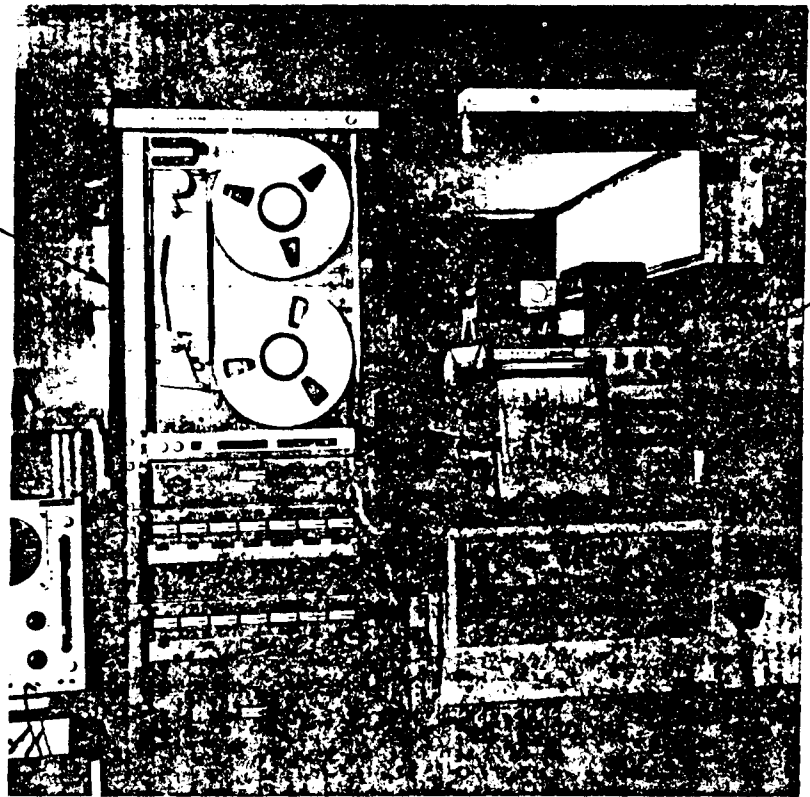
FEMALE



MALE

FIGURE IV-4. LOCATION OF TRI-AXIS ACCELEROMETERS

14 CHANNEL FM
TAPE RECORDER



STRIP CHART
OSCILLOGRAPH

FIGURE IV-5. ELECTRONIC RECORDING EQUIPMENT

V. DETAILS OF DROP TESTS

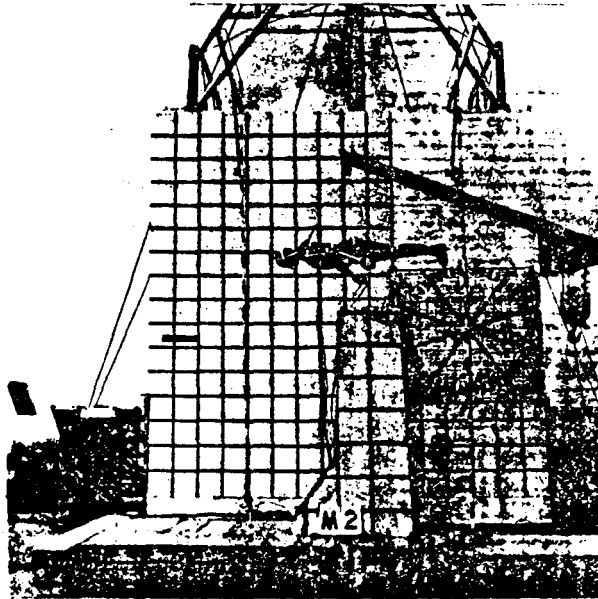
A total of 22 dummy drop tests were conducted; five with the child, eight with the female, and nine with the male. The dummies were dropped from various heights and various attitudes to obtain a wide variety of impact speeds and angular orientations. As an example, Figure V-1 shows the male dummy in position for drop test Number 2. Tables V-1 through V-3 summarize the particulars of each drop test.

As shown in Figure V-2, the prototype was positioned in one of two ways for the drop tests. Photographs of the prototype in these two positions are shown in Figure V-3. Refer to Figure III-2 for the dimensions of the prototype. A polyurethane foam "bumper" was also added to the prototype for tests M-5 through M-9 and its details are shown in Figure V-2. Note that a 6 inch thick pad of polyurethane foam was placed adjacent to the prototype to protect the dummies from impact with the concrete.

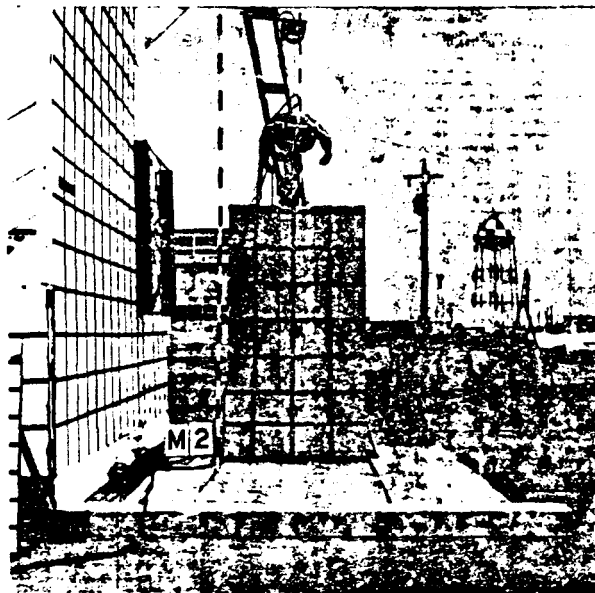
Test Procedure

The procedure followed in each of the test consisted of three basic items, namely, in order, (1) determine columb torque values in dummy's joints, (2) calibrate accelerometers, and (3) hoist dummy to desired height and attitude and conduct drop test.

Determine columb torques. An attempt was made to maintain joint torques at values equal to or slightly higher than that needed to prevent joint rotations under a one "g" environment. In some cases torque adjustments were necessary due to looseness caused by previous drop tests.



CAMERA NO. 1 VIEW



CAMERA NO. 2 VIEW

FIGURE V-1. ADULT MALE DUMMY IN POSITION FOR DROP TEST NO. 2
(M-2)

TABLE V-1. SUMMARY OF CHILD DROP TESTS

<u>TEST NO.</u>	<u>APPROXIMATE HEIGHT OF DROP (FT)¹</u>	<u>POSITION AT RELEASE</u>	<u>TIME FROM RELEASE TO IMPACT² (SEC)</u>	<u>COMMENTS</u>
C-1	1.7	nose down	0.365	Black tape used for targets on dummies in tests C-1 and C-2. Film analysis showed that white tape would be better on subsequent tests.
C-2	3.3	nose down	0.491	
C-3	4.3	nose down	0.561	Lower left leg bent slightly
C-4	8.5	nose down	0.730	
C-5	5.0	buttocks down	0.593	

1 Height above top of prototype.

2 These values were obtained from analysis of the high-speed film. It should be noted that these free-fall times do not agree with those obtained by the free-fall mechanic's formula, i.e.,

$$T = \sqrt{\frac{2d}{g}}$$

where d is drop height and g is gravitational acceleration. The reason for the difference was that a finite amount of lag time occurred as a result of the release mechanism. Before the dummy could obtain a totally free-fall condition, an energy exchange took place, i.e., strain energy in the supporting device was transferred to kinetic energy of the arm which swings away to release the harness.

TABLE V-2. SUMMARY OF FEMALE DROP TESTS

<u>TEST NO.</u>	<u>APPROXIMATE HEIGHT OF DROP (FT)¹</u>	<u>POSITION AT RELEASE</u>	<u>TIME FROM RELEASE TO IMPACT² (SEC)</u>	<u>COMMENTS</u>
F-1	3.6	nose down	0.515	Tests F-1 and F-2 were conducted to assess the repeatability of tests results.
F-2	3.6	nose down	0.514	
F-3	4.0	right side down	Unknown	Bent lower left leg slightly. Ran out of film before impact.
F-4	5.0	oblique	0.575	
F-5	0.0	buttocks down	0.0	Tests F-5 and F-6 conducted to assess sliding and rolling of the dummy against the vehicle surface.
F-6	2.6	buttocks down	0.433	
F-7	(See Comments)	head down	0.399	Dropped head down. Head initially at same height as top of prototype, but offset slightly
F-8	7.0	oblique	0.638	Lower right leg severed at weld connections below knee joint.

1 Height above top of prototype.

2 See footnote 2 of Table V-1.

40

TABLE V-3. SUMMARY OF MALE DROP TESTS

<u>TEST NO.</u>	<u>APPROXIMATE HEIGHT OF DROP (FT)¹</u>	<u>POSITION AT RELEASE</u>	<u>TIME FROM RELEASE TO IMPACT (SEC)³</u>	<u>COMMENTS</u>
M-1	1.3	nose down	0.310	Tests M-1 and M-2 were identical (as far as possible) and were conducted to assess the repeatability of test results.
M-2	1.3	nose down	0.313	
M-3	3/6	oblique (left shoulder down).	0.507	
M-4	4.9	oblique (right shoulder down).	0.603	
M-5	1.6	nose down	0.353	4 inch high by 6 inch wide bumper added to prototype. ² Eyebolt (used to lift dummy) inadvertently left in dummy's head.
M-6	1.6	nose down	0.360	Repeat of M-5 without eyebolt.
M-7	4.0	oblique (left shoulder down)	0.543	Prototype tilted to cause more sliding and rolling.
M-8	4.2	buttocks down	0.561	
M-9	6.0	oblique (left shoulder down).	0.948	Prototype returned to original position.

1 Height above top of prototype.

2 Bumper used for Tests M-5 through M-9.

3 See footnote 2 of Table V-1.

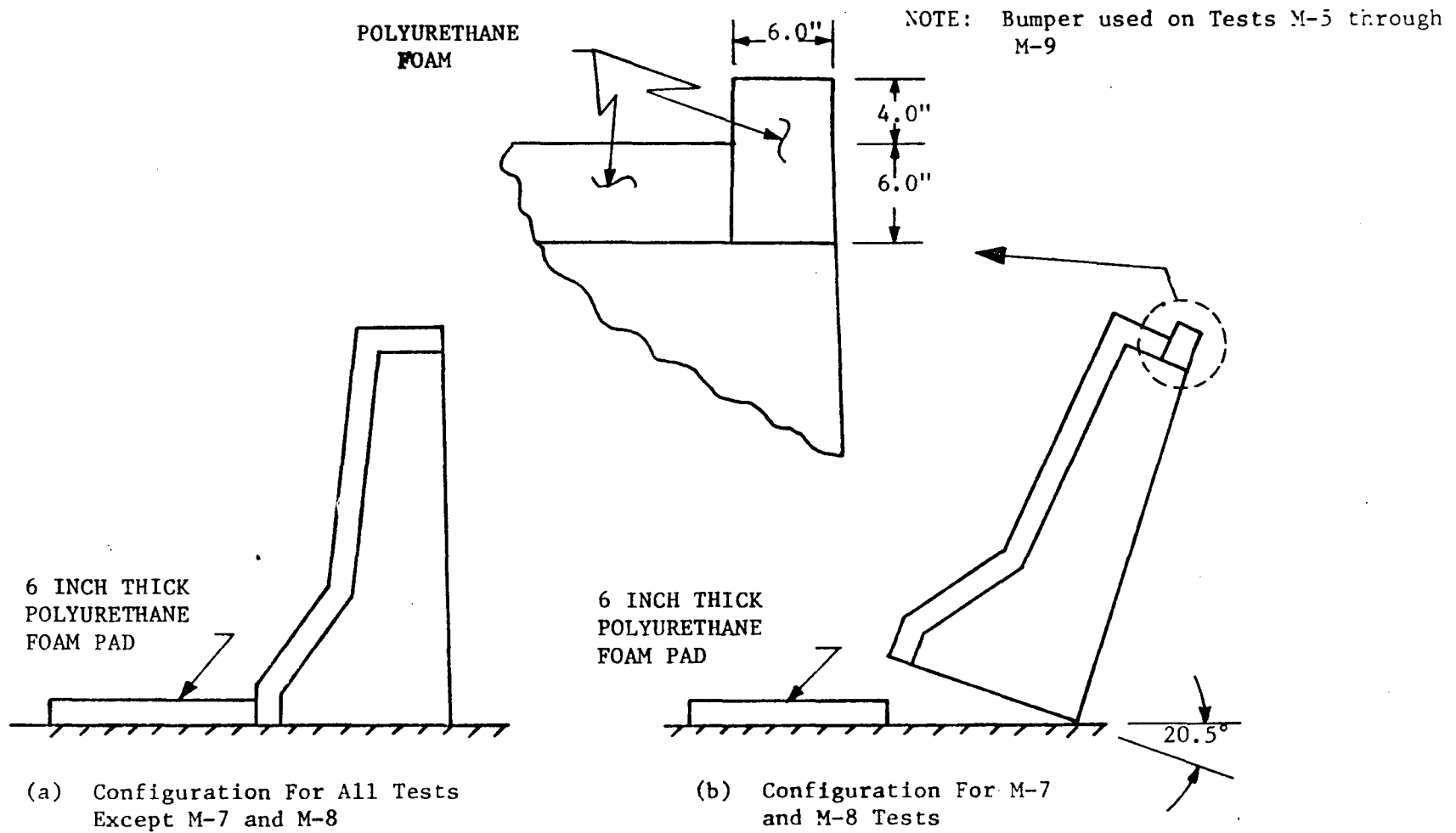
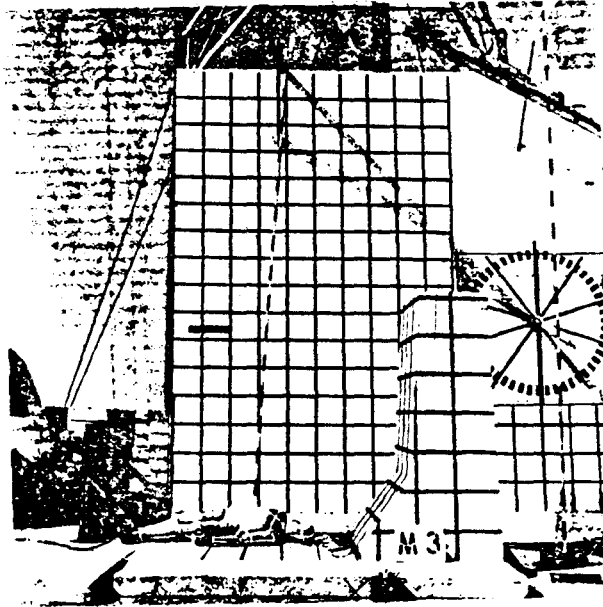
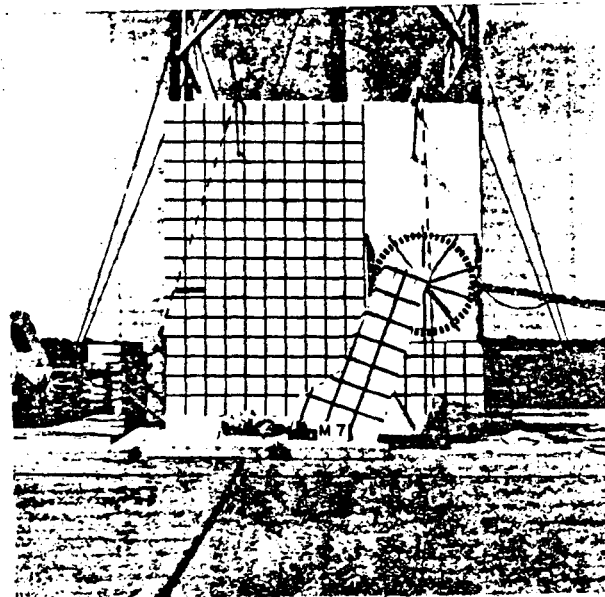


FIGURE V-2. PROTOTYPE CONFIGURATIONS



UPRIGHT POSITION



TILTED POSITION

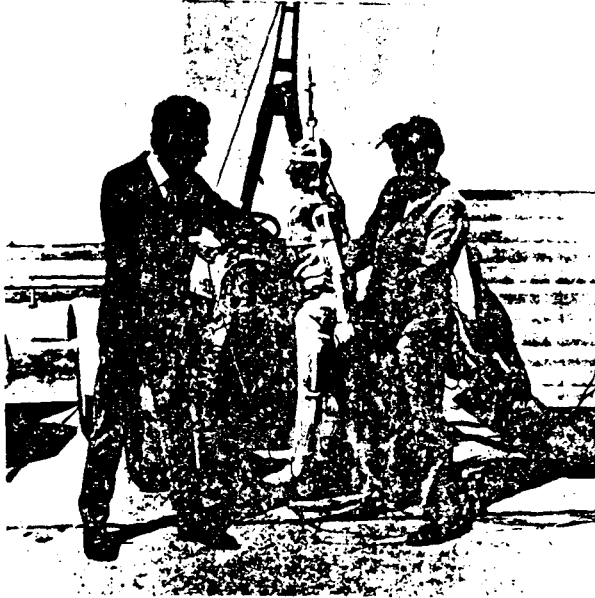
FIGURE V-3. UPRIGHT AND TILTED MOCK-UP POSITIONS

To measure the joint torques, a force sufficient to cause joint rotation was applied at a known distance from the joint. The force was measured by a strain-gage force transducer and recorded on a strip-chart oscillograph. Figure V-4 shows measurements of the force being made on the female dummy. Table V-4 contains the pre-test column joint torques for each test.

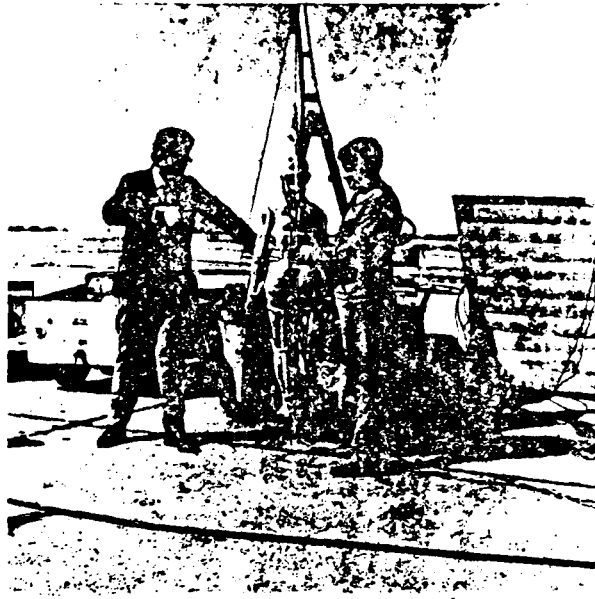
Calibrate accelerometers. Just prior to each drop test, the dummy accelerometers were balanced and calibrated. To balance the lateral and vertical (y and z directions in segment axes) accelerometers, the dummy was placed in a prone position. In this position, these accelerometers were in a zero-g environment. To balance the accelerometers in the fore and aft direction (x direction in segment axis), the dummy was placed on its side.

Resistors simulating a 40 g acceleration were used to calibrate each of the nine accelerometer signals. The calibration was performed just before each test.

Position dummy and conduct test. After the joint torques were measured and the accelerometers were calibrated, the dummy was positioned in the desired attitude and placed in a lifting harness. It was then hoisted to the desired height. The lifting harness for each dummy was fabricated from 0.020 inch diameter music wire. The wire had very high strength properties and was of negligible weight. The length of wire in each harness was sufficient to allow full uninhibited movement of the dummies during testing. It was covered with insulation "spaghetti" where



LEFT SHOULDER TORQUE ABOUT Y-AXIS



LEFT SHOULDER TORQUE ABOUT X-AXIS

FIGURE V-4. MEASUREMENTS OF JOINT TORQUES IN ADULT FEMALE DUMMY

TABLE V-4. COLUMB JOINT TORQUES
(IN NEWTON-LBS)

TEST	HEAD		SHOULDER				ELBOW		HIP				KNEE	
	X	Y	Left		Right		Left	Right	Left		Right		Left	Right
			X	Y	X	Y			X	Y	X	Y		
C-1	94.5	73.5	48.3	20.7	62.1	17.3	67.1	48.8	93.0	65.1	93.0	60.4	46.9	53.6
C-2	94.5*	73.5*	Not Available for Tests C-2 and C-3.											
C-3	94.5*	73.5*												
C-4	94.5*	73.5*	69.0	22.4	75.9	20.7	67.1	36.6	214.0	195.0	251.0	260.2	23.5	40.2
C-5	94.5*	73.5*	65.5	22.4	65.5	20.7	73.2	42.7	158.0	260.2	204.2	240.2	40.2	20.1
F-1	77.9	87.6	63.4	12.5	68.2	43.7	28.0	19.7	70.0	65.4	98.6	112.7	40.3	77.4
F-2	77.9*	87.6*	67.8	39.7	58.8	77.6	71.1	48.2	41.6	77.3	73.1	75.1	34.2	72.1
F-3	77.9*	87.6*	54.8	33.4	60.2	23.5	21.8	23.8	46.2	91.2	91.9	87.2	34.2	103.0
F-4	77.9*	87.6*	67.8	39.7	34.8	25.4	29.5	15.6	363.2	122.3	142.1	89.9	21.8	33.4
F-5	76.2	85.1	67.8	23.5	56.0	25.9	18.5	19.1	254.0	197.5	193.1	167.5	57.2	95.9
F-6	58.5	86.8	77.7	56.6	86.1	117.6	26.9	19.1	47.5	156.0	195.8	191.8	40.3	83.6
F-7	92.8	115.7	57.6	63.4	28.7	58.3	21.8	19.7	85.8	148.1	175.6	182.3	41.2	74.8
F-8	83.9	62.6	85.5	48.0	77.6	83.8	18.5	23.2	89.9	203.6	189.0	161.6	46.2	63.4
M-1	200.0	160.0	199.8	142.0	152.9	182.0	97.9	78.0	200.7	236.7	396.0	211.2	145.9	124.2
M-2	200.0*	160.0*	243.0	162.0	137.2	134.4	83.0	94.1	164.7	198.0	294.8	325.6	140.2	151.2
M-3	200.0*	160.0*	225.9	136.6	147.3	179.2	147.7	92.1	155.7	175.5	240.0	303.6	125.0	122.0
M-4	200.0*	160.0*	225.9	124.2	229.6	220.0	118.7	88.1	245.7	175.5	281.6	255.2	140.2	176.0
M-5	200.0*	160.0*	234.9	232.2	263.2	183.6	128.7	92.0	225.0	72.0	158.4	275.4	102.6	135.0
M-6	200.0*	160.0*	225.9	145.8	186.0	201.6	112.0	70.2	142.2	157.5	156.6	178.6	74.1	138.2
M-7	200.0*	160.0*	225.9	183.6	186.0	218.4	124.5	92.0	153.0	135.0	200.6	176.0	111.7	127.4
M-8	200.0*	160.0*	225.9	152.8	186.0	122.0	124.5	101.4	162.0	139.5	180.4	319.4	96.9	186.8
M-9	200.0*	160.0*	225.9	159.8	186.0	208.9	102.1	127.1	175.5	184.5	224.4	213.8	83.2	159.8

* Estimated

it contacted the dummy's flesh to prevent cutting.

Shortly before the dummy was dropped the photographic and electronic recording equipment was allowed to reach operating speeds. A switch was then depressed which released the dummy and excited a flash bulb. The flash bulb, which can be seen in the high speed film served as a common time reference or event marker between the two cameras. The switch depress was also recorded on the magnetic tape as an event marker for the accelerometer data.

Impact Conditions

After being raised to the desired height, the dummy was guyed with light twine to prevent movement up to the time of release. As a consequence, with the exception of Test C-5 (which had a small rigid body rotation), the dummies fell with only translational motion, as shown by an analysis of the high-speed film. Impact conditions could, therefore be specified in terms of (1) the rigid body impact velocity, (2) coordinates of a reference point on the dummy with respect to a fixed axis system, and (3) the angular orientation of each dummy segment with respect to the fixed axis system.

A total of 32 impact variables (initial conditions) were needed for the TTICVS. These were the impact velocity, the three coordinates of the terminal end of segment Number 1 (see Figure II-2), and 28 angles to define the attitude of the 12 articulated body segments. With this information and known dimensions of the dummy (pivot-to-pivot lengths and shoulder and hip widths), the position and attitude of the dummy on impact could be specified in terms of the fixed axis system.

For convenience, the origin of the fixed axis system used to describe the impact conditions given herein is as shown in Figure V-5 for all tests, i.e., at point 4 on the mock-up. Its orientation is such that the X'-Y' plane is always parallel to the ground plane for all tests (including M-7 and M-8 where the prototype was tilted).

The angular orientation of a particular body segment was specified with three Eulerian angles. With reference to Figure V-6, the orientation of the segment fixed axis system (X_n , Y_n , and Z_n) of segment "n" with respect to the fixed coordinate system (X' , Y' , Z') is given by three angular measures. These are, in order of rotation, ϕ_n , θ_n , and ψ_n . It can be shown that

$$\begin{pmatrix} X' \\ Y' \\ Z' \end{pmatrix} = [T^n] \begin{pmatrix} X_n \\ Y_n \\ Z_n \end{pmatrix} \quad (V-1)$$

where

$$T_{11}^n = \cos\phi_n \cos\theta_n \cos\psi_n - \sin\phi_n \sin\psi_n;$$

$$T_{12}^n = -\cos\phi_n \cos\theta_n \sin\psi_n - \sin\phi_n \cos\psi_n;$$

$$T_{13}^n = \cos\phi_n \sin\theta_n;$$

$$T_{21}^n = \sin\phi_n \cos\theta_n \cos\psi_n + \cos\phi_n \sin\psi_n;$$

$$T_{22}^n = -\sin\phi_n \cos\theta_n \sin\psi_n + \cos\phi_n \cos\psi_n;$$

$$T_{23}^n = \sin\phi_n \sin\theta_n;$$

$$T_{31}^n = -\sin\theta_n \cos\psi_n;$$

$$T_{32}^n = \sin\theta_n \sin\psi_n; \text{ and}$$

$$T_{33}^n = \cos\theta_n.$$

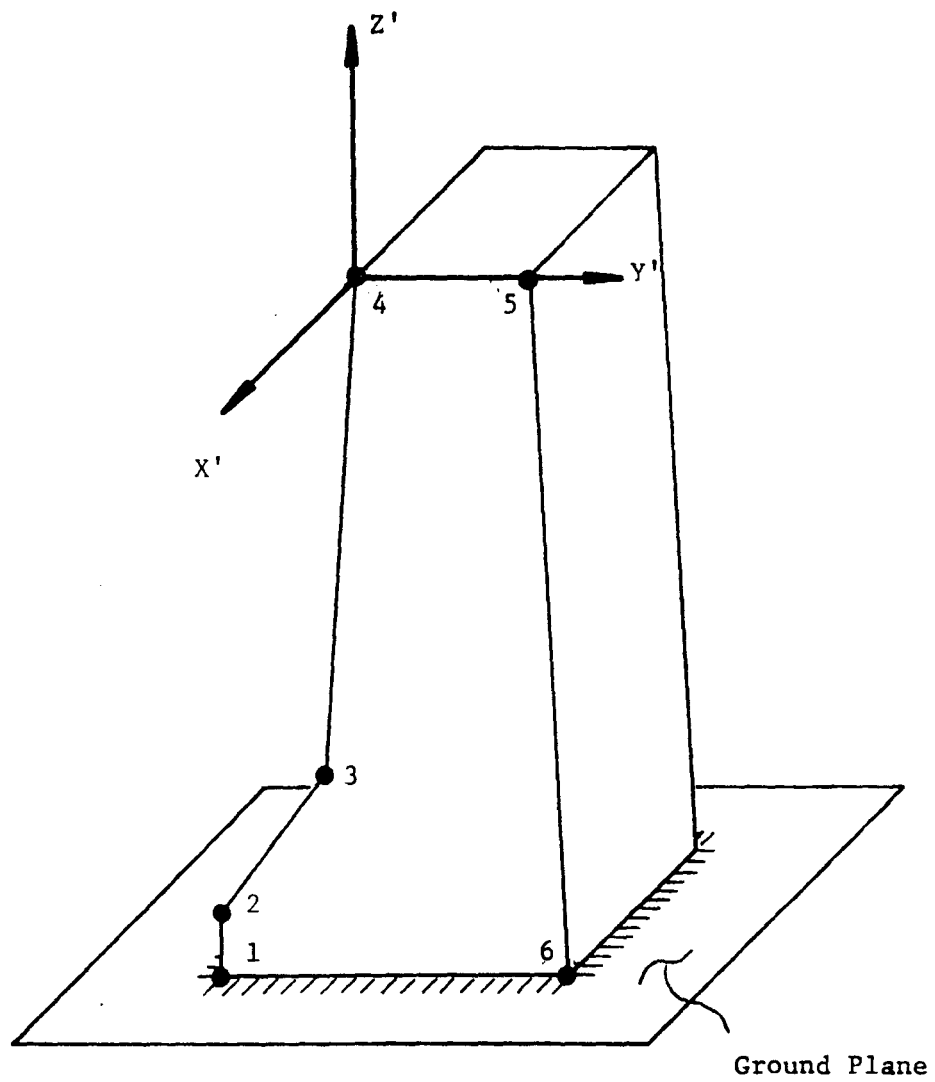


FIGURE V-5. FIXED AXIS ORIENTATION

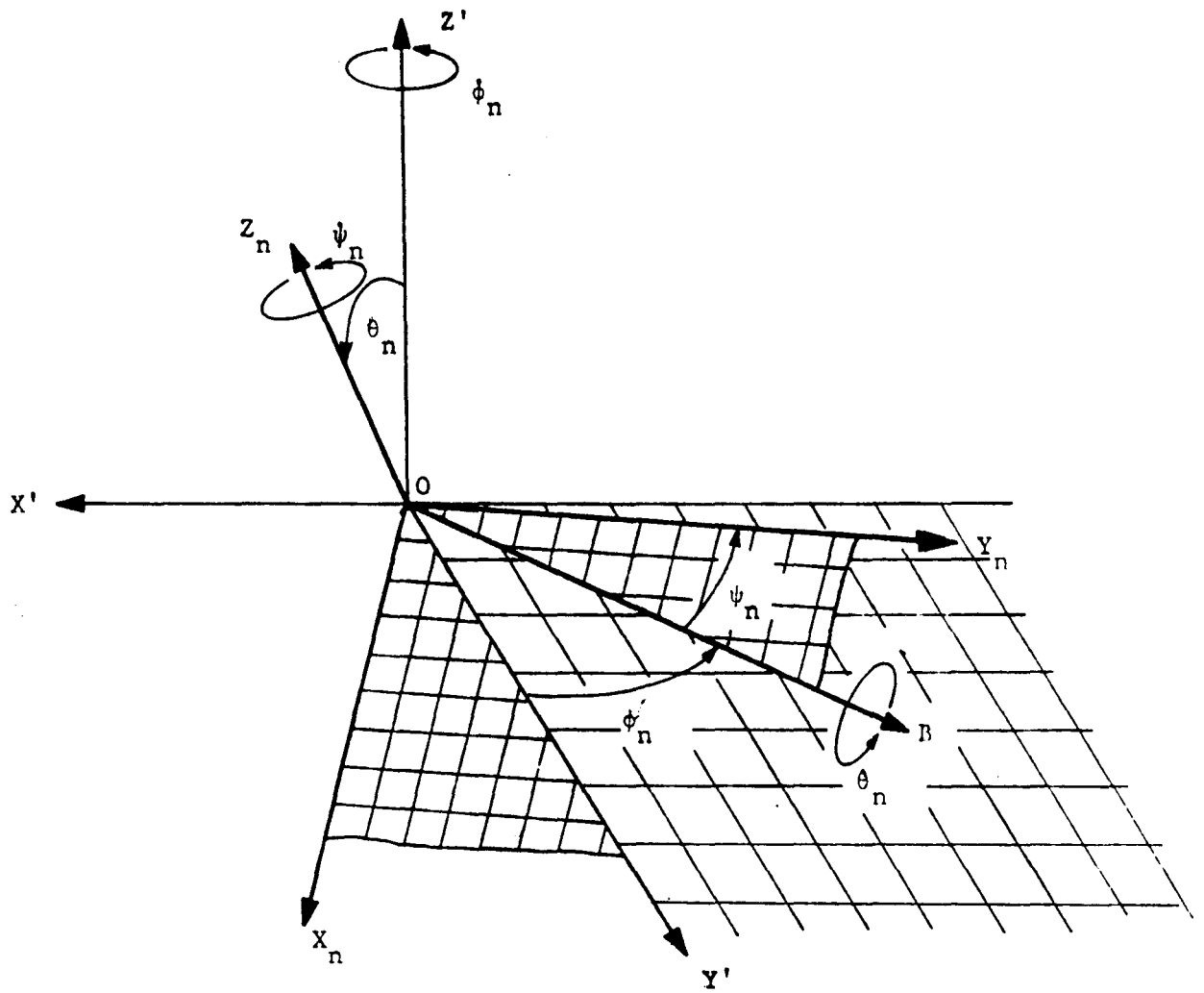


FIGURE V-6. EULERIAN ANGLES

Equations V-1 are used to determine the orientation of segments 1, 2, 3, 4, 5, 6, 9, and 10. Segments 7, 8, 11, and 12 are constrained to move relative to segments 5, 6, 9, and 10, respectively, with only one degree of freedom, as shown in Figure V-7.

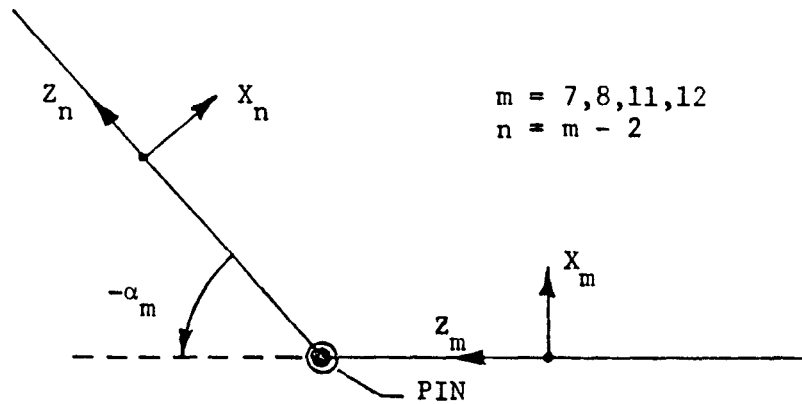


FIGURE V-7. ELBOW AND KNEE CONSTRAINTS

The orientation of segment "m" with respect to the fixed axis system is given by

$$\begin{Bmatrix} X' \\ Y' \\ Z' \end{Bmatrix} = [T^n] \begin{bmatrix} \cos\alpha_m & 0 & \sin\alpha_m \\ 0 & 1 & 0 \\ -\sin\alpha_m & 0 & \cos\alpha_m \end{bmatrix} \begin{Bmatrix} X_m \\ Y_m \\ Z_m \end{Bmatrix} \quad (V-2)$$

Three basic steps were followed in determining the impact conditions.

- (1) A first approximation of the dummy's impact position and orientation was made from the known pre-release attitude of the dummy and from

the high speed film. At test time, before lifting the test dummies for the drops, the orientation of the body extremities (head, arms, legs) relative to the torso were obtained and recorded. The high speed film records (two orthogonal views) were analyzed for determination of orientation of as many of the body segments as could be accurately determined. These were angular orientations with respect to the fixed coordinate system. Location of the reference point was also made with respect to the fixed coordinate system.

From these results, certain body segments were chosen as reference segments to which the orientation of the other body segments were related in terms of direction cosines. These reference segments were normally the torso or leg segments, i.e., large segments whose orientation could easily be determined from the high speed film. The direction cosines of other segments specified with respect to these reference segments were obtained from both the pre-release data and from the film data.

- (2) A small utility computer program, written specifically for assistance in computing impact conditions, took the approximate data from Step 1 and computed approximate Euler angles.
- (3) Results from Step 2 were plotted to scale and then compared with the appropriate frame from the high speed film by use of a stop-action movie projector. If the comparison was not satisfactory, adjustments were made and Steps 2 and 3 were repeated until

convergence was obtained. The computer program of Step 2 was written to allow any body segment, whose Euler angles had been previously computed (by the program), to serve as a reference segment for any other body segment, regardless of the connectivity of the two segments. This was an invaluable feature in converging on an answer.

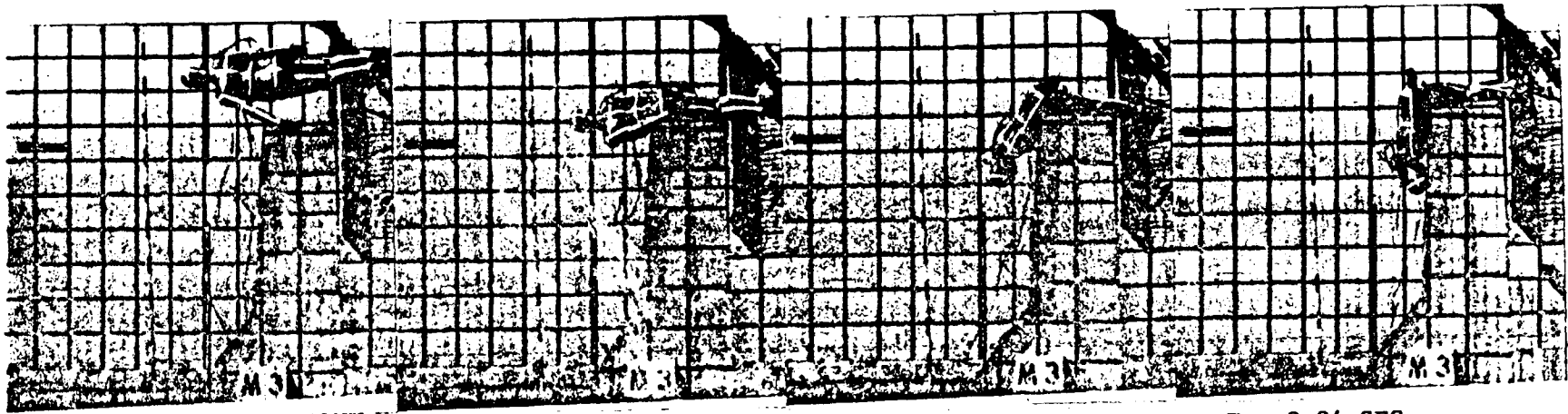
The impact conditions for each test are listed in Appendix D. The coordinates of the reference point on the dummy (terminal end of segment 1) with respect to the fixed axis system are given as X'_{T1} , Y'_{T1} , and Z'_{T1} . The impact velocity is given as \dot{Z}_{T1} .

Test Results

As discussed previously, the dummy kinematics during each drop test were recorded by two high-speed cameras. Figure V-8 shows a sequence of photos taken from the film of camera No. 1 for Test M-3. Figure V-9 shows a sequence of photos taken from camera No. 2 for the same test. It should be noted that the photos shown in Figures V-8 and V-9 have been cropped and do not show the complete frame.

The accelerations were recorded on FM magnetic tape for a permanent record. The tapes were played back through an oscillograph to provide hard copies of the results for presentation in this report.

Figure V-10 shows the accelerometer records for Test C-2 (no head Z-accelerometer data due to malfunction). Complete accelerometer data for all tests are given in Appendix E. Figure V-10 (and each figure in Appendix F) is a photographically reduced copy of the original oscillograph copy.

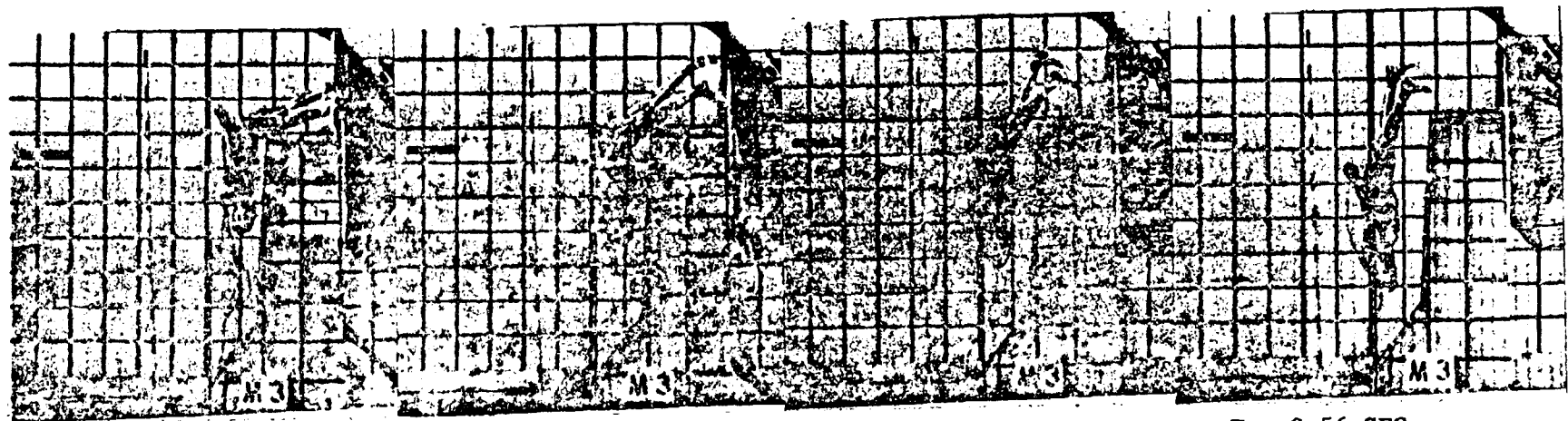


T = 0.00 SEC

T = 0.08 SEC

T = 0.16 SEC

T = 0.24 SEC



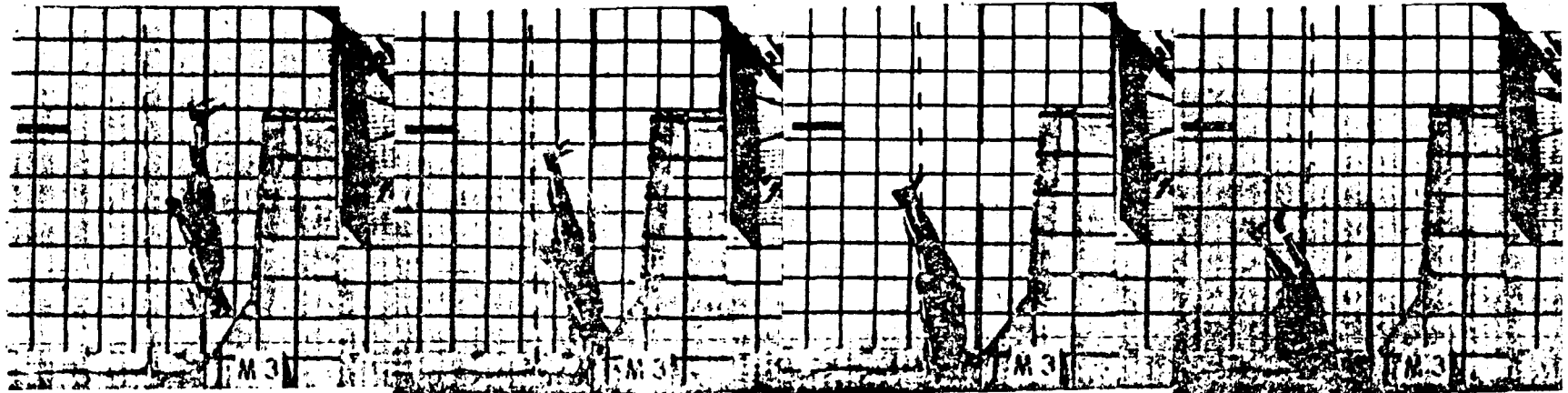
T = 0.32 SEC

T = 0.40 SEC

T = 0.48 SEC

T = 0.56 SEC

FIGURE V-8. HIGH SPEED FILM FRAMES OF TEST M-3, CAMERA NO. 1



T = 0.64 SEC

T = 0.72 SEC

T = 0.80 SEC

T = 0.88 SEC



T = 0.96 SEC

T = 1.04 SEC

T = 1.12 SEC

T = 1.20 SEC

FIGURE V-8. CONTINUED

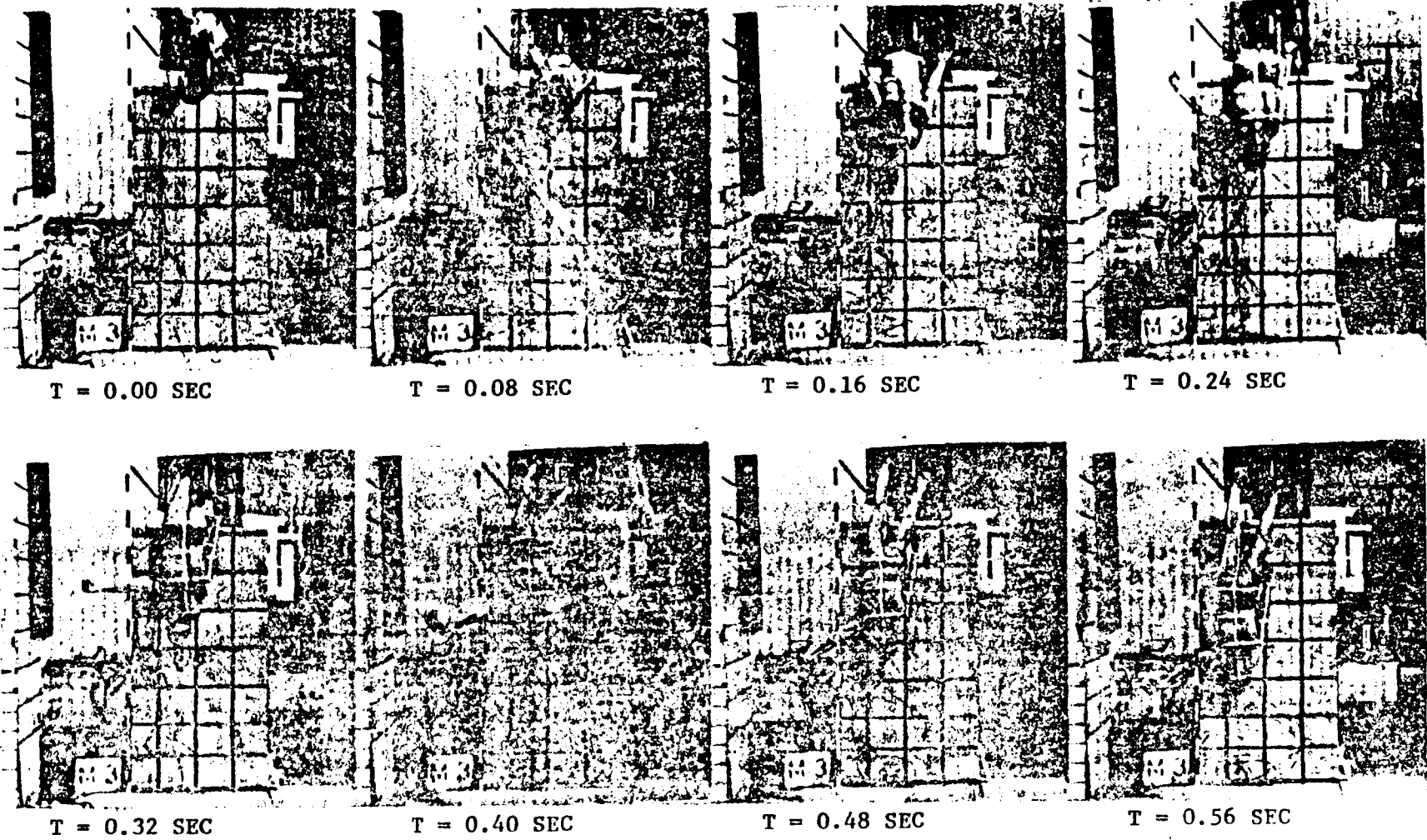


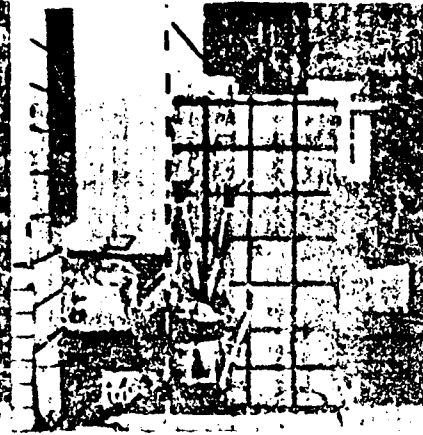
FIGURE V-9. HIGH SPEED FILM FRAMES OF TEST M-3, CAMERA NO. 2



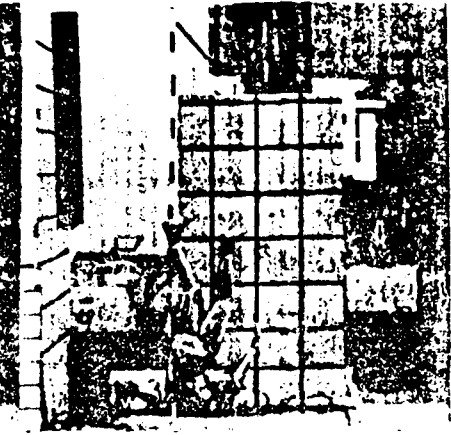
T = 0.64 SEC



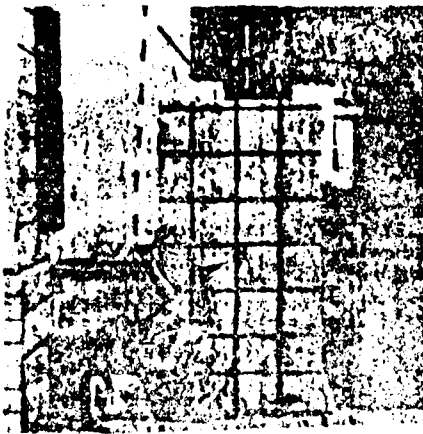
T = 0.72 SEC



T = 0.80 SEC



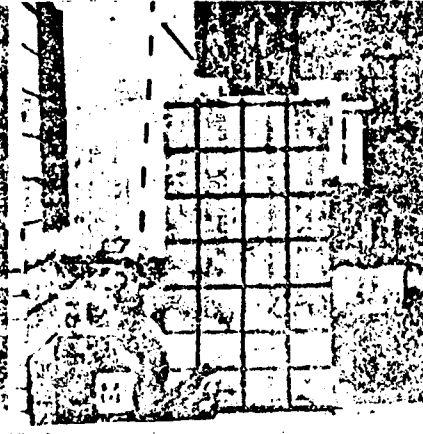
T = 0.88 SEC



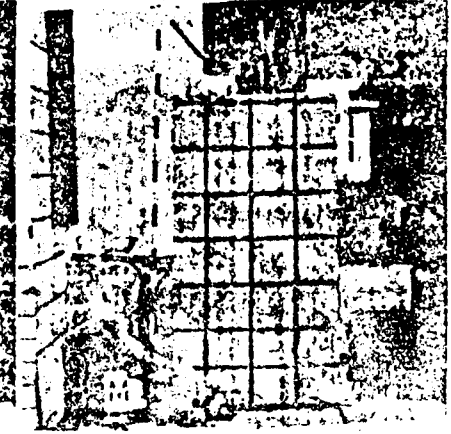
T = 0.96 SEC



T = 1.04 SEC



T = 1.12 SEC



T = 1.20 SEC

FIGURE V-9. CONTINUED

TEST C-2
HEAD

+
40 G's
+

X ✓
Y ✓

TIME AFTER RELEASE (SEC)

0.0 0.1 0.2 0.3 0.4 0.5 0.6 0.7 0.8 0.9 1.0

100 Hz SIGNAL
PEAK TO PEAK TIME = 1/100 SEC

DUMMY RELEASE

EVENT MARKER

TEST C-2
CHEST

X ✓
Y ✓
Z ✓

TEST C-2
PELVIS

X ✓
Y ✓
Z ✓

FIGURE V-10. TYPICAL ACCELEROMETER DATA

Several points are noted on Figure V-10, and are applicable to all the plots in Appendix F. A summary of the important features follows.

- (1) The direction of the arrow to the left of each accelerometer plot indicates the positive direction and its length is equivalent to 40 G's. Positive X, Y, and Z directions for the head, chest, and pelvis are as shown in Figure II-2 for segments 3, 2, and 4, respectively.
- (2) Three time scales are included on each Figure, one each for the head, chest, and pelvis accelerometer data. The scale factor is as shown on the "head" accelerometer values of Figure V-10.
- (3) A common "event" marker and a common 100 Hz signal appear at the bottom of the head, chest, and pelvis accelerometer data. The event marker shows the time at which the dummy release switch was depressed. This point is seen as the initial discontinuity in the event marker line. The next discontinuity in the event marker line represents the time at which the dummy release switch was released, and has no significance.

It is to be noted that the plots in Figure V-10 (and Appendix F) were obtained from three separate oscillograph records, one each for the head, chest, and pelvis. The three records were placed adjacent to each other as shown such that the common time reference (dummy release point) for each was in alignment.

(4) In general, each accelerometer plot is characterized by three significant events. These are the initial impact with the mock-up, then a free-fall phase, and finally, impact with the simulated wind shield and the ground.

VI. CONCLUSIONS

The objective of the drop tests described in this volume was to provide a data base from which the Texas Transportation Institute's Collision Victim Simulator could be validated in the pedestrian mode. This objective was met in that a wide variety of kinematic and accelerometer data, for three different size dummies, were obtained. In most of the tests, three-dimensional motion occurred. The kinematics were recorded on high-speed film and the accelerometer data was recorded on magnetic tape.

Detailed measurements of dummy properties and of the mock-up surface properties were made. Each dummy's mass distribution, segment moments of inertia, joint damping properties, geometry, and surface force-deformation properties were measured. Force-deformation properties of the mock-up surface (polyurethane foam) were experimentally and analytically determined. Measurements of the coefficient of friction between the mock-up surface and the dummy's skin were also made.

No attempt was made in this volume to draw any conclusions regarding the significance of the drop tests as related to the pedestrian accident itself. In this regard, some observations and findings are given in Volume V.

Although the tests were conducted to provide data for validation of the TTICVS, the results could also be used to validate other simulators. The NHTSA should be contacted regarding the availability of the film and accelerometer data.

REFERENCES

1. Young, R. D., "A Three-Dimensional Mathematical Model of an Automobile Passenger," Research Report 140-2, Texas Transportation Institute, College Station, Texas, August 1970.
2. McHenry, R. R., and Naab, K. N., "Computer Simulation of the Automobile Crash Victim in a Frontal Collision--A Validation Study," Report No. YB-2126-V-1R, Cornell Aeronautical Laboratory, Inc., July 1966.

APPENDIX A

DERIVATION OF FORCE-DEFORMATION
RELATIONSHIPS FOR RIGID SPHERES PENETRATING
POLYURETHANE FOAM

APPENDIX A

DERIVATION OF FORCE-DEFORMATION RELATIONSHIPS FOR RIGID SPHERES PENETRATING POLYURETHANE FOAM

An effort was made to derive theoretical force-deformation equations for rigid spheres penetrating polyurethane foam, the material used to cover the mock vehicle exterior. The spheres were intended to represent the idealized shape of different body segments. The assumptions made in the derivation were as follows:

- (1) The shear strength of the foam was negligible, i.e., the resistance to sphere penetration was due to compression of the foam immediately below the sphere only (a punching action); and
- (2) The stress-strain curve for the foam could be idealized by a piecewise-linear representation.

Shown in Figure A1 are the geometric variables of the problem. It can be shown that:

$$\beta = \cos^{-1} \left[\frac{R-y}{R} \right] \quad (A1)$$

and $a = y - R(1 - \cos\theta)$ (A2)

The projected area (in direction of penetration) of the differential area, dA , is given by:

$$dA = 2\pi R^2 \cos\theta \sin\theta d\theta \quad (A3)$$

The differential force, dF , is computed as:

$$dF = \sigma_{\theta} dA \quad (A4)$$

where σ_{θ} is the compressive stress at θ . The value of σ_{θ} is computed from the stress-strain relationship of the foam, i.e.:

$$\sigma_{\theta} = \sigma_{\theta}(\epsilon_{\theta}) \quad (A5)$$

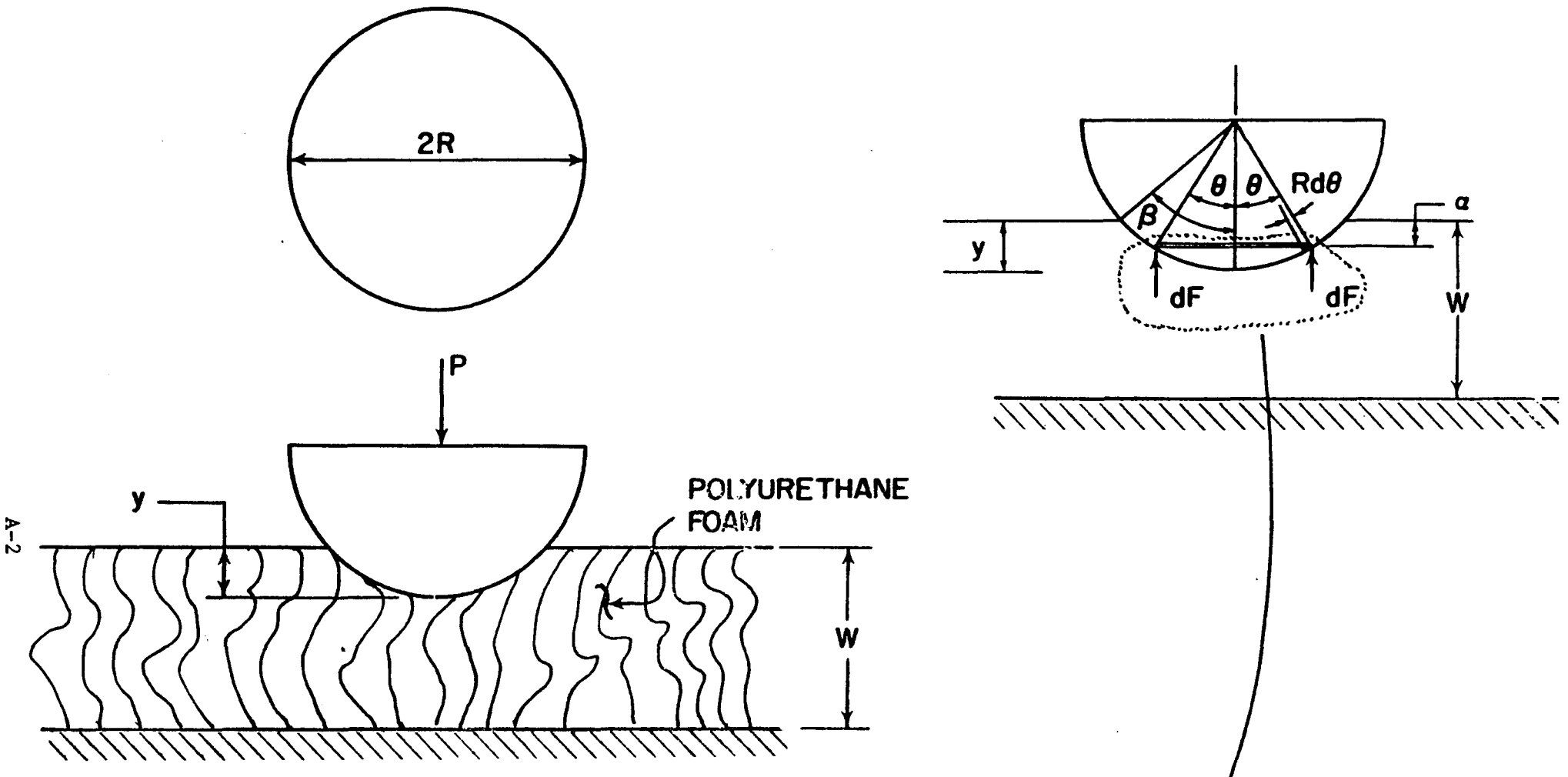
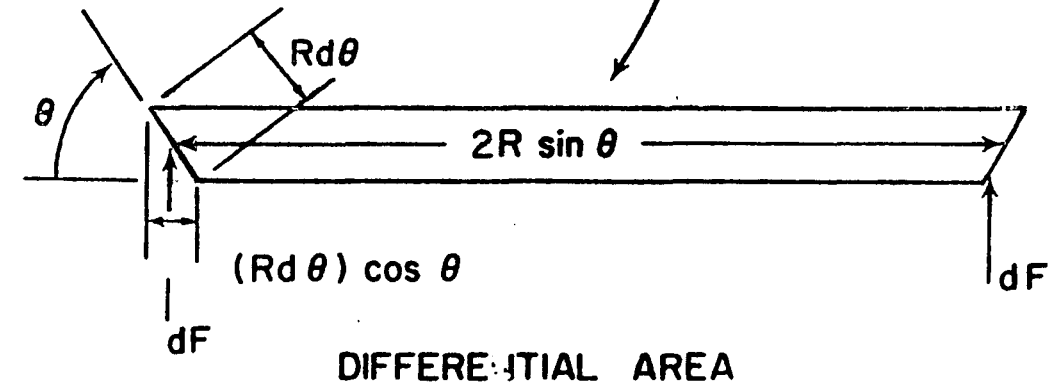
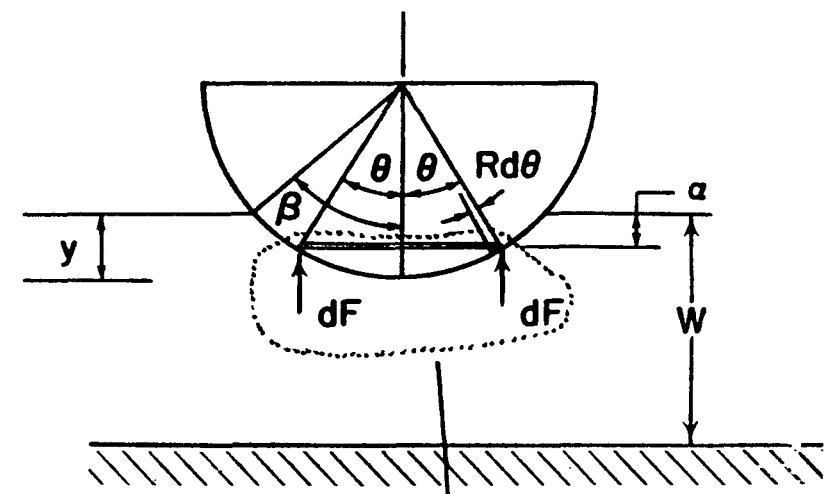


FIGURE A-1. GEOMETRIC VARIABLES OF SPHERE AND FOAM



DIFFERENTIAL AREA

FIGURE A1. GEOMETRIC VARIABLES OF SHPERE AND FOAM

where ϵ_θ is the axial strain at θ and is computed by:

$$\epsilon_\theta = \frac{a}{w} = \frac{y-R(1-\cos\theta)}{w} \quad (A6)$$

Thus, the total load, P, needed for the sphere to penetrate the foam to a depth y is given by:

$$P = \int_0^\beta \sigma_\theta 2\pi R^2 \cos\theta \sin\theta d\theta \quad (A7)$$

A typical stress-strain curve for polyurethane foam in compression is shown in Figure A2. Also shown is the idealized curve assumed for this analysis. The four parameters used to define the idealized curve are σ_Y , ϵ_1 , ϵ_2 , and E_3 , and the stress-strain equations are as follows:

$$\sigma = \begin{cases} \frac{\sigma_Y}{\epsilon_1} \epsilon & \text{for } 0 \leq \epsilon \leq \epsilon_1 \\ \sigma_Y & \text{for } \epsilon_1 \leq \epsilon \leq \epsilon_2 \\ \sigma_Y + E_3 (\epsilon - \epsilon_2) & \text{for } \epsilon \geq \epsilon_2 \end{cases} \quad (A8)$$

With the stress-strain relationships of Equations A8 and the strain relationship of Equation A6, the load P can be computed from Equation A7. Due to the nature of the idealized stress-strain curve, it was necessary to develop equations for P for three basic ranges of penetration, y. These ranges are as follows:

- I. When $y \leq W\epsilon_1$;
- II. When $W\epsilon_1 < y \leq W\epsilon_2$; and
- III. When $y > W\epsilon_2$

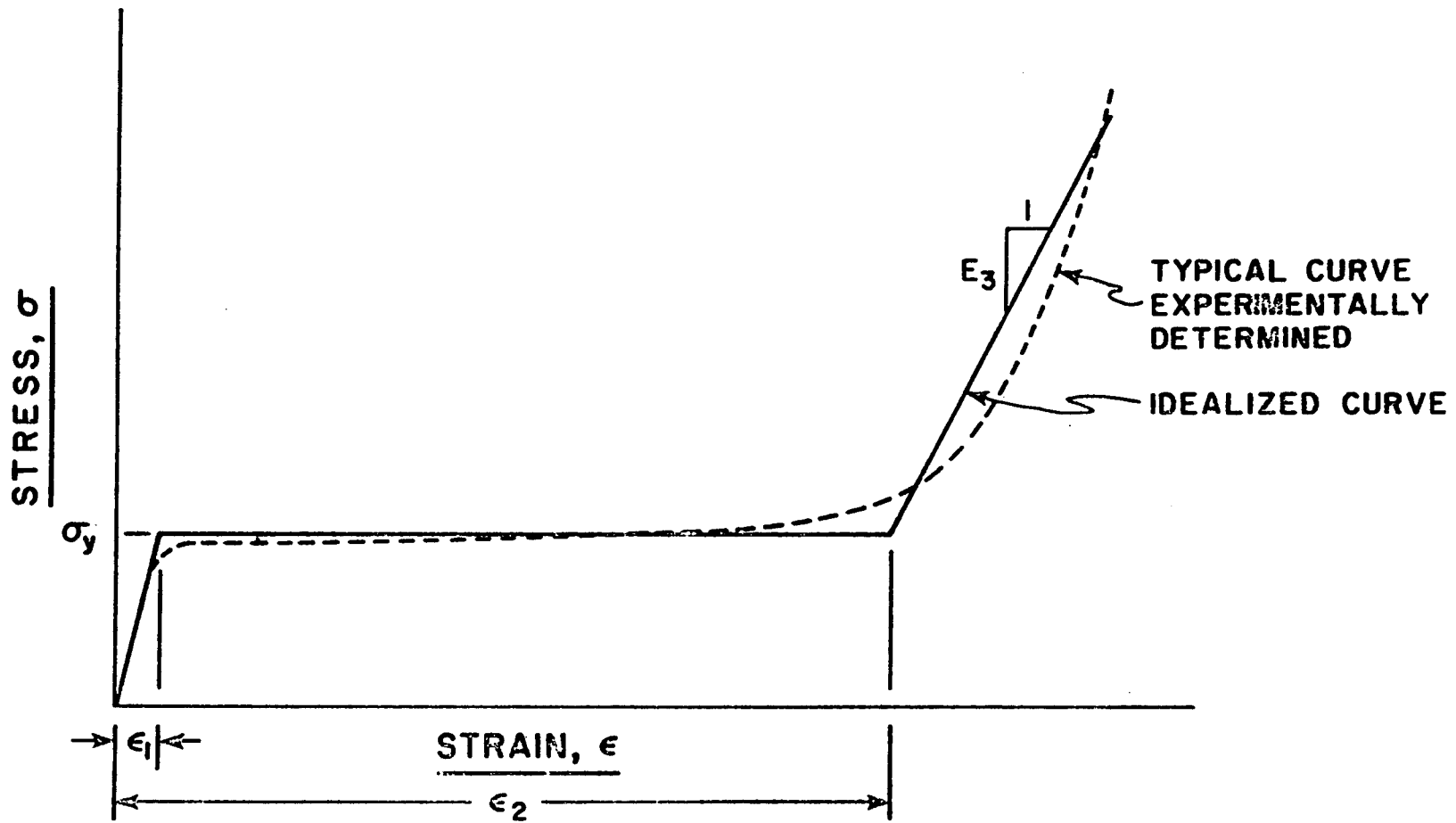


FIGURE A-2. STRESS-STRAIN PARAMETERS

Note that in the following equations, β is as defined in Equation A1 unless $y \geq R$, in which case $\beta = 90$ degrees.

$$\text{I. } y \leq W\epsilon_1$$

$$P = \frac{2\pi\sigma_Y R^2}{W\epsilon_1} \int_0^\beta [y-R(1-\cos\theta)] \cos\theta \sin\theta \, d\theta$$

or

$$P = \frac{2\pi\sigma_Y R^2}{W\epsilon_1} \left[(y-R) \left(\frac{1}{2}\right) \sin^2\beta - \frac{R}{3} \cos^3\beta + \frac{R}{3} \right] \quad (\text{A9})$$

$$\text{II. } W\epsilon_1 < y \leq W\epsilon_2$$

Define θ_1 as:

$$\theta_1 = \cos^{-1} \left[1 - \frac{y-W\epsilon_1}{R} \right]$$

Then, if $y < R + W\epsilon_1$

$$P = 2\pi R^2 \sigma_Y \int_0^{\theta_1} \cos\theta \sin\theta \, d\theta$$

$$+ \frac{2\pi\sigma_Y R^2}{W\epsilon_1} \int_{\theta_1}^\beta [y-R(1-\cos\theta)] \cos\theta \sin\theta \, d\theta$$

or

$$P = \pi R^2 \sigma_Y \sin^2\theta_1 + \frac{2\pi\sigma_Y R^2}{W\epsilon_1} \left[(y-R) \left(\frac{1}{2}\right) (\sin^2\beta - \sin^2\theta_1) - \frac{R}{3} (\cos^3\beta - \cos^3\theta_1) \right] \quad (\text{A10})$$

If $y > R + W\epsilon_1$

$$\theta_1 = 90 \text{ degrees}$$

and

$$P = \pi R^2 \sigma_Y \quad (\text{A11})$$

III. $y > W\epsilon_2$

Define θ_2 as

$$\theta_2 = \cos^{-1} \left[1 - \frac{y - W\epsilon_2}{R} \right]$$

Then, if $y < R + W\epsilon_1$

$$\begin{aligned} P &= 2\pi R^2 \int_0^{\theta_2} \left\{ \sigma_Y + E_3 \left[\frac{y-R(1-\cos\theta)}{W} - \epsilon_2 \right] \right\} \cos\theta \sin\theta \, d\theta \\ &+ 2\pi R^2 \sigma_Y \int_{\theta_2}^{\theta_1} \cos\theta \sin\theta \, d\theta \\ &+ \frac{2\pi\sigma_Y R^2}{W\epsilon_1} \int_{\theta_1}^{\theta_2} [y-R(1-\cos\theta)] \cos\theta \sin\theta \, d\theta \end{aligned}$$

or

$$\begin{aligned} P &= 2\pi R^2 \left\{ \left[\sigma_Y + \frac{E_3}{W}(y-R) - E_3\epsilon_2 \right] \left(\frac{1}{2} \right) \sin^2\theta_2 \right. \\ &- \frac{E_3}{3W} (\cos^3\theta_2 - 1) \left. \right\} + \pi R^2 \sigma_Y (\sin^2\theta_1 - \sin^2\theta_2) \\ &+ \frac{2\pi\sigma_Y R^2}{W\epsilon_1} \left[(y-R) \left(\frac{1}{2} \right) (\sin^2\theta_2 - \sin^2\theta_1) \right. \\ &- \left. \frac{R}{3} (\cos^3\theta_2 - \cos^3\theta_1) \right] \quad (\text{A12}) \end{aligned}$$

If $R + W\epsilon_1 \leq y < R + W\epsilon_2$,

then

$$\beta = \theta_1 = 90^\circ$$

and

$$P = 2\pi R^2 \left\{ \left[\sigma_Y + \frac{E_3}{W} (y-R) - E_3 \epsilon_2 \right] \left(\frac{1}{2} \right) \sin^2 \theta_2 - \frac{E_3 R}{3W} (\cos^3 \theta_2 - 1) \right\} + \pi R^2 \sigma_Y (\cos^2 \theta_2) \quad (A13)$$

If $y > R + W\epsilon_2$

then

$$\beta = \theta_1 = \theta_2 = 90^\circ$$

and

$$P = \pi R^2 \left(\sigma_Y - \frac{E_3 R}{3W} + \frac{E_3 Y}{W} - E_3 \epsilon_2 \right) \quad (A14)$$

The accuracy of the above equations were evaluated by comparing their predictions with actual lab tests of spheres penetrating foam. A small computer program was written to compute P versus y as determined from these equations. The comparison of the theoretical versus experimental results is given in Chapter III of this report.

Figure A3 shows a plot of the experimentally determined stress-strain curve for the type of foam used on the mock vehicle exterior. Also shown in Figure A3 is the idealized stress-strain curve for the foam.

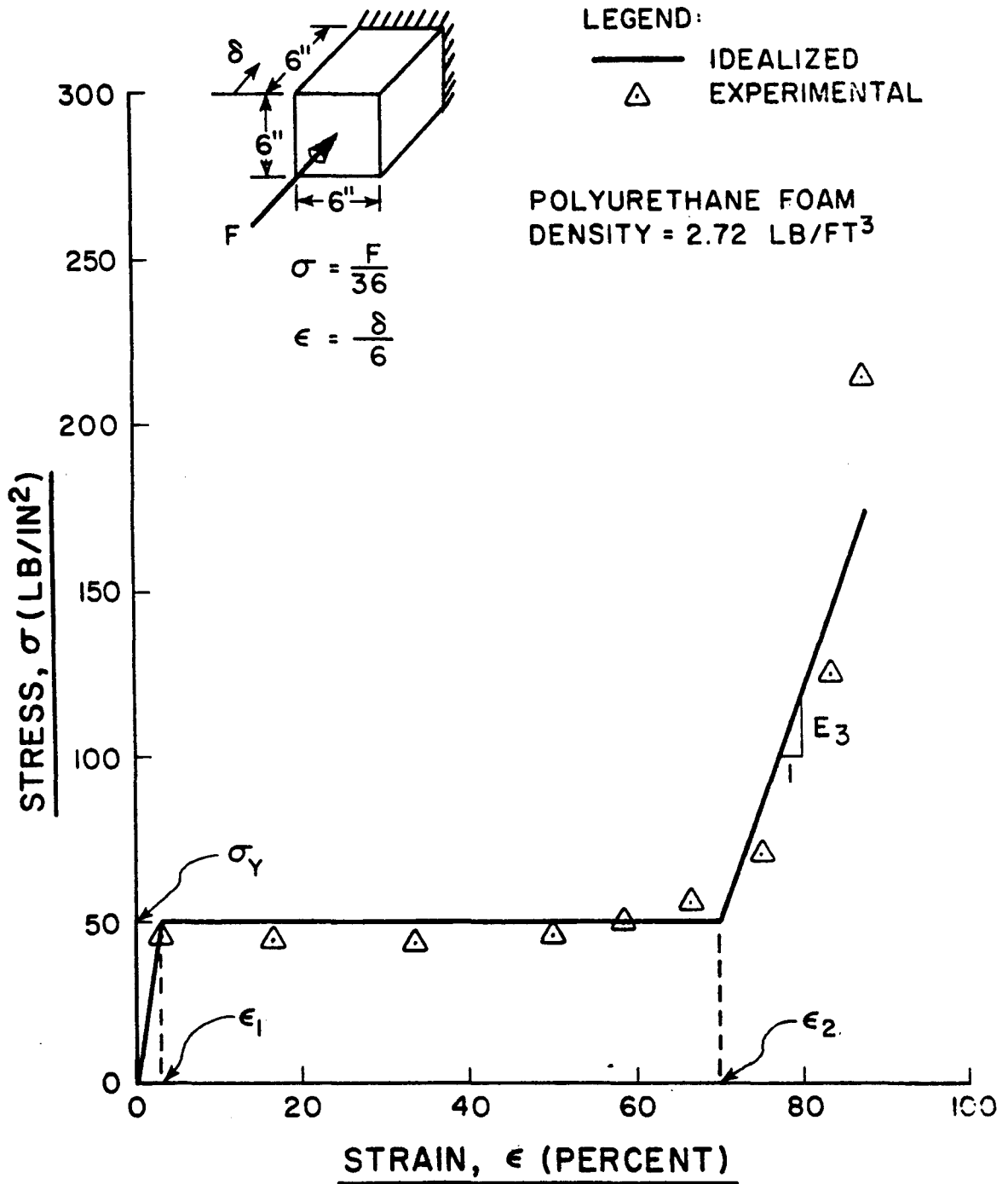


FIGURE A-3. STRESS-STRAIN CURVE FOR FOAM

For the idealized curve:

$$\epsilon_1 = 0.03 \text{ in./in.};$$

$$\epsilon_2 = 0.76 \text{ in./in.};$$

$$\sigma_Y = 45.0 \text{ lb/in.}^2; \text{ and}$$

$$E_3 = 3174 \text{ lb/in.}^2$$

APPENDIX B

ESTIMATION OF MASS DISTRIBUTION AND MOMENTS AT
INERTIA OF DUMMY TORSOS

APPENDIX B

ESTIMATION OF MASS DISTRIBUTION AND MOMENTS AT INERTIA OF DUMMY TORSOS

The three dummies used for testing in this project did not disassemble into the same number of segments as represented in the mathematical model (see Figure II-2). The male and female dummy torsos could not be separated into three discreet segments. Similarly, the child torso-plus-head combination could not be separated into the required four segments. For this reason, it was necessary to measure the inertial properties for the complete torso or else the torso-plus-head combination, and then obtain estimates of the inertial properties for each of the hypothetical segments. Regardless of the method of analysis employed to distribute the inertial properties to the idealized segments, the combined properties of these segments were made equal to the measured properties of the complete dummy torso or torso-plus-head combination.

Figure B-1a shows most of the major components that provide structural integrity to the female torso and indicates the assumed divisions for the three hypothetical segments. The structural components of the male torso are very similar to that of the female, while the child torso-plus-head combination, Figure B-1b, is somewhat different. In all cases, the dummy torsos were divided into the three most "natural" segments; namely, a long rigid chest portion, a short flexible "spinal column", and a short rigid lower back segment.

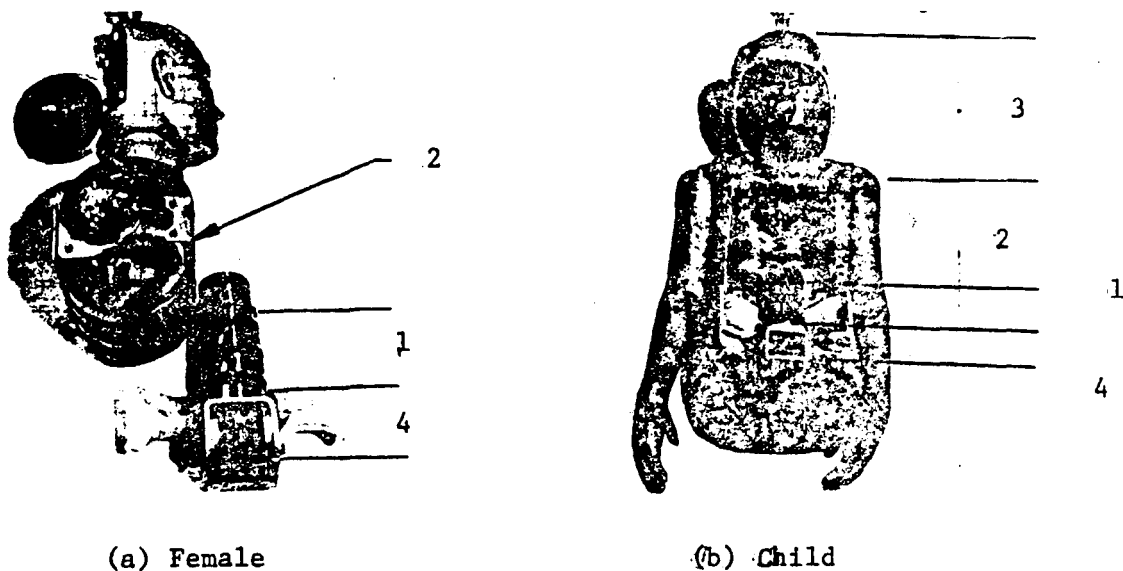


FIGURE B-1. / DISASSEMBLED DUMMY TORSOS AND ASSUMED SEGMENTS

In order to estimate the inertial properties of the individual male and female torso segments, the following assumptions were made:

- (1) The dummy torso can be idealized as a series of simple geometric shapes as shown in Figure B-2.
- (2) Each of the mass components in Figure B-2 is rigidly attached to one of the hypothetical segments.
- (3) The various mass components have a uniform mass density.
- (4) The center of gravity of each segment lies along the Z-axis shown in Figure B-2 and at the midpoint of each segment.

Using the above assumptions, the procedure used was to estimate the mass of the lower torso, segments 1 and 4. This was accomplished by disassembling the torso and weighing the skin (m_{1a}), padding (m_{1b}), "spinal

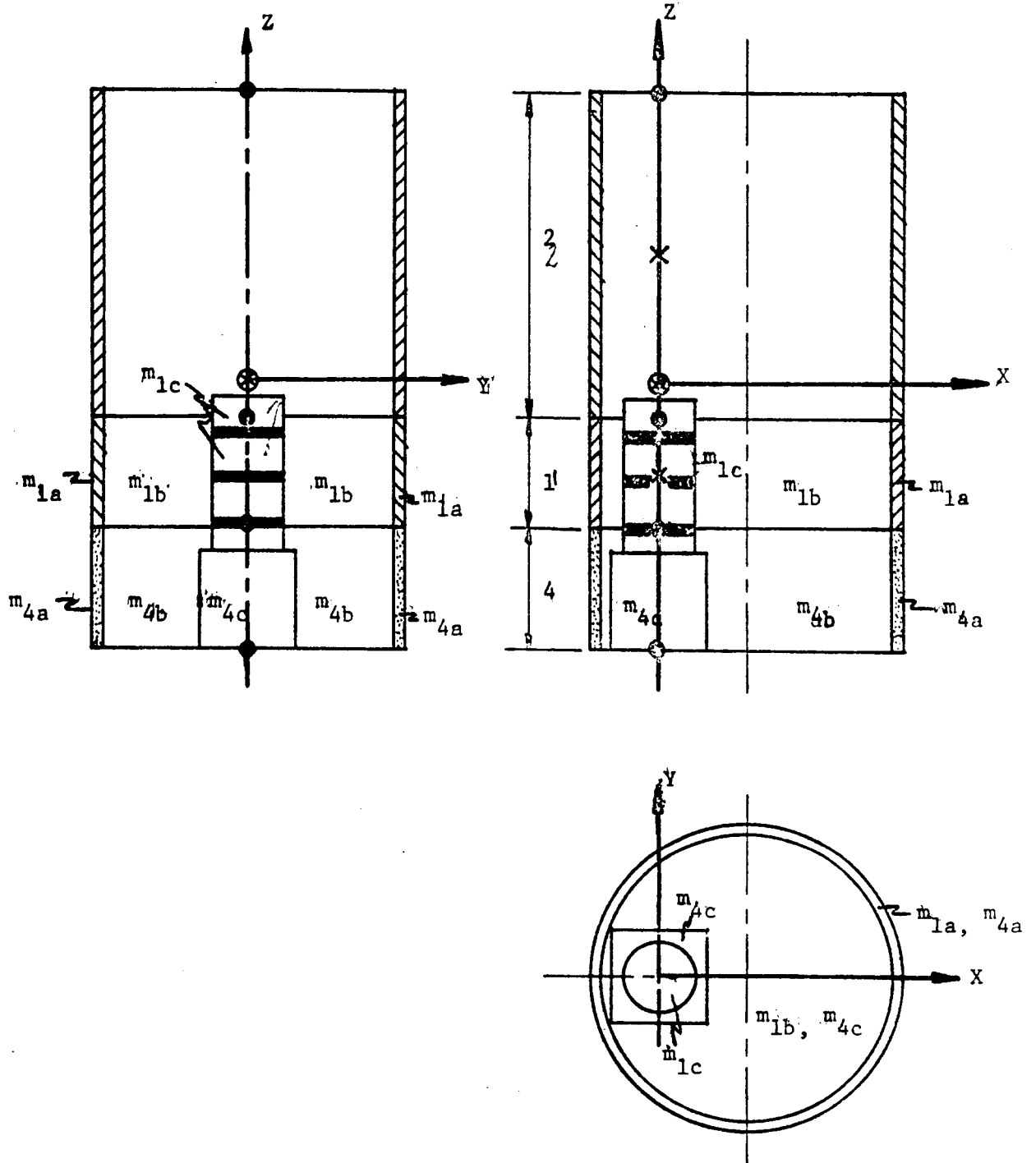


FIGURE B-2. IDEALIZED TORSO MODEL FOR MALE AND FEMALE DUMMIES

column" (m_{1c}), and miscellaneous hardware in the lower back segment (m_{4c}). Using these measured values and assumption 4 above, it was found that the computed center of gravity, for the three segments combined, deviated from the position measured for the complete dummy torsos. Masses m_{1b} were then calculated such that the computed and measured center of gravities would coincide. These values are summarized in Table B-1.

TABLE B-1 MASSES FOR MALE AND FEMALE TORSOS

MASS DESIGNATION	MALE		FEMALE	
	MASS (lbm)	TOTAL SEGMENT MASS (lbm)	MASS (lbm)	TOTAL SEGMENT MASS (lbm)
m_{1a}	2.1		1.5	
m_{1b}	5.3*		1.4*	
m_{1c}	10.1		7.0	
m_1		17.5		9.9
m_{4a}	2.3		1.2	
m_{4b}	8.4*		1.4*	
m_{4c}	12.7		5.9	
m_4		23.4		8.5
m_2		50.7**		25.5**
		$\Sigma m = 91.6$		$\Sigma m = 43.9$

* These values are estimates such that the resultant of all masses passes through the measured center of gravity.

** Obtained by subtracting masses of segments 1 and 4 from the total torso mass.

For the male and female, moments of inertia at the center of gravity and about axes X, Y, and Z were computed for the two lower torso segments based on the assumed simple geometry and calculated masses. The assumed geometries for masses connected to these segments are categorized in Table B-2 and their dimensions and locations are listed in Table B-3. Employing the parallel axis theorem, the moments of inertia for segment 2 were computed such that the combined inertial properties of segments 1, 2, and 4 were the same as those measured for the complete torso. The moments of inertia for these segments are summarized in Table B-4.

TABLE B-2. ASSUMED GEOMETRY OF MASS COMPONENTS FOR MALE AND FEMALE TORSO

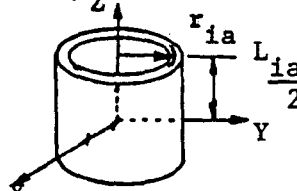
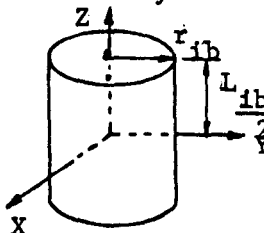
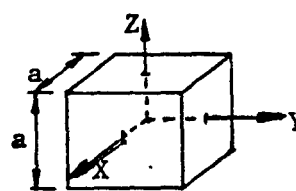
MASS DESIGNATION	ASSUMED SHAPE	MOMENTS OF INERTIA
m_{1a}, m_{4a}	Thin-walled circular cylinder 	$I_x = I_y = \frac{m_{ia}}{12} 6r_{ia}^2 + L_{ia}^2$ $I_z = m_{ia} r_{ia}^2$
m_{1b}, m_{4b}	Solid Circular Cylinder 	$I_x = I_y = \frac{m_{ib}}{12} 3r_{ib}^2 + L_{ib}^2$ $I_z = 1/2 m_{ib} r_{ib}^2$
m_{1c}	Same as Above	
m_{4c}	Cube 	$I_x = I_y = I_z = 1/6 m_{4c} a^2$

TABLE B-3. DIMENSIONS FOR IDEALIZED DUMMY TORSO

MASS DESIGNATION	DIMENSION	MALE (in)	FEMALE (in)
m_{1a}, m_{4a}	r_{ia}	6.25	4.25
	L_{ia}	4.5, 5.0	4.5, 3.5
	\bar{X}_a	3.5	1.5
m_{1b}, m_{4b}	r_{ib}	6.0	4.0
	L_{ib}	4.5, 5.0	4.5, 3.5
	\bar{X}_b	3.5	1.5
m_{1c}	r_{ie}	1.5	1.5
	L_{ic}	5.0	4.5
	\bar{X}_c	0.0	0.0
m_{4c}	a	4.0	4.0
	X_c	0.0	0.0

TABLE B-4. INERTIAL PROPERTIES FOR MALE AND FEMALE TORSO SEGMENTS

SEGMENT DESCRIPTION and No. from Fig. II-2	WEIGHT (lb)	LENGTH OF SEGMENT (in)	LOCATION OF C.G. (ρ)*in.	MOMENT OF INERTIA (in-lb-sec ²)		
				X	Y	Z
<u>Male</u>						
Middle Torso - 1	17.5	5.0	2.25	0.328	0.562	0.72
Upper Torso - 2	50.7	13.5	6.75	4.77	3.42	1.74
Lower Torso - 4	23.4	5.0	2.5	0.456	0.806	1.05
<u>Female</u>						
Middle Torso - 1	9.94	4.5	2.25	0.100	0.117	0.136
Upper Torso - 2	25.52	10.0	5.36	2.018	1.666	0.882
Lower Torso - 4	8.48	3.5	1.75	0.104	0.118	0.15

The child dummy torso-plus-head combination did not separate into the various mass components used in the male and female analysis. For this reason, a very simple analysis was used. The most important part of this analysis was to obtain the inertial properties for the child head and neck. Because of the similarity in size between the female and child head and neck, the inertial properties for the child were extrapolated from the measured properties of the female head. A mass distribution for the remaining segments was then assumed such that the center of gravity computed for the four segments was positioned at the measured center of gravity.

The moments of inertia for the lower two segments were computed assuming the shape to be that of a solid circular cylinder. These moments of inertia plus those of the head, obtained from the female to child extrapolation, were used to compute the required moments of inertia at the center of gravity of the upper torso segment such that the moments of inertia for the assemblage of segments were the same as those measured for the child torso-plus-head combination. These properties are summarized in Table B-5.

TABLE B-5. INERTIAL PROPERTIES FOR CHILD TORSO SEGMENTS

SEGMENT DESCRIPTION AND No. FROM Fig. II-2	WEIGHT (lb)	LOCATION OF C.G. (ρ)*in.	MOMENT OF INERTIA (in-lb-sec ²)		
			X	Y	Z
Middle Torso - 1	2.86	1.25	0.024	0.024	0.041
Upper Torso - 2	12.24	5.53	0.703	0.624	0.232
Head and Neck - 3	9.06	4.7	0.151	0.151	0.093
Lower Torso - 4	2.86	1.25	0.026	0.026	0.044

Because of the simplicity involved in the above discussion, some justification should be given for its use. It was noted from the high-speed film of the drop tests, that the dummies' torsos tended to move as a rigid body i.e., bending along the length of the "spinal column" was relatively small. This implies that the properties of the hypothetical torso segments would not greatly affect the simulations provided that the combined properties of these segments were the same as those measured for the complete dummy torsos. For this reason, an exhaustive study to obtain "exact" inertial properties for the hypothetical segments was unwarranted. Hence, the estimations reported here are based on simple engineering assumptions and are not purported to be "exact".

One further complication arose during the efforts made to obtain a working data base for the child dummy. The upper and lower arm segments could not be separated; hence, the inertial properties for the entire arm assemblage were measured. The mass distribution applying to this system was estimated in the following manner:

- (1) The center of gravity for the assemblage of upper and lower arm segments was located in the two configurations shown in Figure B-3.
- (2) Equations relating the separate masses and the location of their center of gravities to the total mass and the location of the measured center of mass for the assemblage were formulated. (Equations B-1 through B-3).
- (3) A unique solution to these equations was obtained by assuming the center of mass to lie at the midpoint, $\delta_a = L_a/2$, for the upper arm segment.

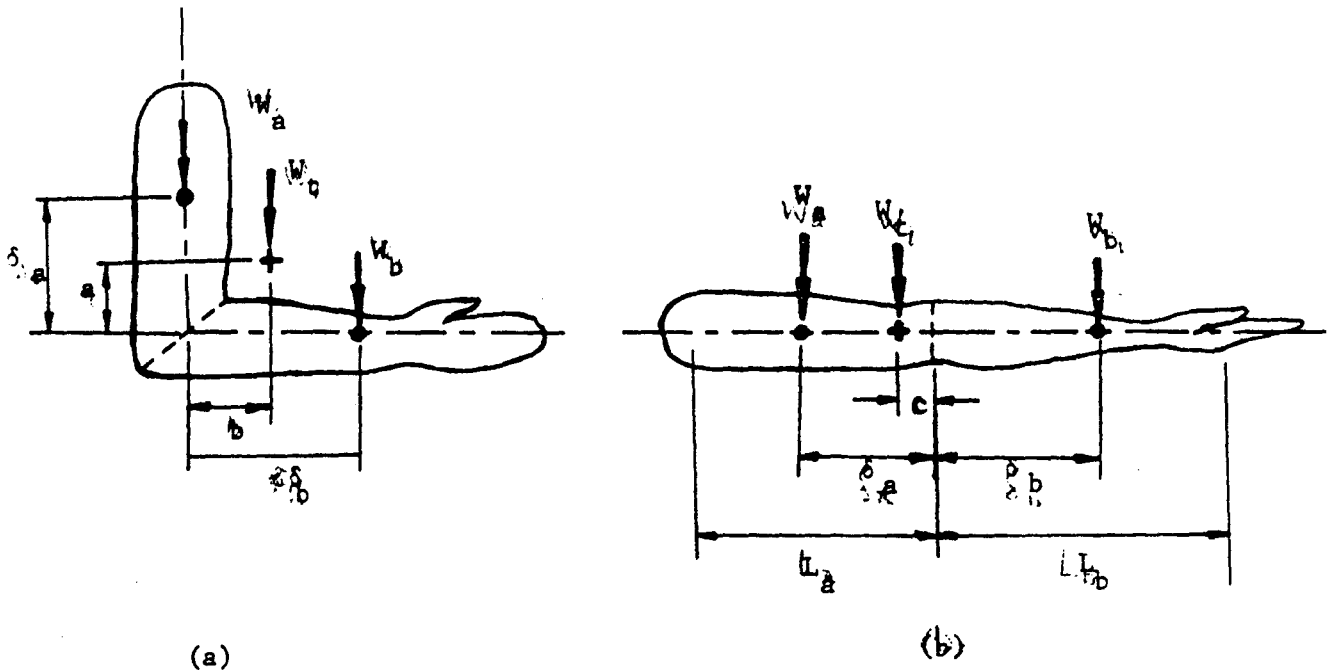


FIGURE B-3. DIMENSIONS FOR CHILD ARM SEGMENTS

$$\delta_A W_A = aW_T \dots\dots\dots (B-1)$$

$$\delta_B W_B = bW_T \dots\dots\dots (B-2)$$

$$W_A + W_B = W_T \dots\dots\dots (B-3)$$

where

W_T = total weight of arm assemblage

W_A, W_B = weight of upper and lower arm segments, respectively

δ_A, δ_B = location of center of gravity for upper and lower arm segments, respectively

a, b = location of center of gravity for the complete arm assemblage in the configuration shown in Figure B-3a

c = location of center of gravity for the complete arm assemblage in

the configuration shown in Figure B-3b

The measured values locating the center of gravity are listed in Table B-6.

TABLE B-6. CENTER OF GRAVITY LOCATIONS FOR CHILD ARMS

Arm Assemblage	Dimensions		
	a (in)	b (in)	c (in)
Left Arm	2.25	1.5	0.75
Right Arm	2.13	1.62	0.75

Using the above values and assumption 3, the masses of each segment were computed. The moments of inertia for the upper arms were computed assuming the segments to have the shape of a right circular cylinder. The remainder of the measured total moments of inertia were associated with the lower arm segment. These values are summarized in Table B-7.

TABLE B-7. INERTIAL PROPERTIES FOR CHILD ARM SEGMENTS

SEGMENT DESCRIPTION AND NO. FROM FIG. II-2	WEIGHT (lb)	LOCATION OF C.G. (ρ)*in.	MOMENT OF INERTIA (in-lb-sec ²)		
			X	Y	Z
Left Upper Arm-5	1.78	3.8	0.0268	0.0268	0.0060
Right Upper Arm-6	1.66	3.8	0.0249	0.0249	0.0067
Left Forearm-7	1.23	7.431	0.0522	0.0546	0.0060
Right Forearm	1.31	7.31	0.0530	0.0517	0.0067

APPENDIX C

STATIC FORCE-DEFORMATION CURVES
OF DUMMY SEGMENTS

FORCE DEFORMATION PROPERTIES OF CHILD DUMMY SEGMENTS — SKULL CAP —

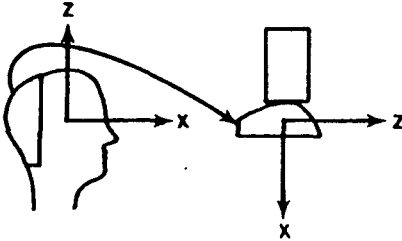
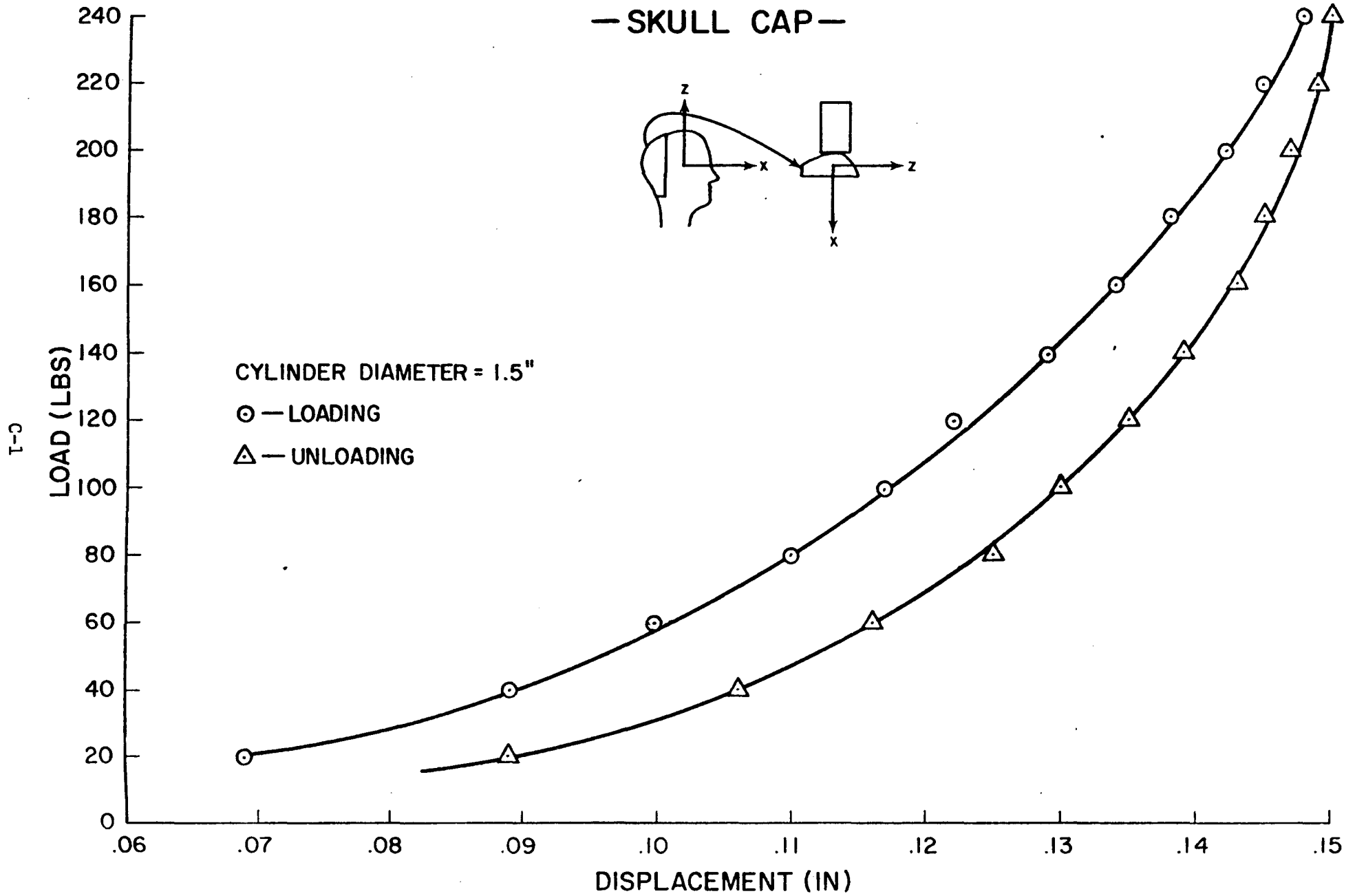


FIGURE C-1.

LOAD DEFORMATION PROPERTIES OF CHILD DUMMY SEGMENTS — CHEST —

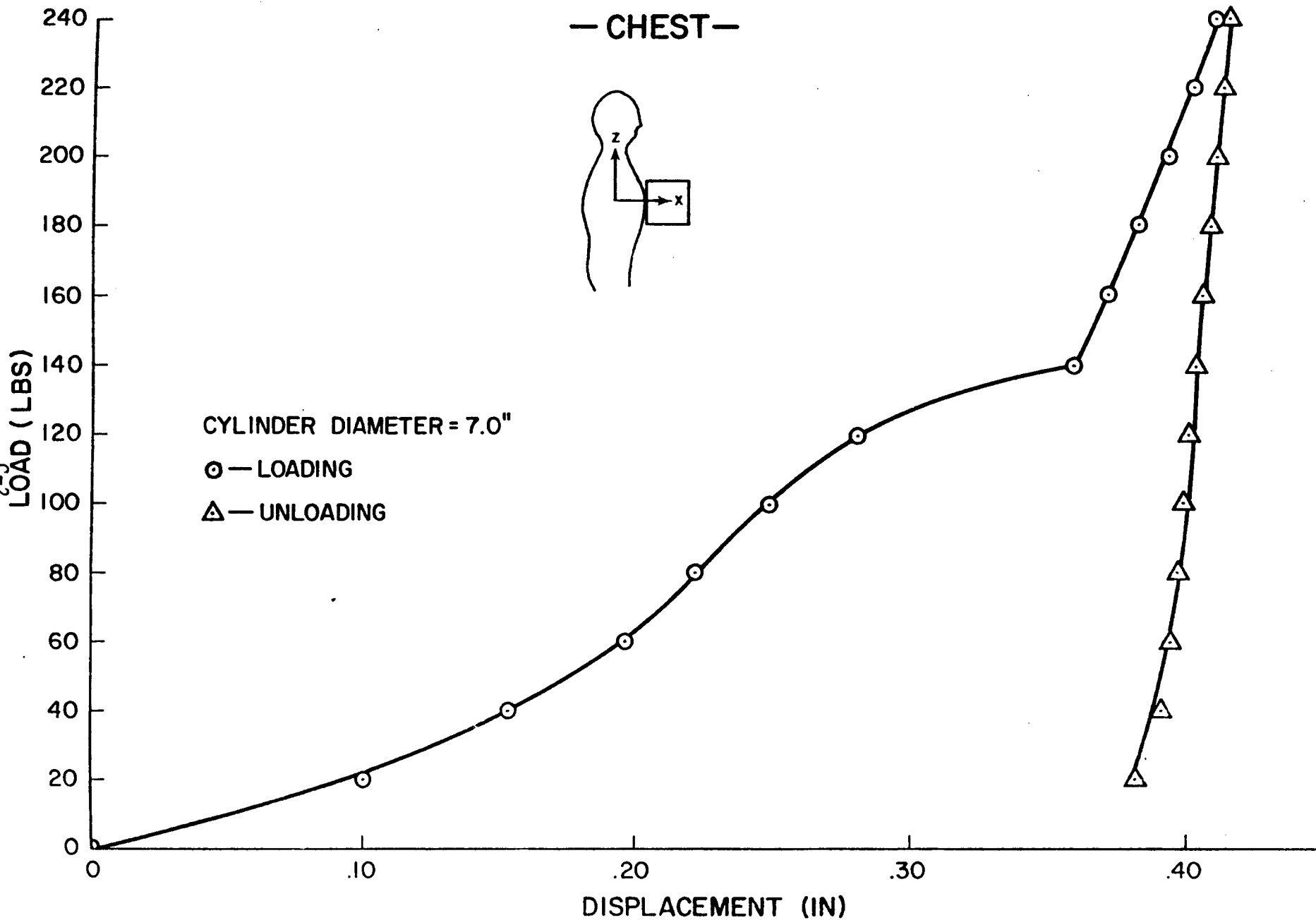


FIGURE C-2.

LOAD DEFORMATION PROPERTIES OF CHILD DUMMY SEGMENTS

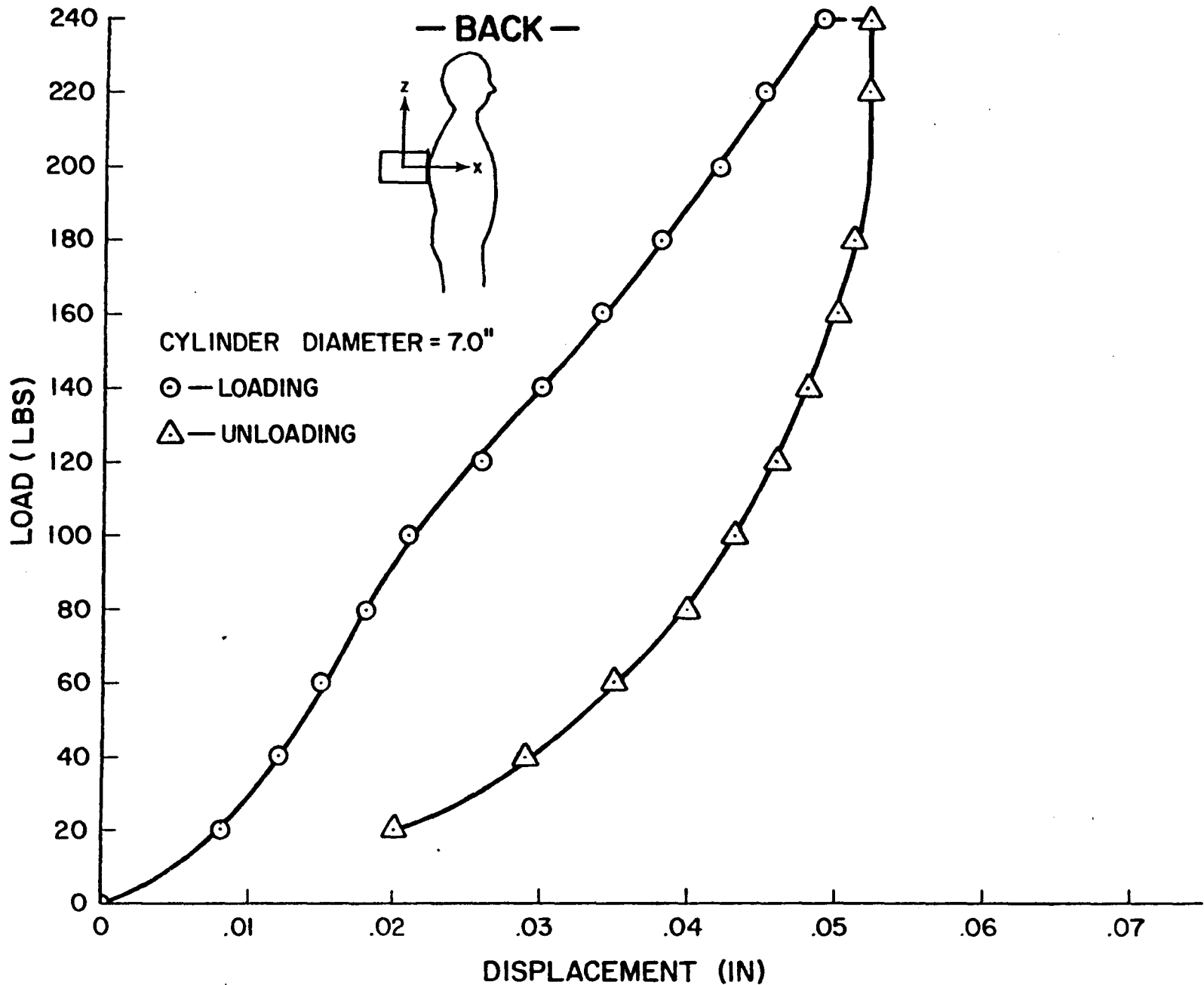


FIGURE C-3.

C-3

FORCE DEFORMATION PROPERTIES OF CHILD DUMMY SEGMENTS — POSTERIOR —

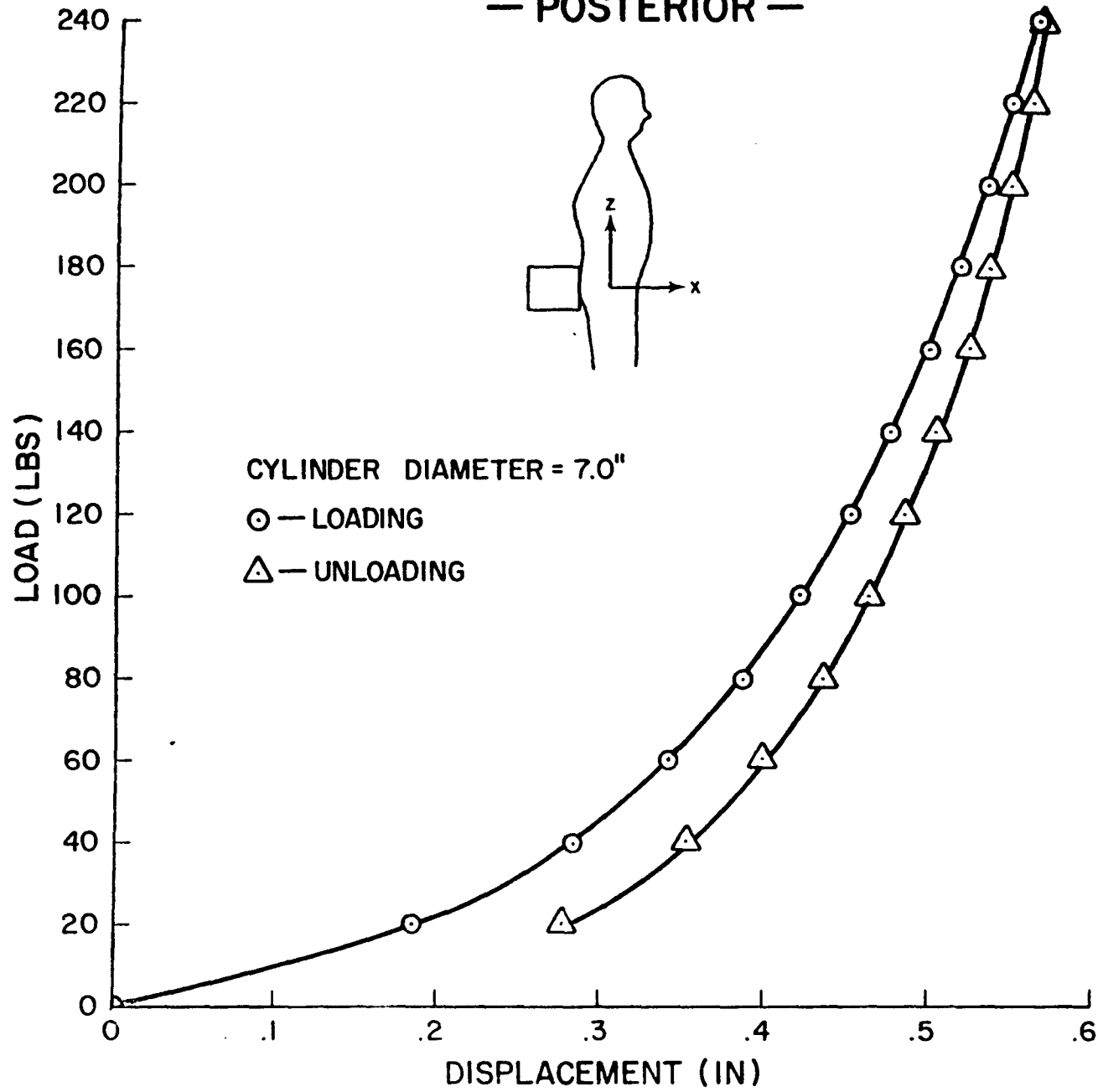
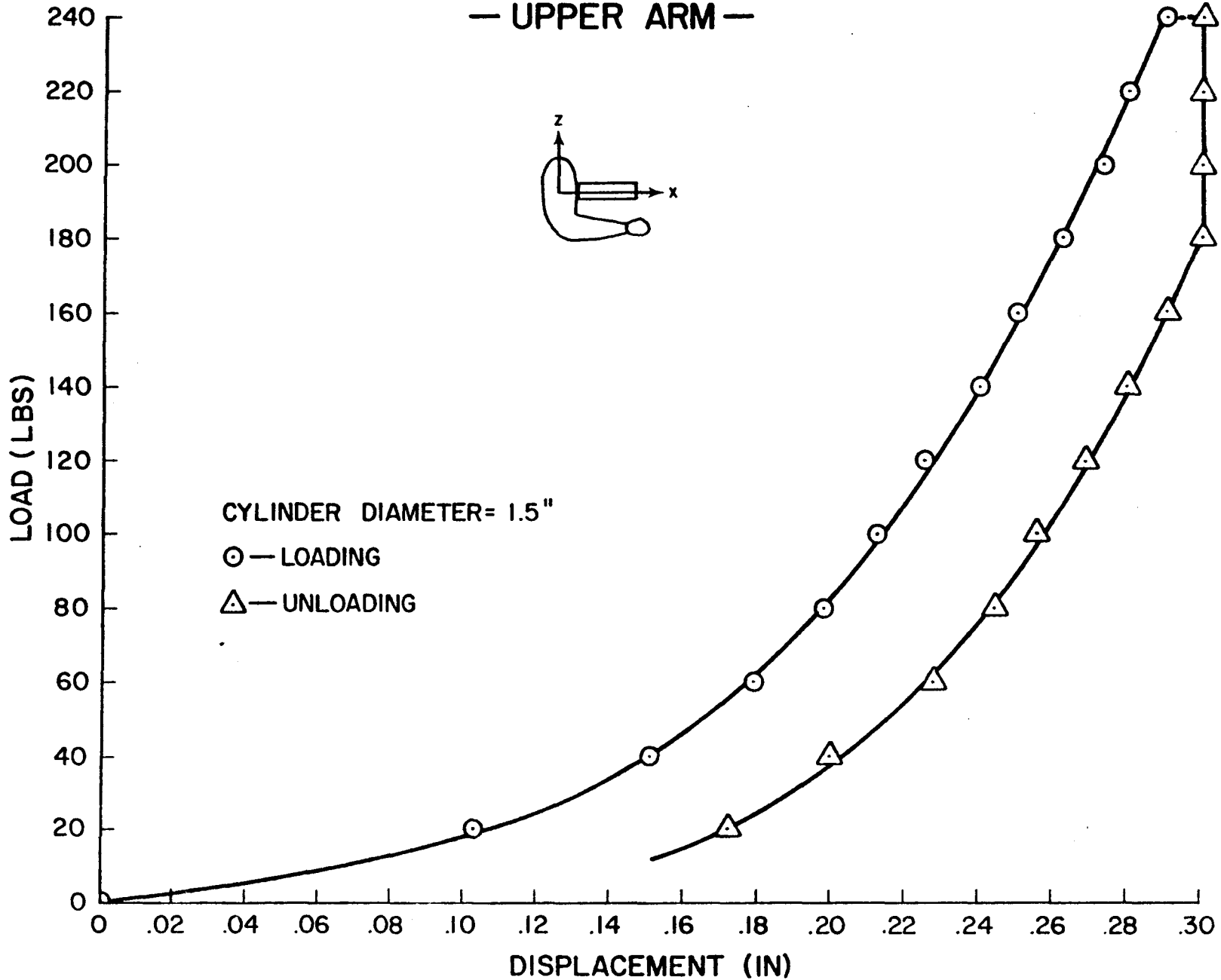


FIGURE C-4.

C-4

LOAD DEFORMATION PROPERTIES OF CHILD DUMMY SEGMENTS

— UPPER ARM —



CYLINDER DIAMETER= 1.5"

○ — LOADING

△ — UNLOADING

DISPLACEMENT (IN)

FIGURE C-5.

C-5

LOAD DEFORMATION PROPERTIES OF CHILD DUMMY SEGMENTS — LOWER ARM —

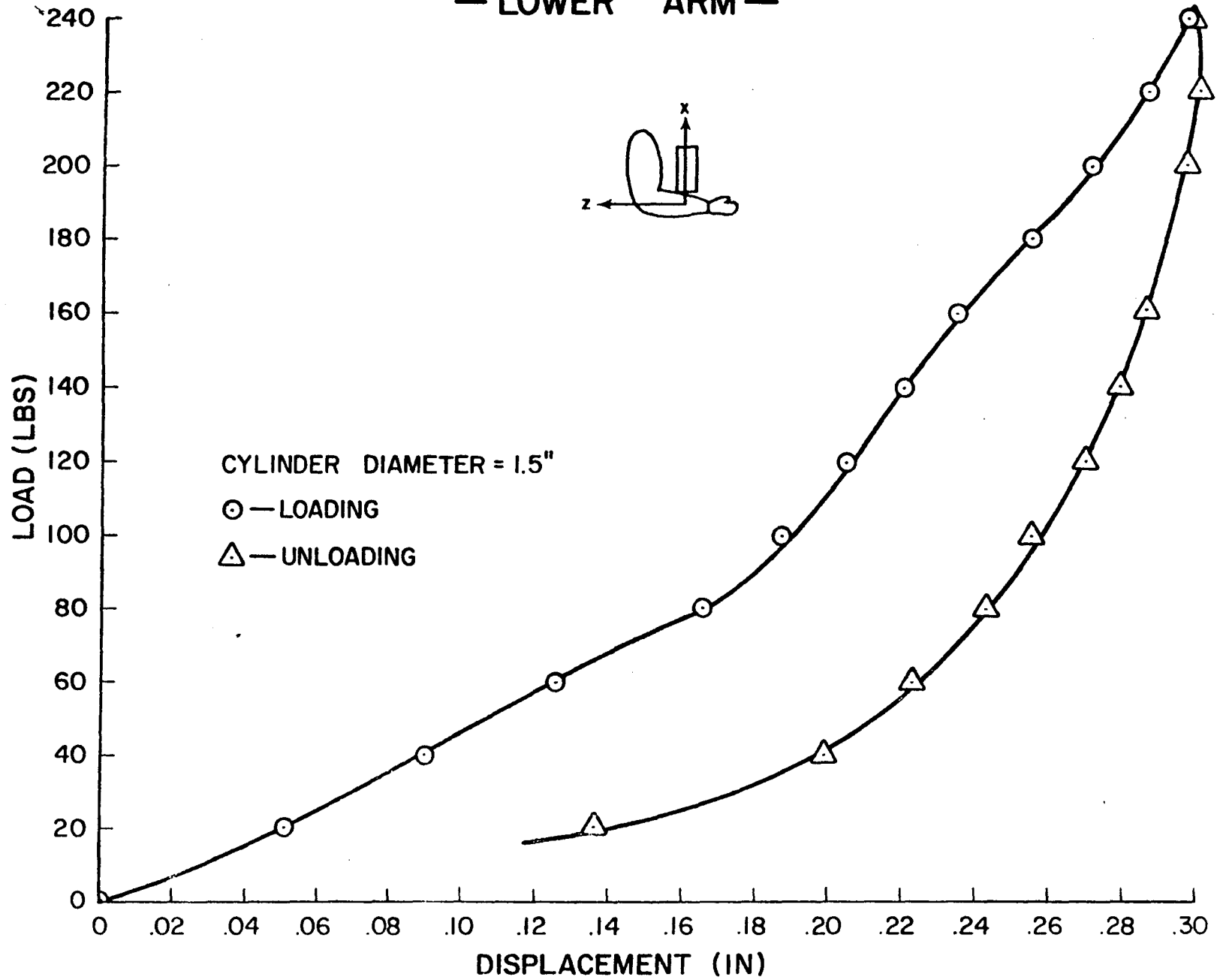


FIGURE C-6.

LOAD DEFORMATION PROPERTIES OF CHILD DUMMY SEGMENTS — UPPER LEG —

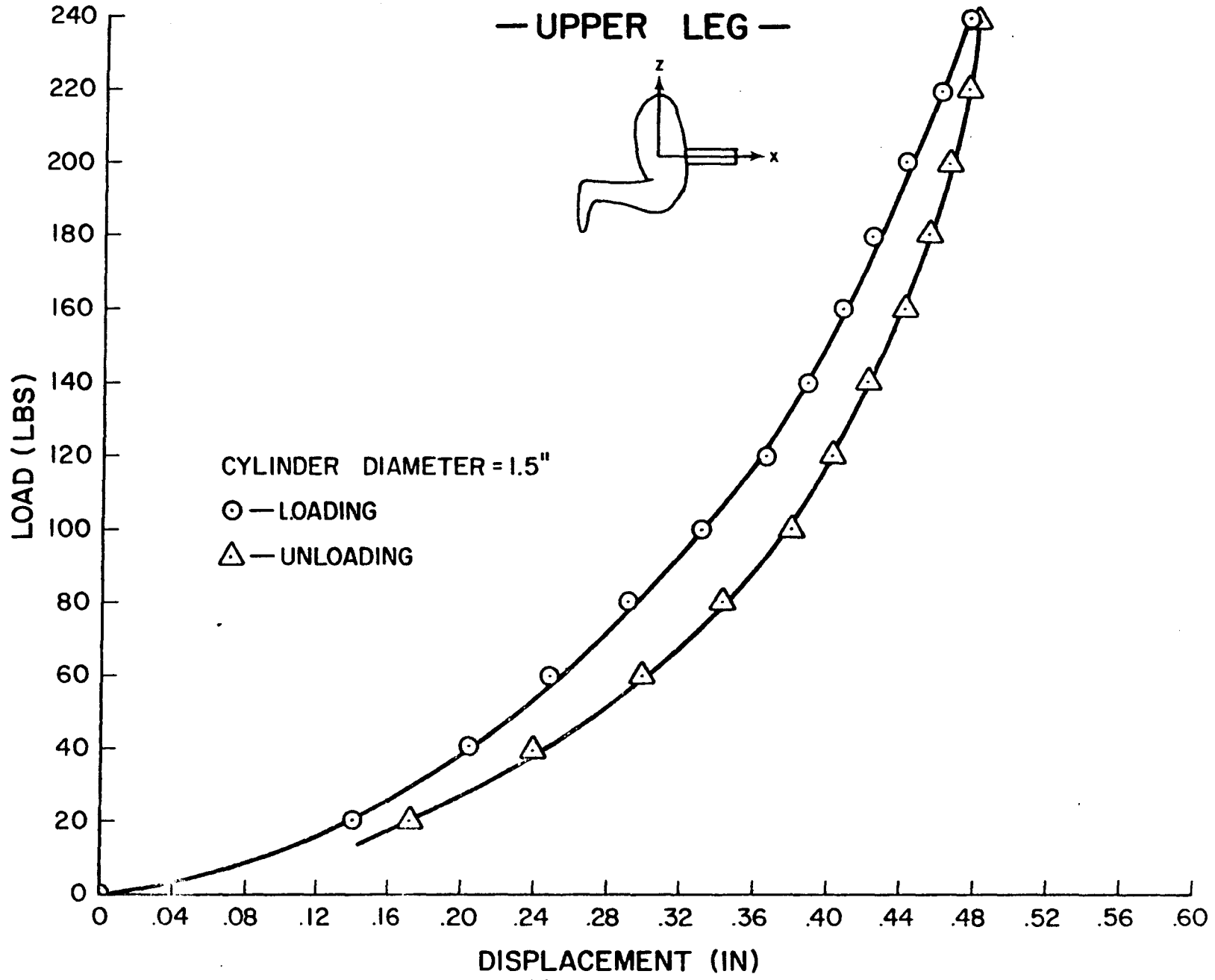
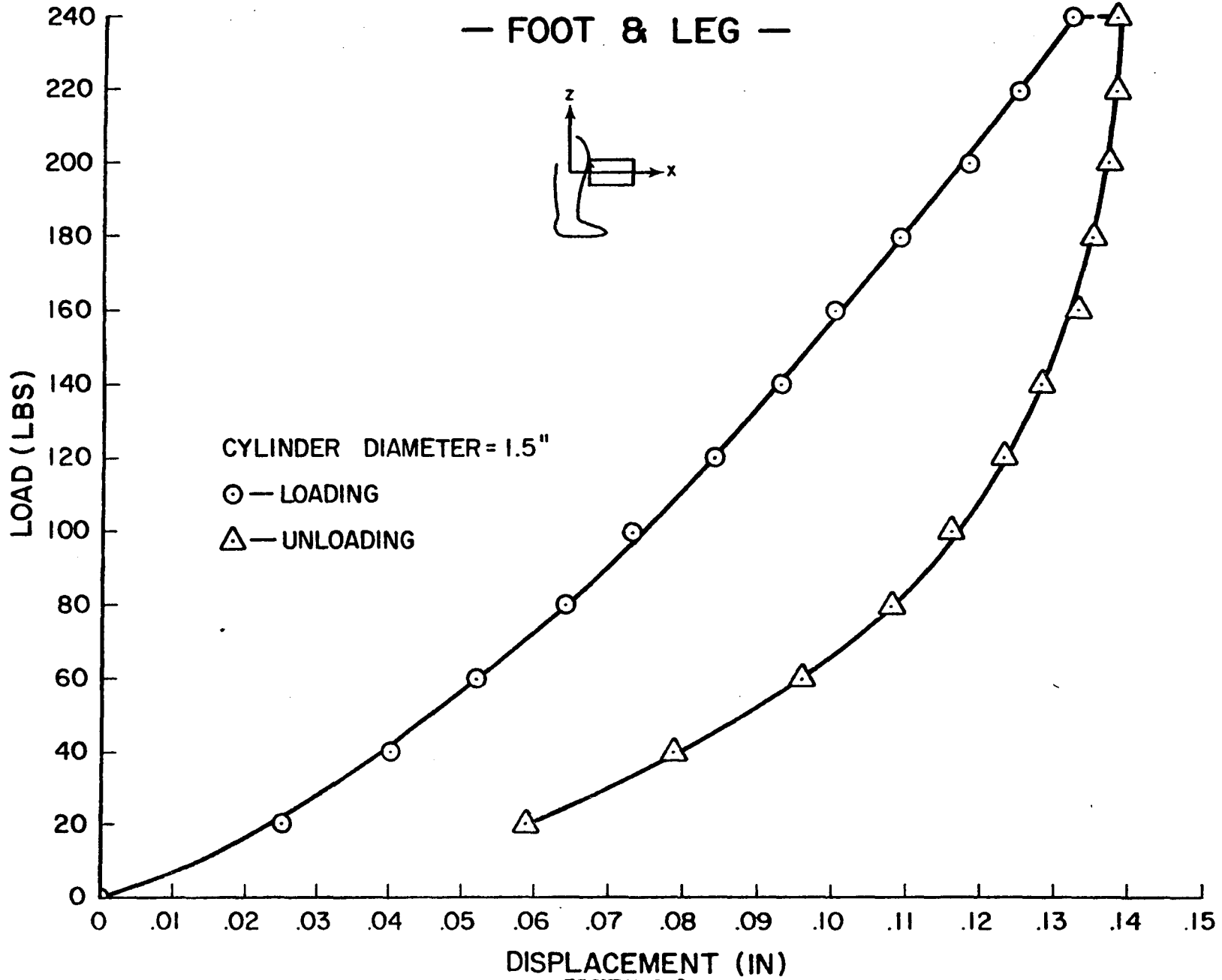


FIGURE C-7.

C-7

LOAD DEFORMATION PROPERTIES OF CHILD DUMMY SEGMENTS — FOOT & LEG —

8-0



CYLINDER DIAMETER = 1.5"

○ — LOADING

△ — UNLOADING

DISPLACEMENT (IN)

FIGURE C-8.

LOAD DEFORMATION PROPERTIES OF FEMALE DUMMY SEGMENTS — SKULL CAP —

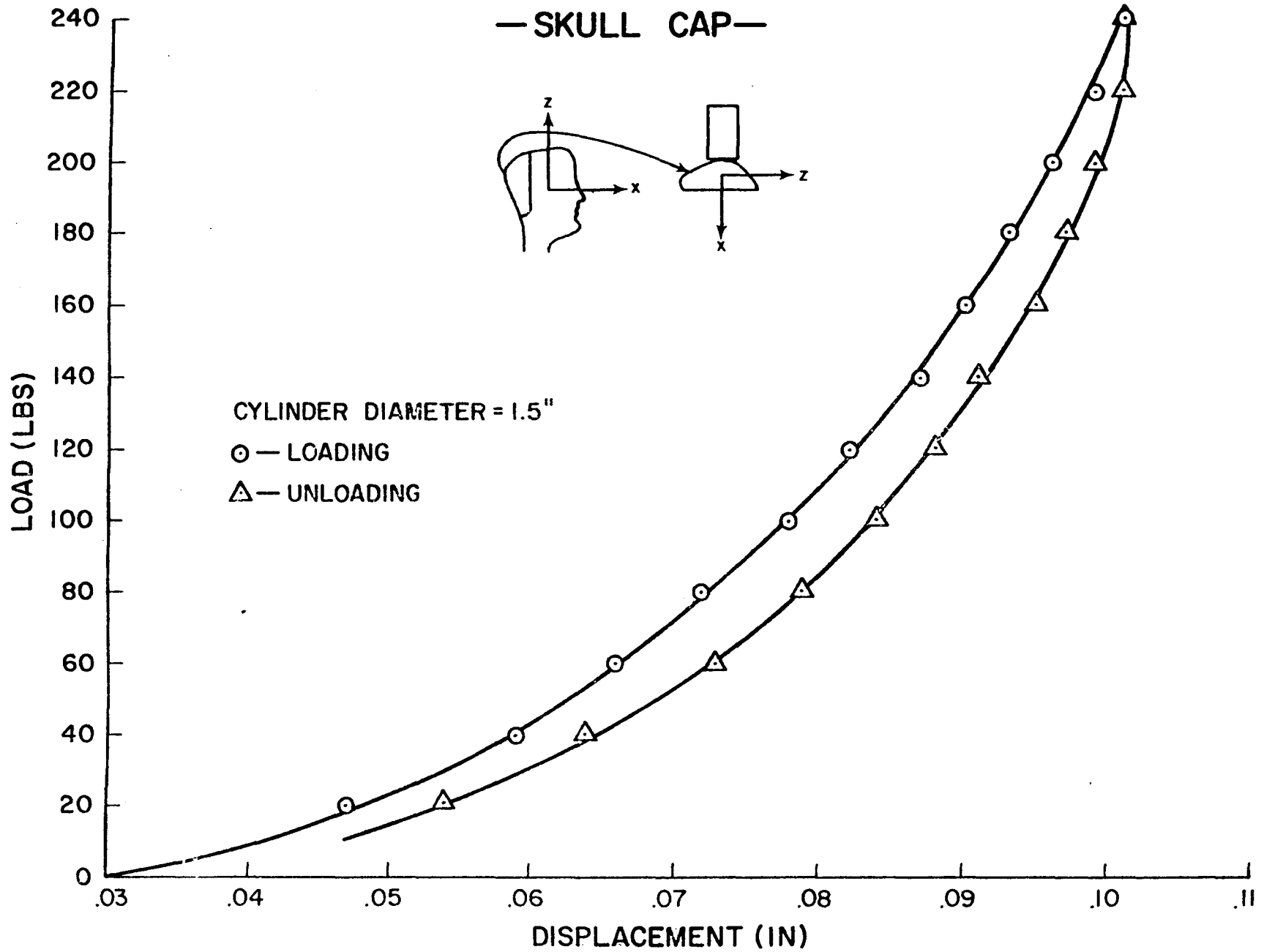


FIGURE C-9.

FORCE DEFORMATION PROPERTIES OF FEMALE DUMMY SEGMENTS - CHEST -

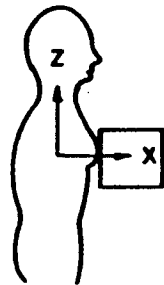
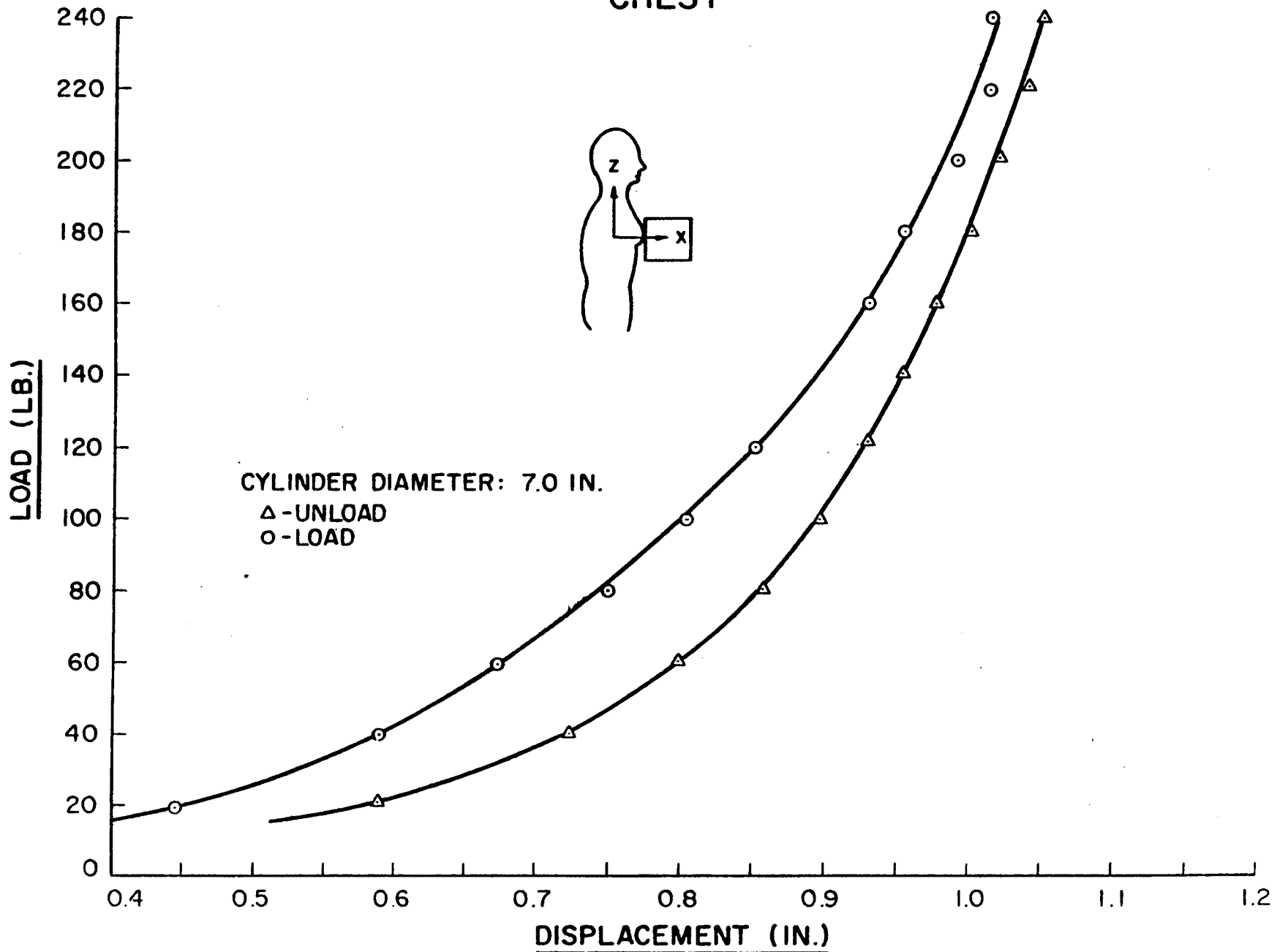
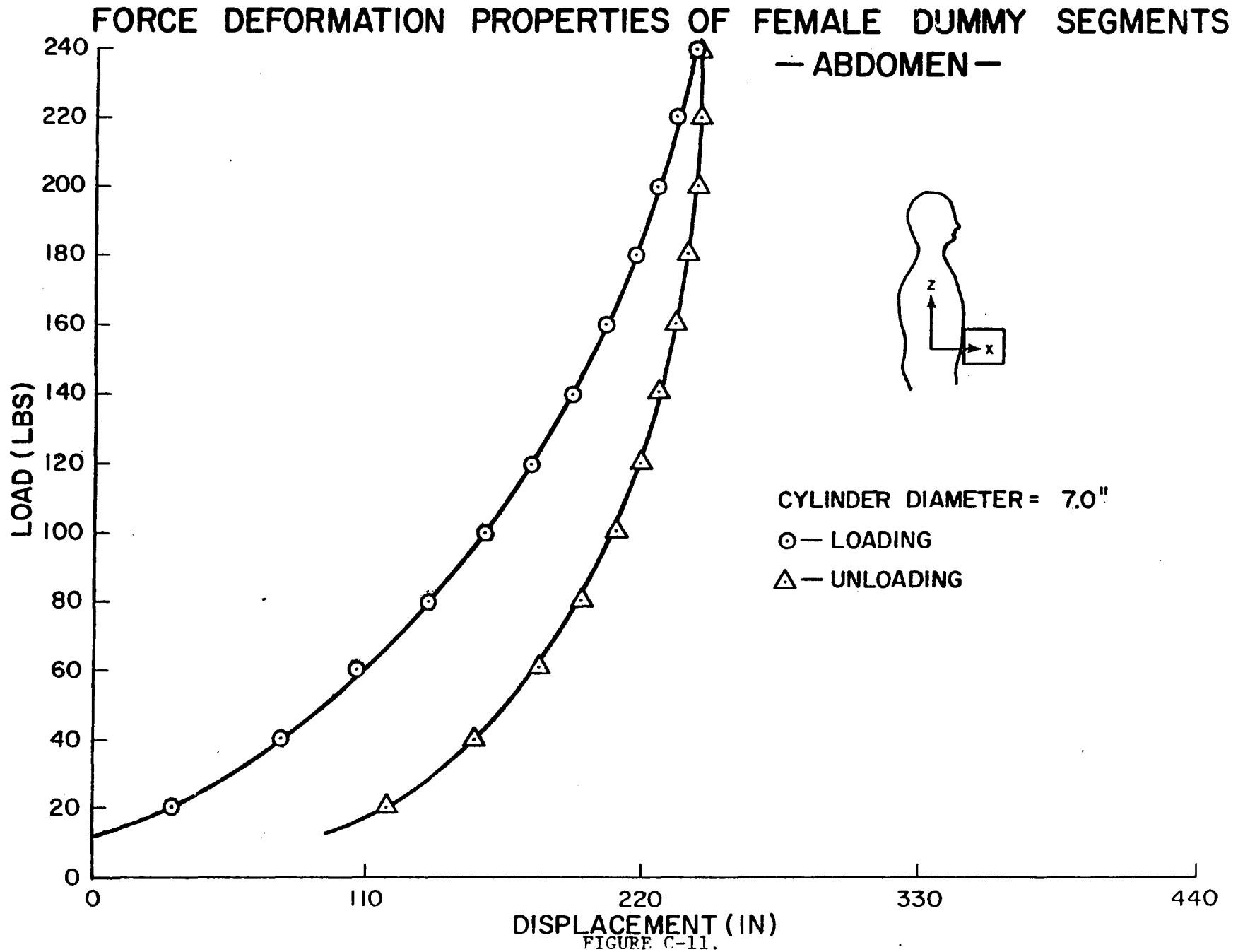


FIGURE C-10.

TI-2



FORCE DEFORMATION PROPERTIES OF FEMALE DUMMY SEGMENTS — POSTERIOR —

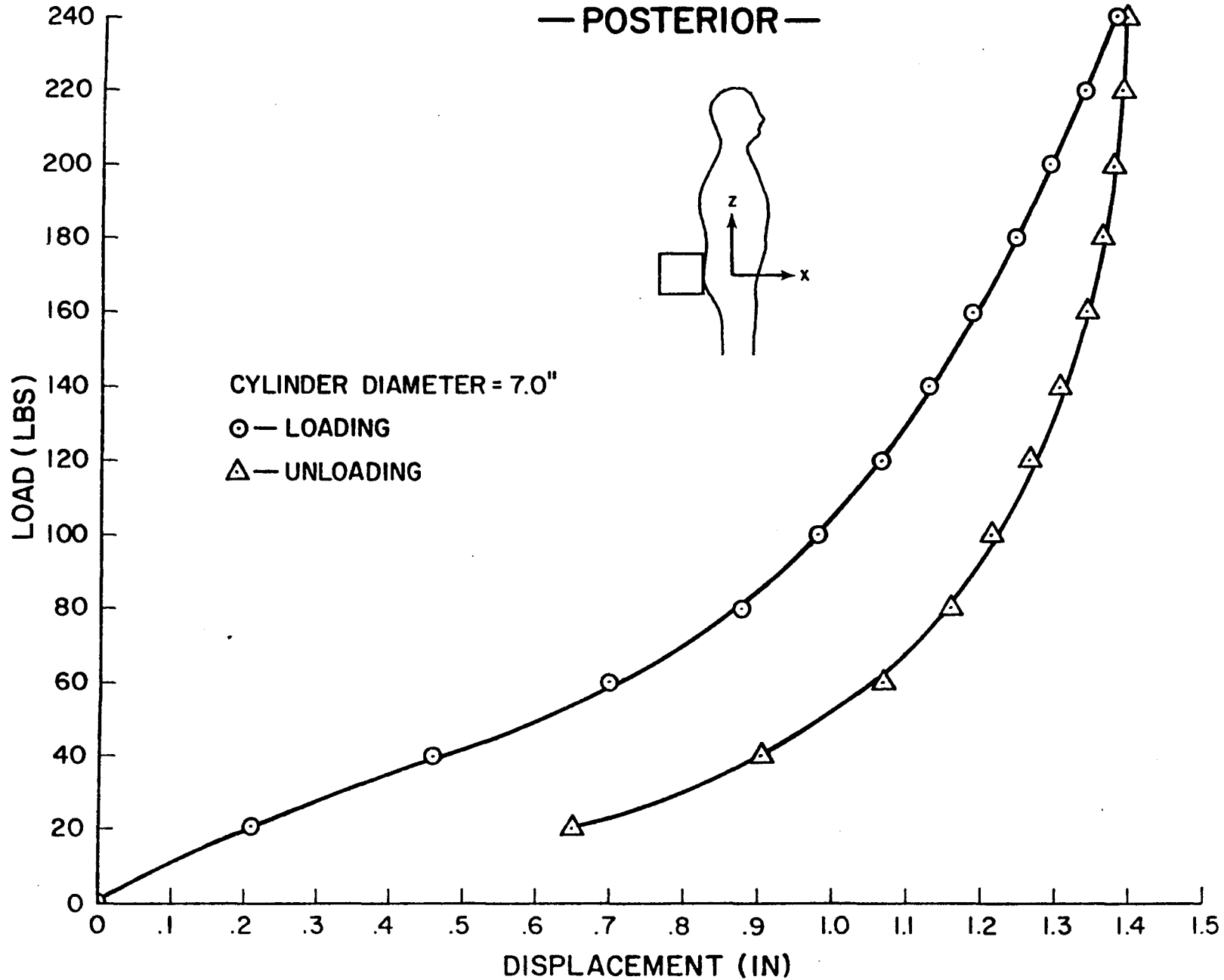


FIGURE C-12.

LOAD DEFORMATION PROPERTIES OF FEMALE DUMMY SEGMENTS

— UPPER ARM —

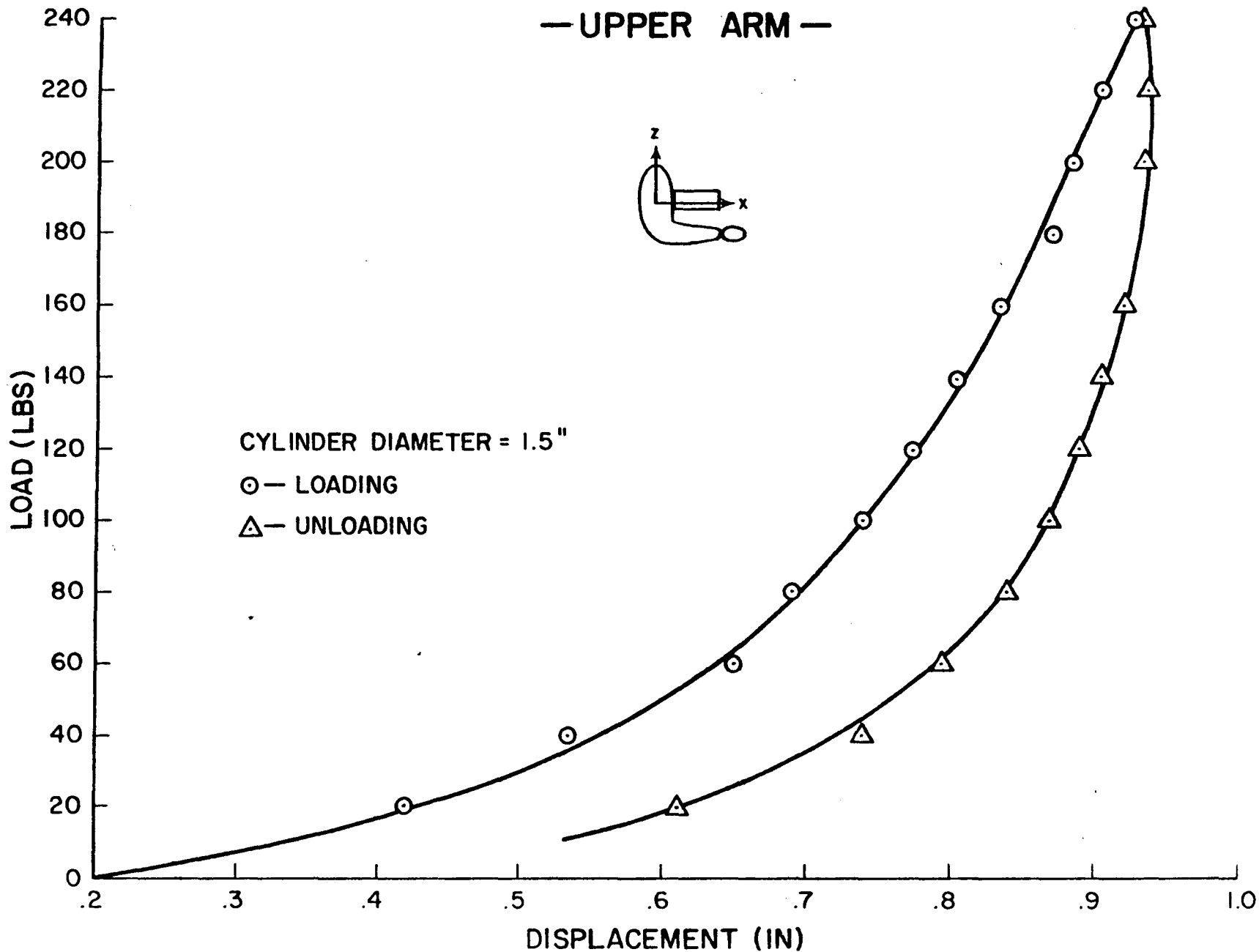
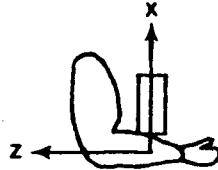


FIGURE C-13.

LOAD DEFORMATION PROPERTIES OF FEMALE DUMMY SEGMENTS

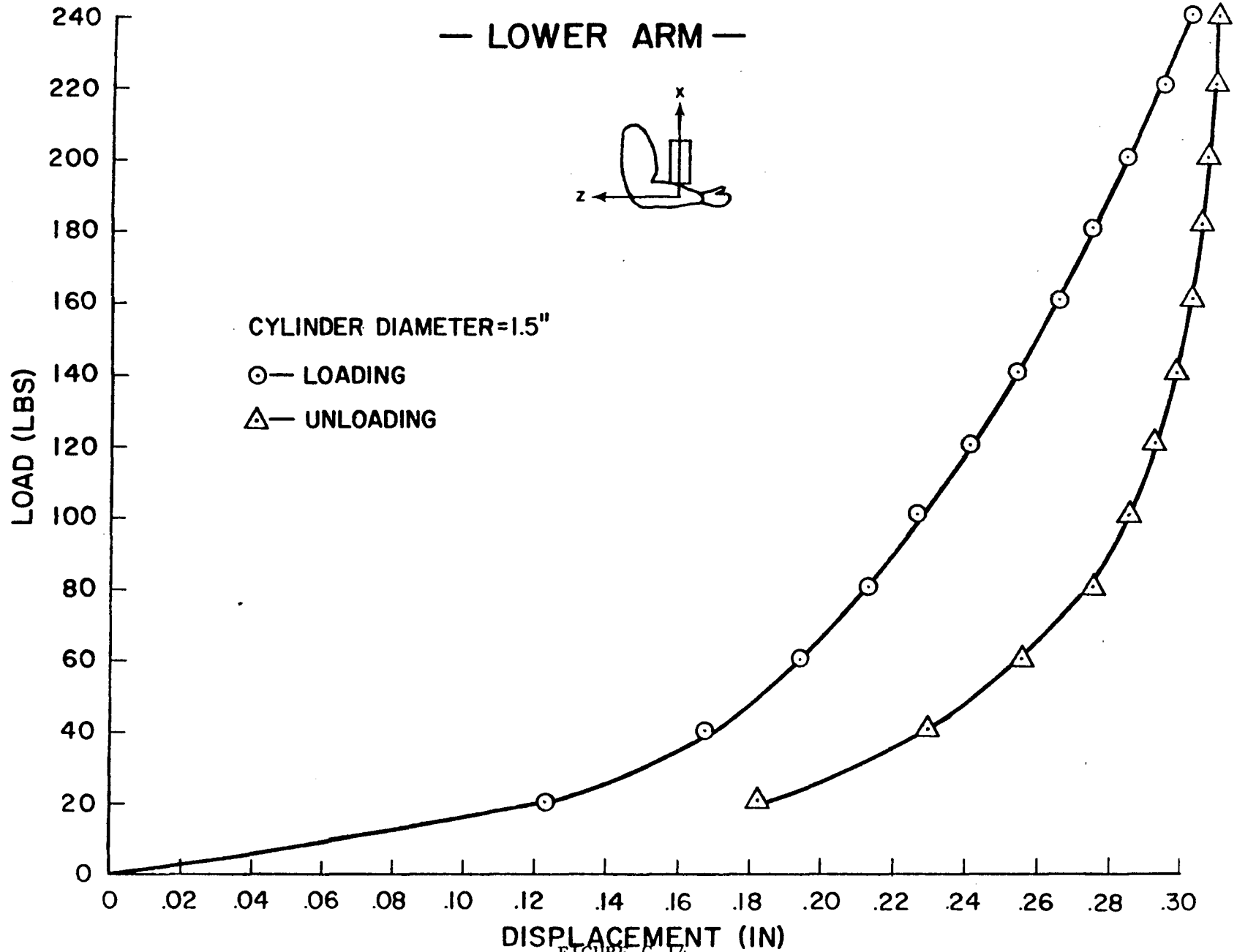
— LOWER ARM —



CYLINDER DIAMETER=1.5"

⊙ — LOADING

△ — UNLOADING

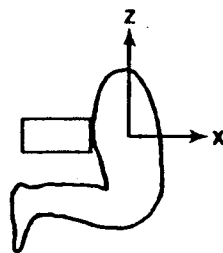


C-14

FIGURE C-14.

LOAD DEFORMATION PROPERTIES OF FEMALE DUMMY SEGMENTS

— UPPER LEG —



CYLINDER DIAMETER = 2.5"

○ — LOADING

△ — UNLOADING

CONTACT MADE WITH
TRANSDUCER BOX

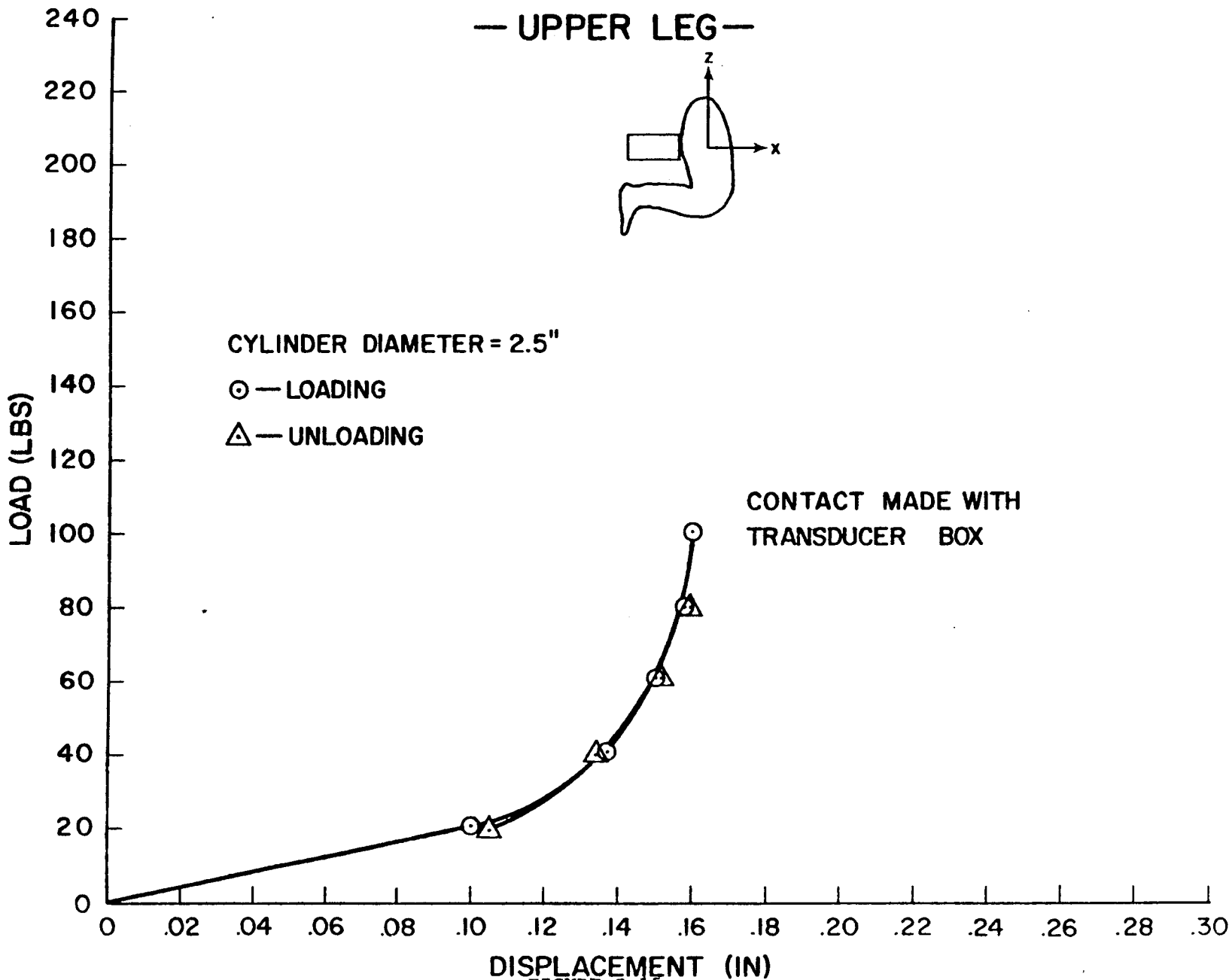


FIGURE C-15.

LOAD DEFORMATION PROPERTIES OF FEMALE DUMMY SEGMENTS

— UPPER LEG —

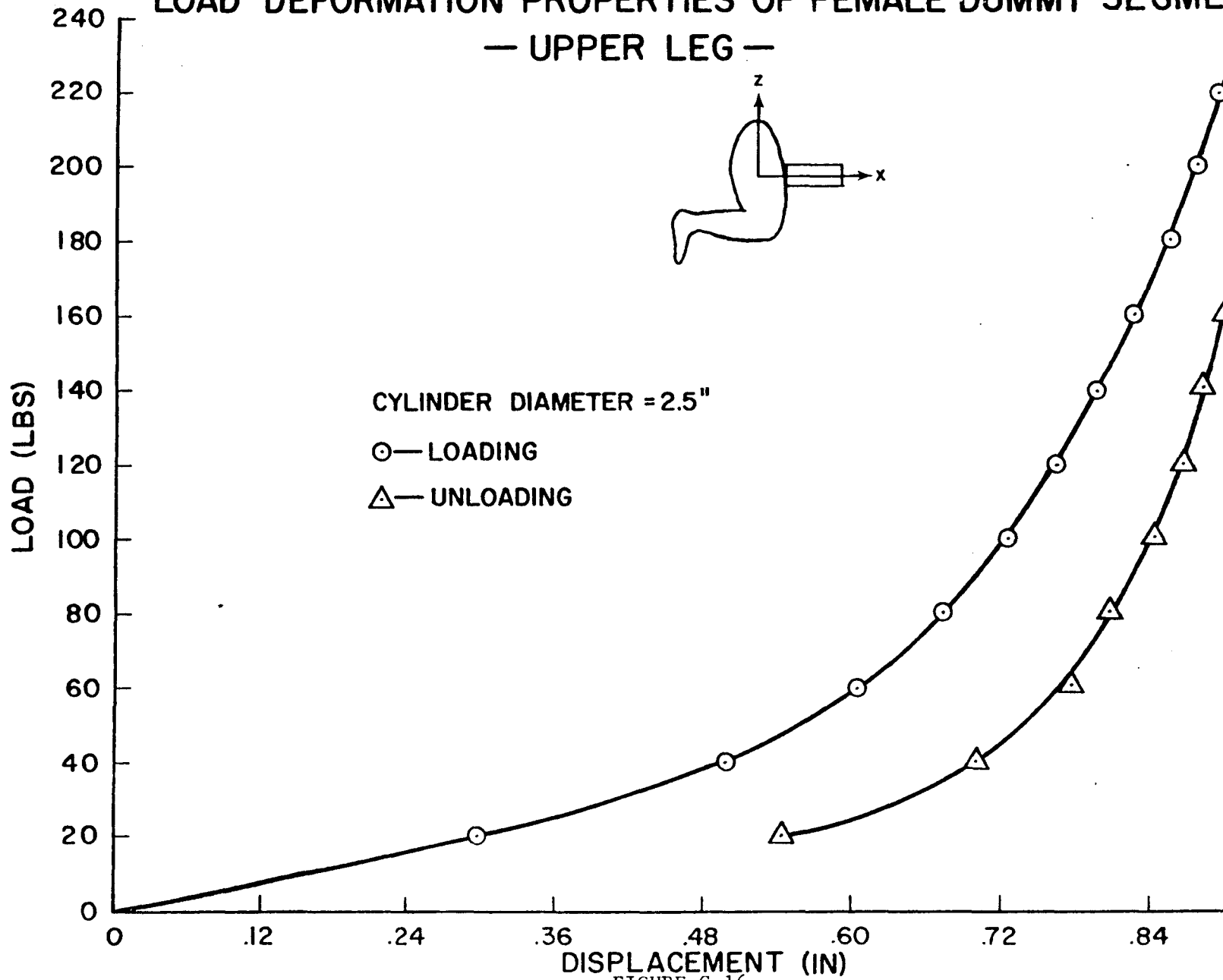
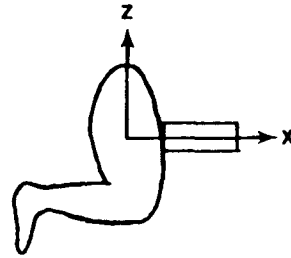
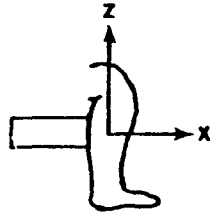


FIGURE C-16.

LOAD DEFORMATION PROPERTIES OF FEMALE DUMMY SEGMENTS

— FOOT & LEG —



CYLINDER DIAMETER = 1.5"

○ — LOADING

△ — UNLOADING

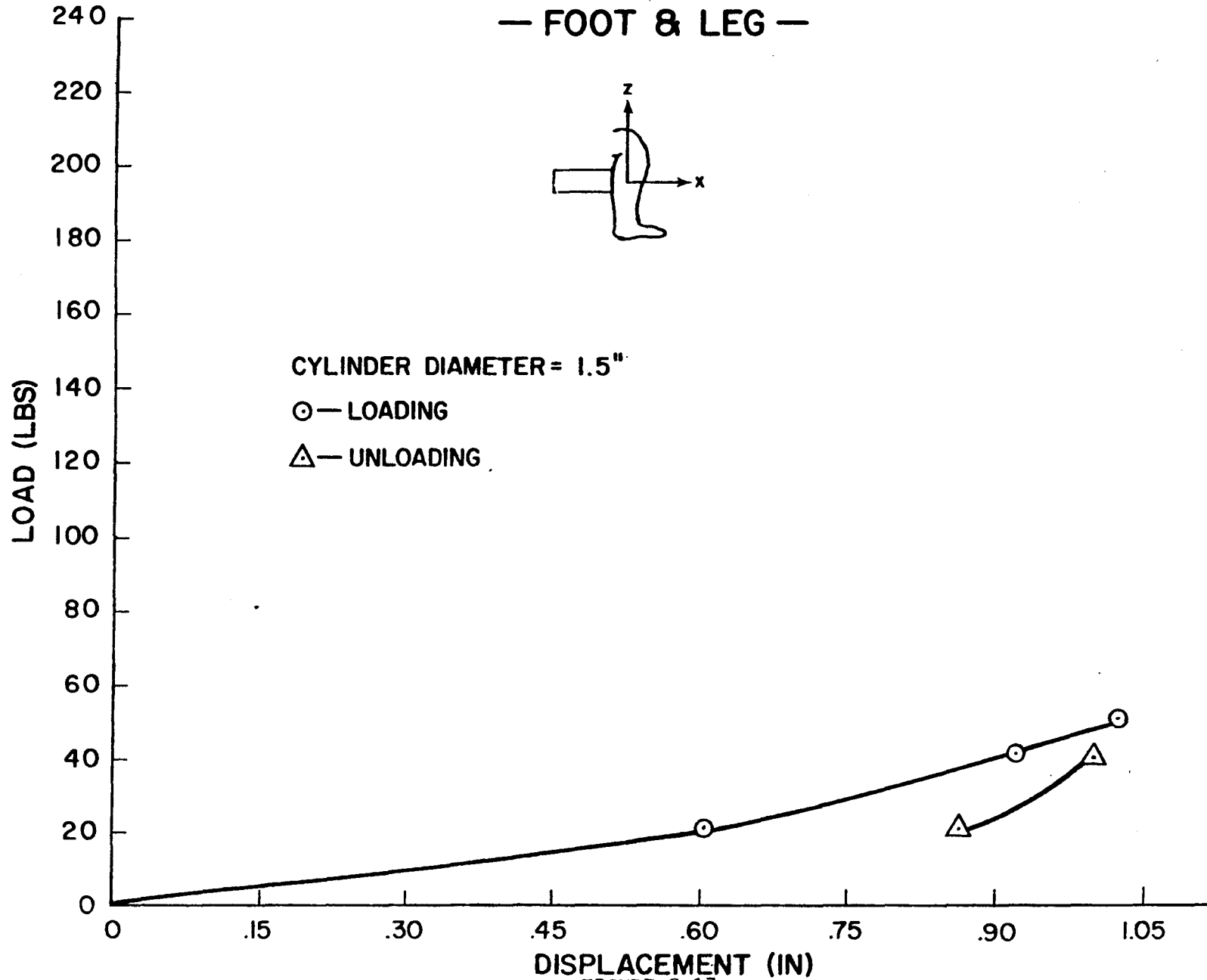


FIGURE C-17.

LOAD DEFORMATION PROPERTIES OF MALE DUMMY SEGMENT -SCULL CAP-

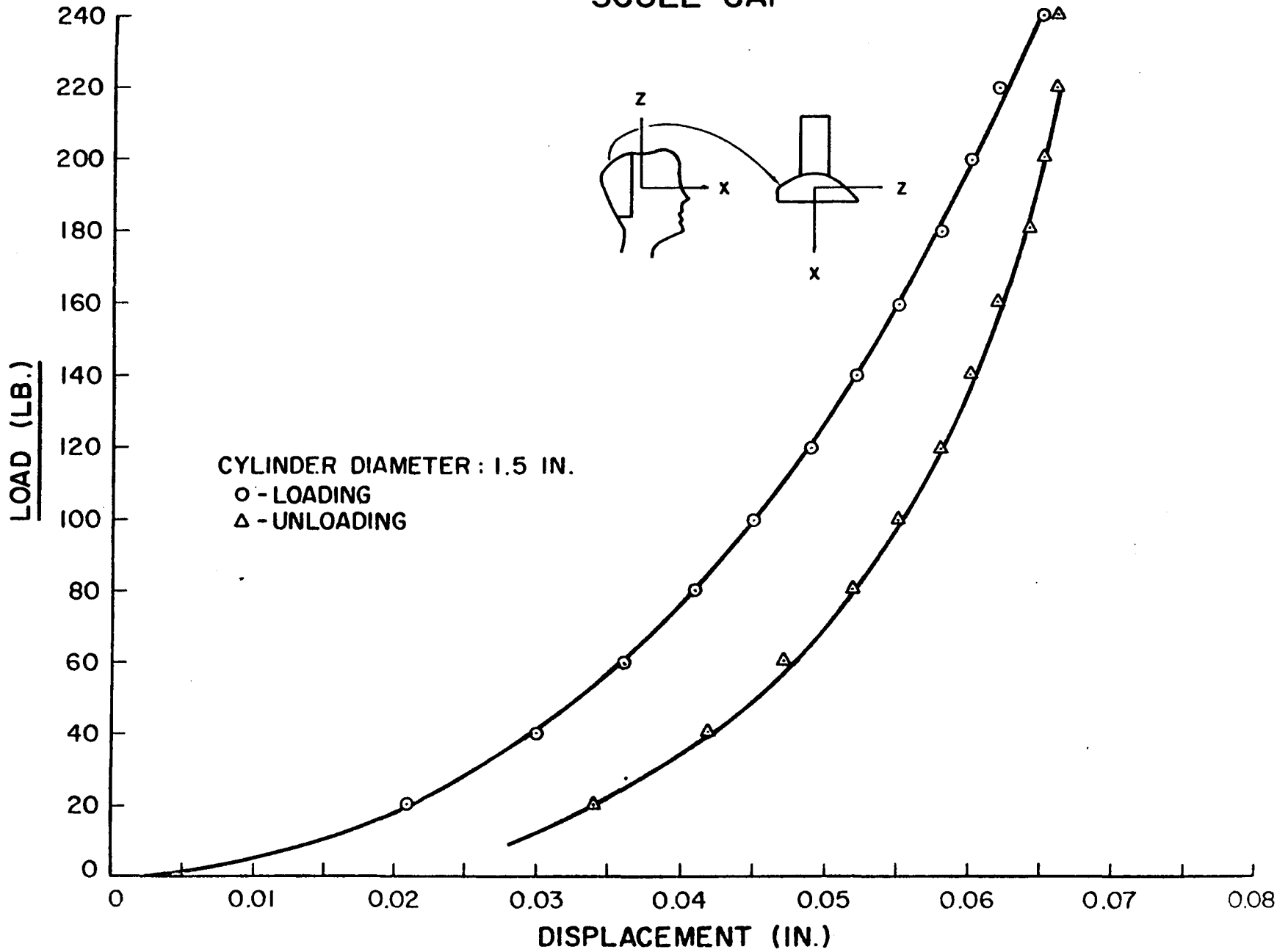


FIGURE C-18.

C-18

FORCE DEFORMATION PROPERTIES OF MALE DUMMY SEGMENTS - CHEST (FRONT) -

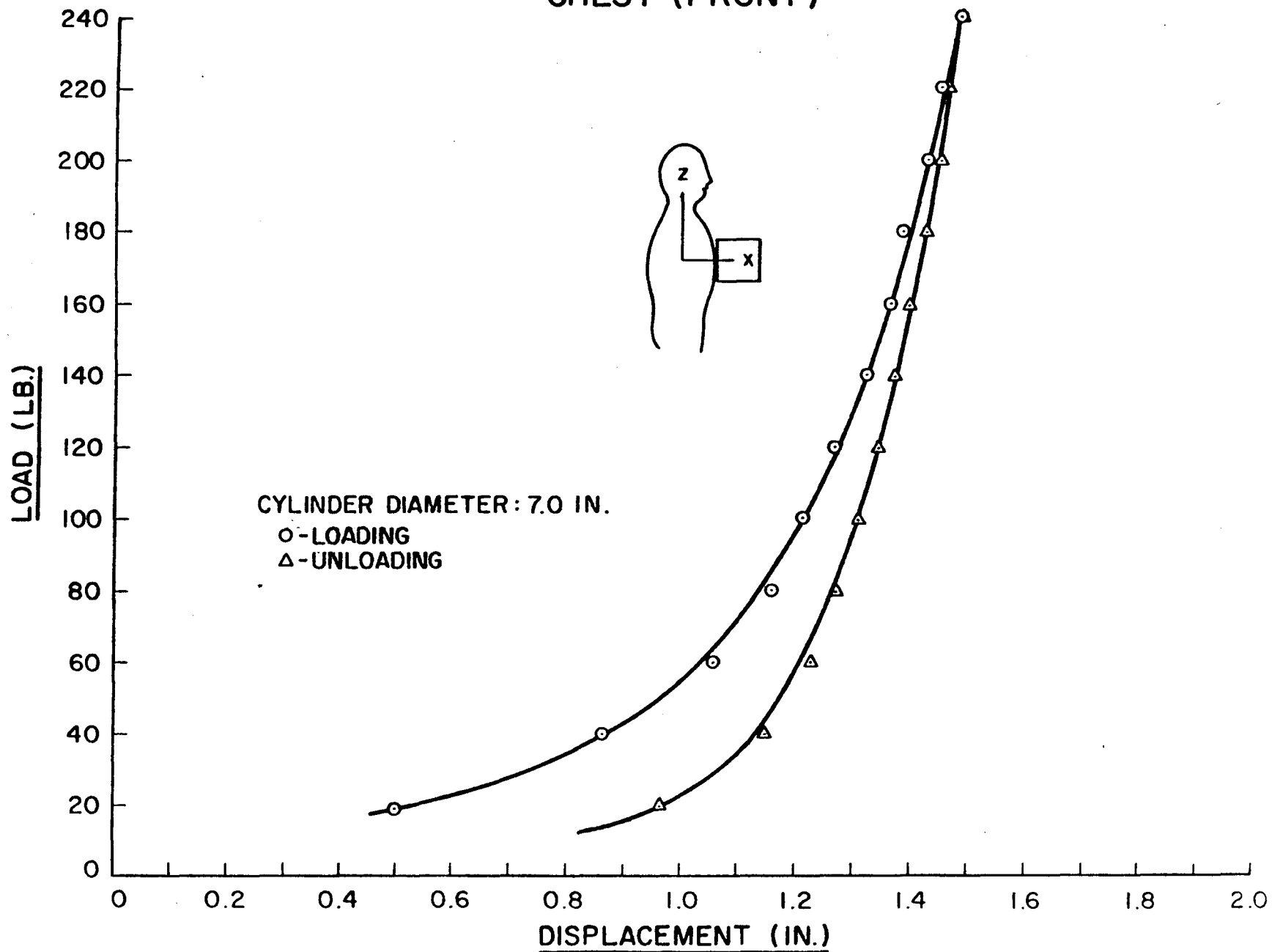


FIGURE C-19.

FORCE DEFORMATION PROPERTIES OF MALE DUMMY SEGMENTS — ABDOMEN —

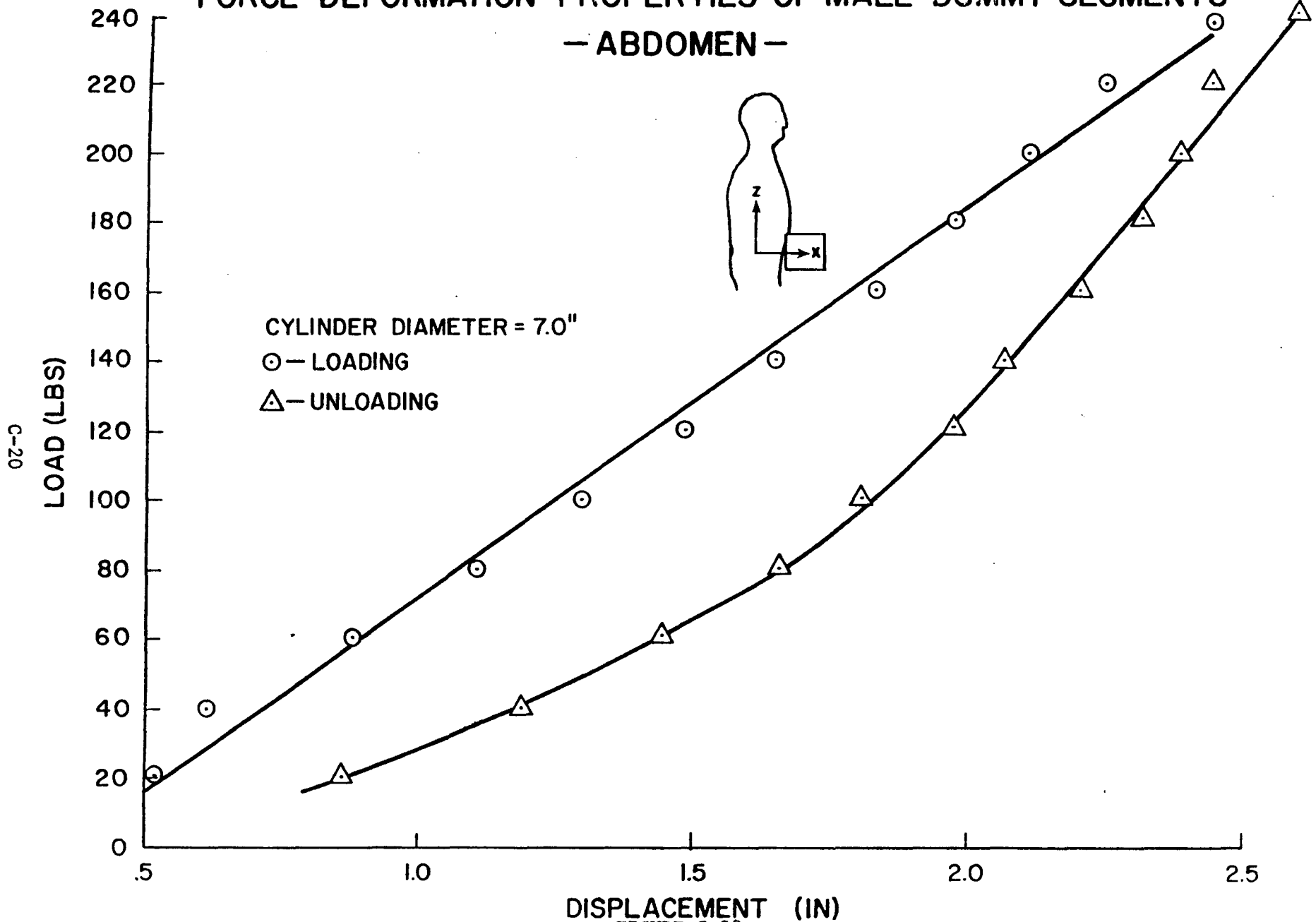


FIGURE C-20.

FORCE DEFORMATION PROPERTIES OF MALE DUMMY SEGMENTS

— POSTERIOR —

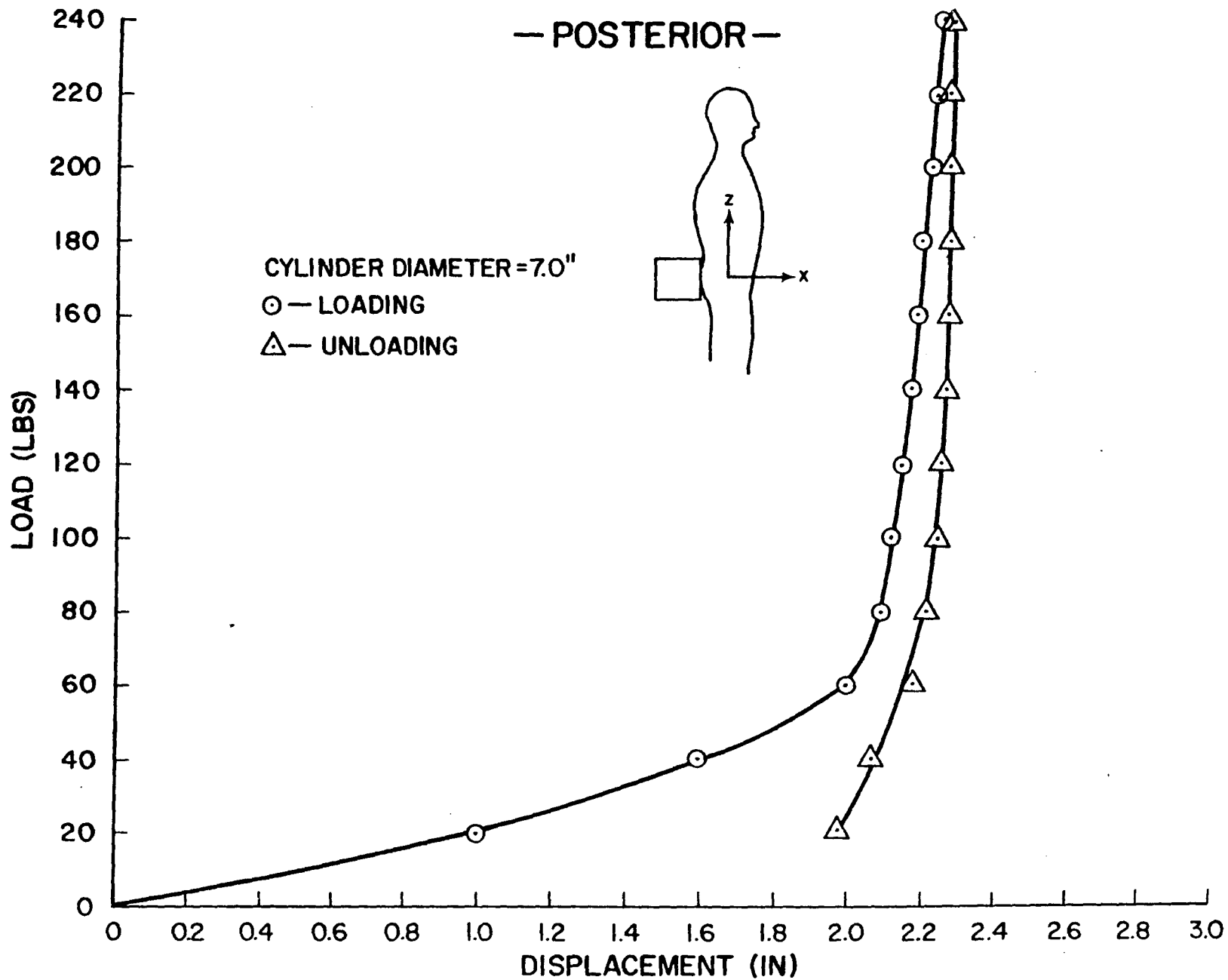
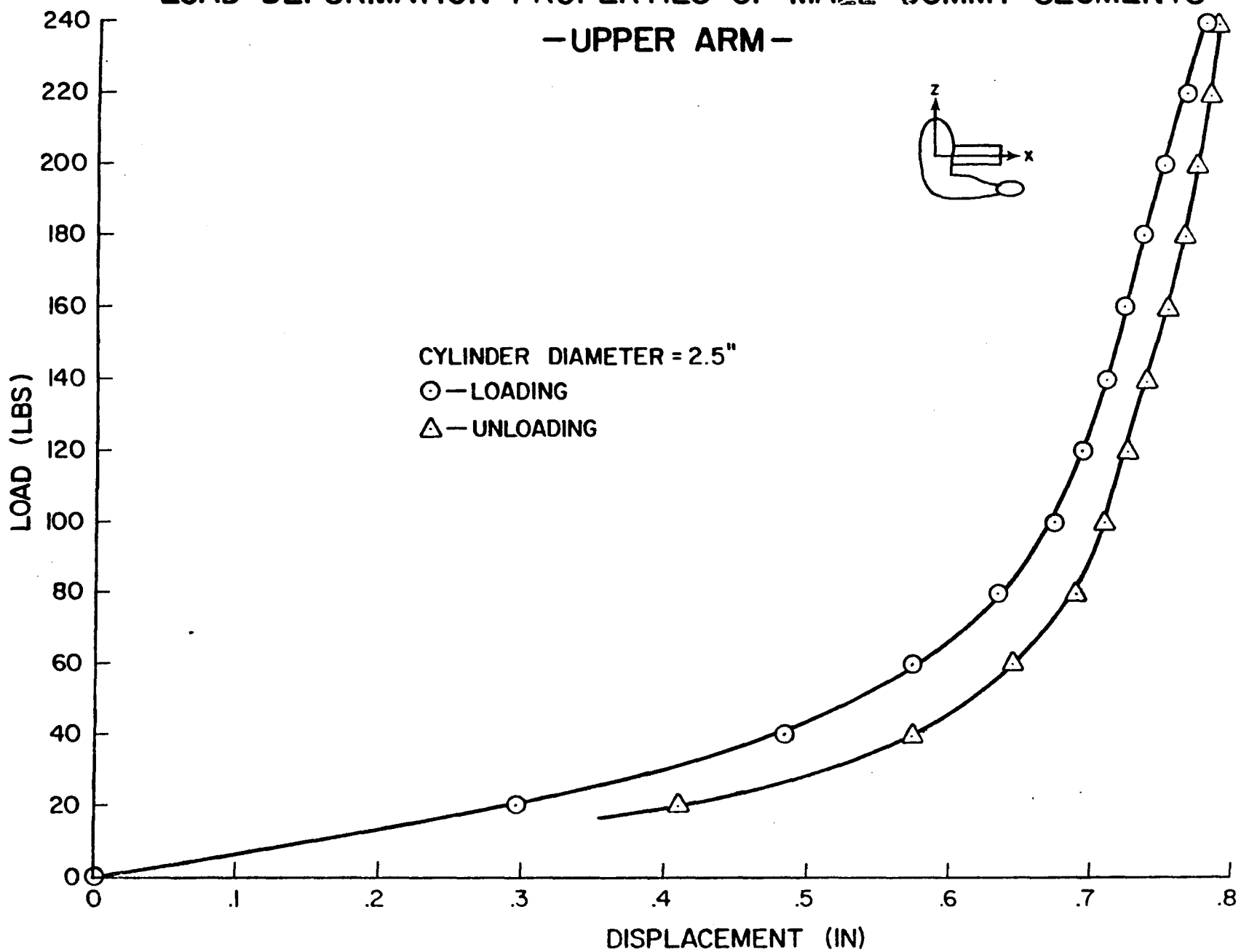


FIGURE C-21.

LOAD DEFORMATION PROPERTIES OF MALE DUMMY SEGMENTS — UPPER ARM —

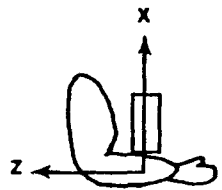


DISPLACEMENT (IN)

FIGURE C-22.

LOAD DEFORMATION PROPERTIES OF MALE DUMMY SEGMENTS

— LOWER ARM —



CYLINDER DIAMETER = 2.5"

○ — LOADING

△ — UNLOADING

C-23

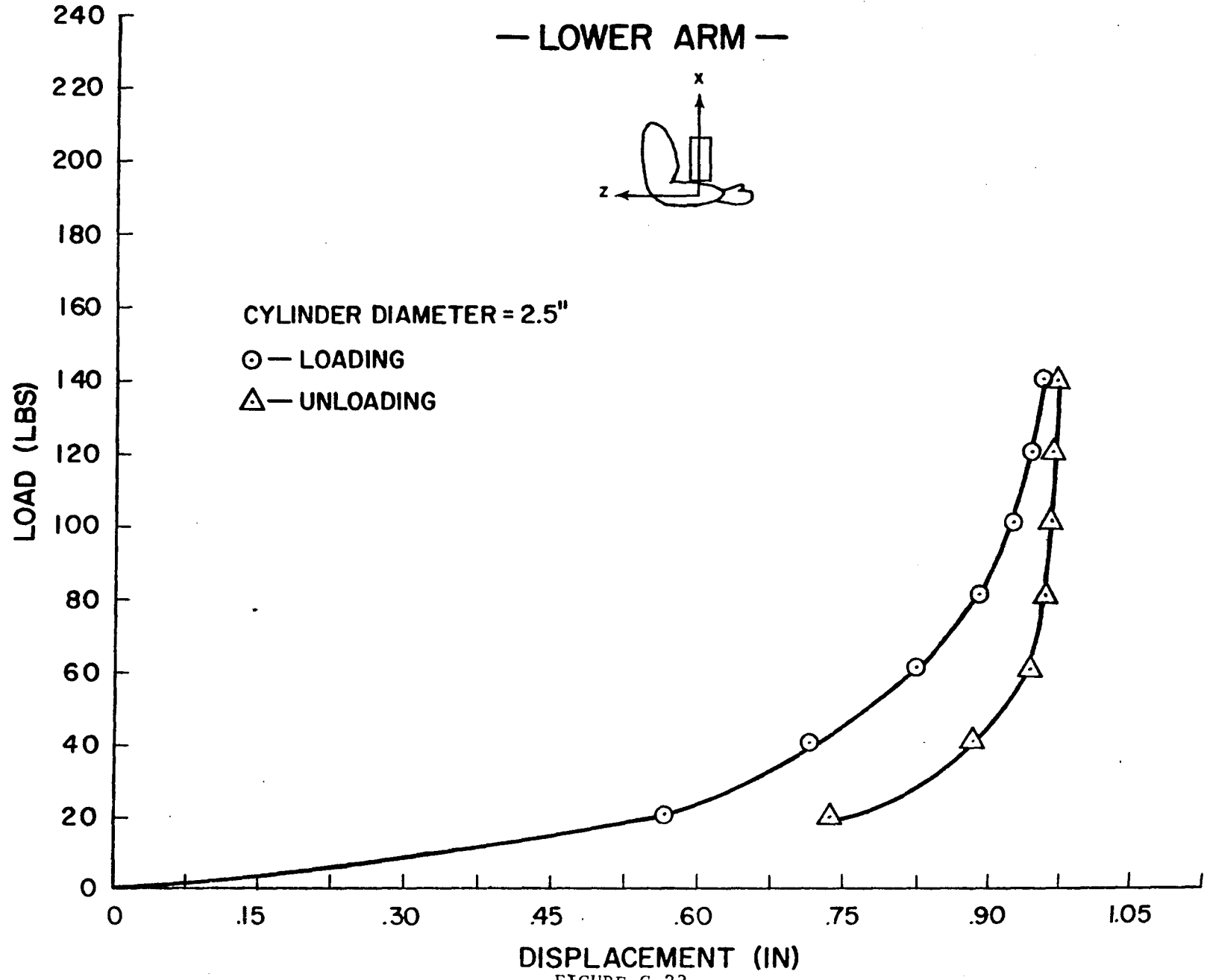
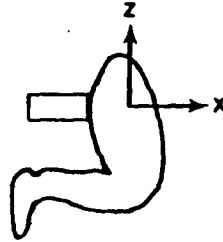


FIGURE C-23.

FORCE DEFORMATION PROPERTIES OF MALE DUMMY SEGMENTS

— UPPER LEG —



CYLINDER DIAMETER = 5.0"

○ — LOADING

△ — UNLOADING

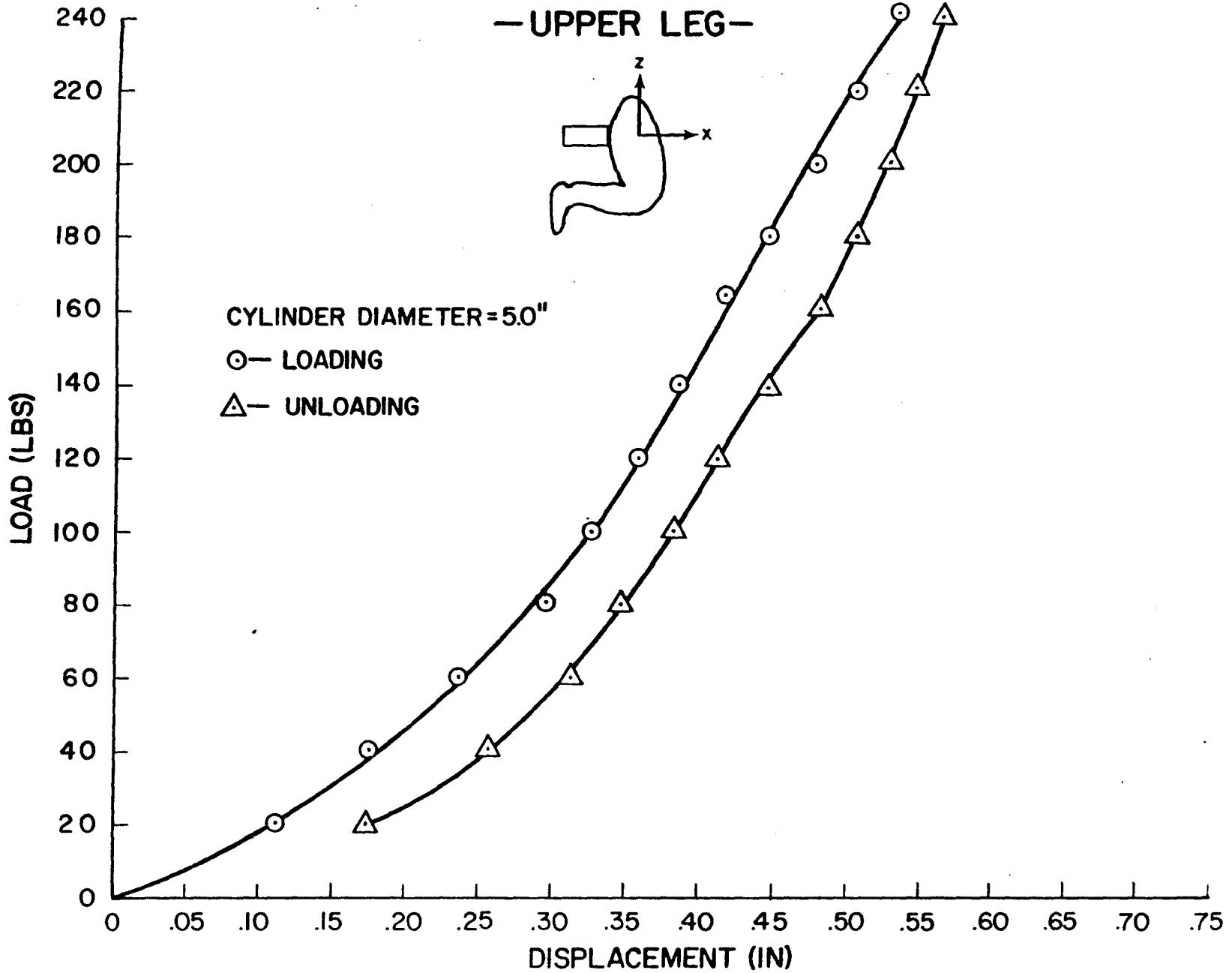


FIGURE C-24.

LOAD DEFORMATION PROPERTIES OF MALE DUMMY SEGMENTS

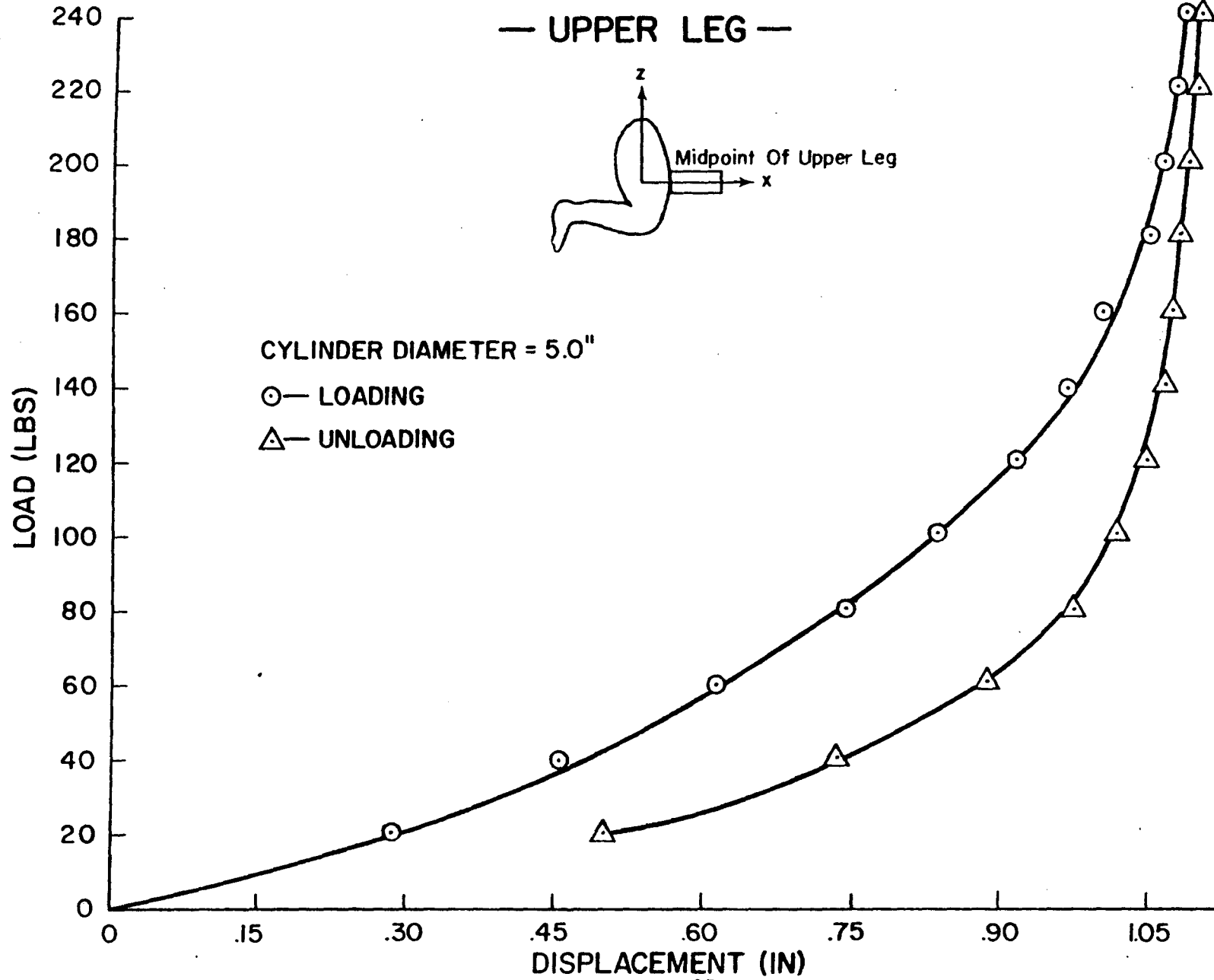
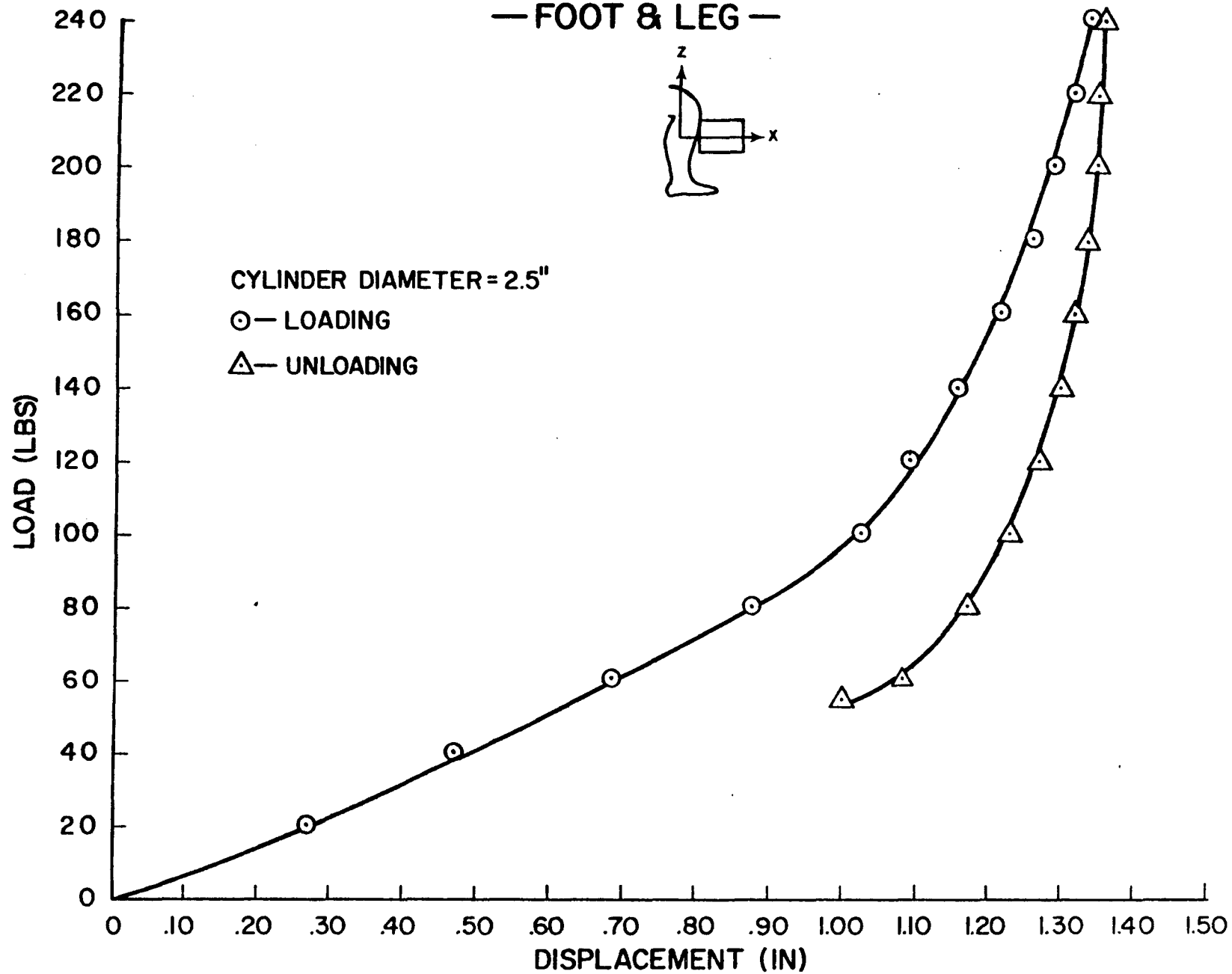


FIGURE C-25.

LOAD DEFORMATION PROPERTIES OF MALE DUMMY SEGMENTS — FOOT & LEG —



C-26

FIGURE C-26.

LOAD DEFORMATION PROPERTIES OF MALE DUMMY SEGMENTS — FOOT & LEG —

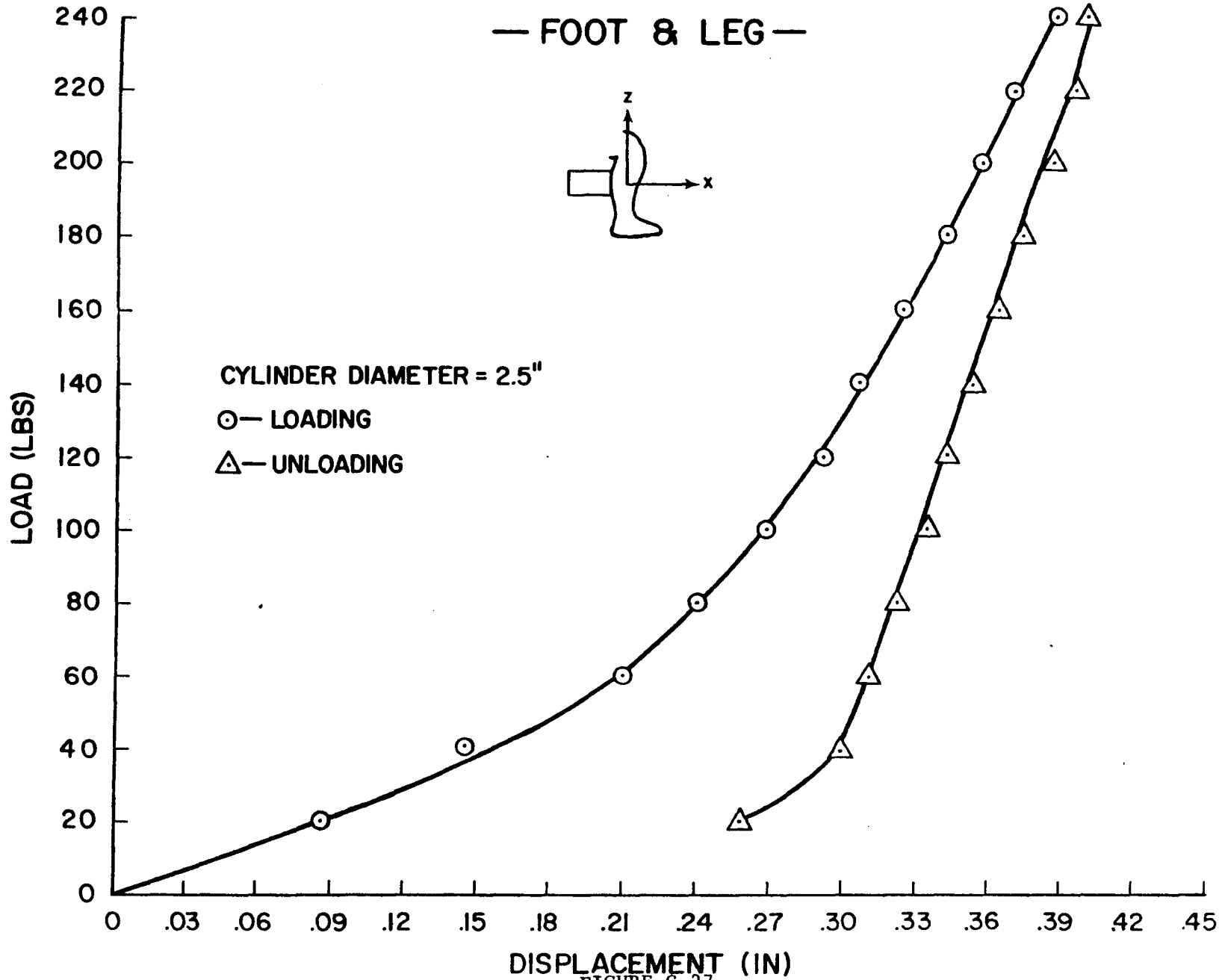


FIGURE C-27.

APPENDIX D

TABULATION OF IMPACT CONDITIONS

TABLE D-1. IMPACT CONDITIONS, TEST C-1

$$X'_{T1} = -24.0 \text{ in.}$$

$$Y'_{T1} = 4.2 \text{ in.}$$

$$Z'_{T1} = 6.6 \text{ in.}$$

$$\dot{Z}_{T1} = -123.6 \text{ in./sec}$$

SEGMENT NO.	ANGLES (RADIANS)			
	ϕ	θ	ψ	α
1	-1.5708	1.5708	0.0	-
2	-1.5708	1.5708	0.0	-
3	-1.5708	1.9155	0.0	-
4	-1.5708	1.5708	0.0	-
5	-1.5708	1.5708	0.0	-
6	-1.5708	1.5708	0.0	-
9	-1.5708	1.2741	0.0	-
10	-1.5708	1.2741	0.0	-
7	-	-	-	-0.0698
8	-	-	-	-0.5048
11	-	-	-	0.3011
12	-	-	-	0.3011

TABLE D-2. IMPACT CONDITIONS, TEST C-2

$$X'_{T1} = -24.0 \text{ in.}$$

$$Y'_{T1} = -2.7 \text{ in.}$$

$$Z'_{T1} = 6.6 \text{ in.}$$

$$\dot{Z}_{T1} = -176.4 \text{ in./sec}$$

SEGMENT NO.	ANGLES (RADIANS)			
	ϕ	θ	ψ	α
1	-1.5708	1.6319	-0.0262	-
2	-1.5708	1.6319	-0.0262	-
3	-1.5708	1.9330	-0.0262	-
4	-1.5708	1.6319	-0.0262	-
5	-1.5707	1.6275	-0.0262	-
6	-1.5707	1.6216	-0.0262	-
9	-1.5691	1.5665	-0.0261	-
10	-1.5691	1.5665	-0.0261	-
7	-	-	-	-0.2138
8	-	-	-	-0.650
11	-	-	-	0.0916
12	-	-	-	0.0916

TABLE D-3. IMPACT CONDITIONS, TEST C-3

$$X'_{T1} = -24.0 \text{ in.}$$

$$Y'_{T1} = 2.3 \text{ in.}$$

$$Z'_{T1} = 6.6 \text{ in.}$$

$$\dot{Z}_{T1} = -196.8 \text{ in./sec}$$

SEGMENT NO.	ANGLES (RADIAN)			
	ϕ	θ	ψ	α
1	-1.5708	1.5708	0.0785	-
2	-1.5708	1.5708	0.0785	-
3	-1.5708	1.8239	0.0785	-
4	-1.5708	1.5708	0.0785	-
5	-1.5667	1.6230	0.0786	-
6	-1.5667	1.6230	0.0786	-
9	-1.5691	1.5665	-0.0261	-
10	-1.5691	1.5665	-0.0261	-
7	-	-	-	0.1004
8	-	-	-	0.1004
11	-	-	-	0.2094
12	-	-	-	0.2094

TABLE D-4. IMPACT CONDITIONS, TEST C-4

$$X'_{T1} = -12.0 \text{ in.}$$

$$Y'_{T1} = -5.0 \text{ in.}$$

$$Z'_{T1} = 6.0 \text{ in.}$$

$$\dot{Z}_{T1} = -255.6 \text{ in./sec}$$

SEGMENT NO.	ANGLES (RADIANS)			
	ϕ	θ	ψ	α
1	-1.5708	1.5490	0.2094	-
2	-1.5708	1.5490	0.2094	-
3	1.6061	-1.7279	-2.9614	-
4	-1.5708	1.5490	0.2094	-
5	-1.5708	1.5708	0.2094	-
6	-1.5708	1.5708	0.2094	-
9	1.5166	-1.3090	-2.8304	-
10	-1.6250	1.3090	0.3112	-
7	-	-	-	0.0017
8	-	-	-	0.0017
11	-	-	-	0.0019
12	-	-	-	0.0019

TABLE D-5. IMPACT CONDITIONS, TEST C-5

$$X'_{T1} = -24.0 \text{ in.}$$

$$Y'_{T1} = -15.5 \text{ in.}$$

$$Z'_{T1} = 6.0 \text{ in.}$$

$$\dot{Z}_{T1} = -217.2 \text{ in./sec}$$

SEGMENT NO.	ANGLES (RADIANS)			
	ϕ	θ	ψ^*	α
1	-1.5708	1.5708	-2.6180	-
2	-1.5708	1.5708	-2.6180	-
3	-1.5708	1.5708	-2.6180	-
4	-1.5708	1.5708	-2.6180	-
5	-1.5708	1.5708	-2.6180	-
6	-1.6363	1.8103	-2.6108	-
9	-1.3908	1.8715	-2.5913	-
10	-1.3908	1.8715	-2.5913	-
7	-	-	-	0.0
8	-	-	-	0.0
11	-	-	-	0.6981
12	-	-	-	0.6981

* $\dot{\psi}_n = .23 \text{ rad/sec}$ $n = 1, 2, 3, 4, 5, 6, 9, 10$

i.e. (body has rigid body rotation only)

TABLE D-6. IMPACT CONDITIONS, TEST F-1

$$X'_{T1} = -30.0 \text{ in.}$$

$$Y'_{T1} = -4.3 \text{ in.}$$

$$Z'_{T1} = 6.0 \text{ in.}$$

$$\dot{Z}_{T1} = -183.6 \text{ in./sec}$$

SEGMENT NO.	ANGLES (RADIANs)			
	ϕ	θ	ψ	α
1	-1.5656	1.5969	0.0347	-
2	-1.5656	1.5969	0.0347	-
3	-1.5694	1.4879	0.0344	-
4	-1.5656	1.5969	0.0347	-
5	-1.5629	1.6753	-0.0205	-
6	-1.5629	1.6753	-0.0205	-
9	-1.5708	1.4486	0.0349	-
10	-1.5708	1.4486	0.0349	-
7	-	-	-	-0.2880
8	-	-	-	-0.30
11	-	-	-	0.0
12	-	-	-	0.0087

TABLE D-7. IMPACT CONDITIONS, TEST F-2

$$X'_{T1} = -24.0 \text{ in.}$$

$$Y'_{T1} = -6.5 \text{ in.}$$

$$Z'_{T1} = 6.5 \text{ in.}$$

$$\dot{Z}_{T1} = -183.6 \text{ in./sec}$$

SEGMENT NO.	ANGLES (RADIANS)			
	ϕ	θ	ψ	α
1	-1.5654	1.6039	0.0347	-
2	-1.5654	1.6039	0.0347	-
3	-1.5692	1.4948	0.0347	-
4	-1.5654	1.6039	0.0347	-
5	-1.5526	1.9527	0.0373	-
6	-1.5526	1.9527	0.0373	-
9	-1.5708	1.4486	0.0349	-
10	-1.5696	1.4835	0.0333	-
7	-	-	-	-0.2880
8	-	-	-	-0.5236
11	-	-	-	0.0175
12	-	-	-	0.0436

TABLE D-8. IMPACT CONDITIONS, TEST F-3

Note: Due to a loss of high-speed film, impact conditions could not be determined for Test F-3.

TABLE D-9. IMPACT CONDITIONS, TEST F-4

$$X'_{T1} = -24.0 \text{ in.}$$

$$Y'_{T1} = -4.5 \text{ in.}$$

$$Z'_{T1} = 11.0 \text{ in.}$$

$$\dot{Z}_{T1} = -205.2 \text{ in./sec}$$

SEGMENT NO.	ANGLES (RADIANS)			
	ϕ	θ	ψ	α
1	-1.4893	1.4869	1.0823	-
2	-1.4893	1.4869	1.0823	-
3	-1.4893	1.4869	1.0780	-
4	-1.4893	1.4869	1.0823	-
5	0.4719	-1.0866	-1.6833	-
6	-2.0702	1.2226	1.2103	-
9	-1.5708	1.4443	1.0908	-
10	1.5326	-1.3260	-2.0398	-
7	-	-	-	-1.4661
8	-	-	-	-0.6894
11	-	-	-	1.3962
12	-	-	-	0.0

TABLE D-10. IMPACT CONDITIONS, TEST F-5

$$X'_{T1} = -14.0 \text{ in.}$$

$$Y'_{T1} = -11.0 \text{ in.}$$

$$Z'_{T1} = 1.2 \text{ in.}$$

$$\dot{Z}_{T1} = 0.0 \text{ in./sec}$$

SEGMENT NO.	ANGLES (RADIANs)			
	ϕ	θ	ψ	α
1	-1.5708	1.3788	-3.0892	-
2	-1.5708	1.3788	-3.0892	-
3	-1.5572	1.6403	-3.0906	-
4	-1.5708	1.3788	-3.0892	-
5	-1.5599	1.5880	-3.0907	-
6	-1.5599	1.5880	-3.0907	-
9	-1.5499	1.7797	-3.0896	-
10	-1.5499	1.7797	-3.0896	-
7	-	-	-	-1.3264
8	-	-	-	-1.5708
11	-	-	-	0.2618
12	-	-	-	0.0873

TABLE D-11. IMPACT CONDITIONS, TEST F-6

$$X'_{T1} = -21.0 \text{ in.}$$

$$Y'_{T1} = -13.5 \text{ in.}$$

$$Z'_{T1} = 6.7 \text{ in.}$$

$$\dot{Z}_{T1} = -154.8 \text{ in./sec}$$

SEGMENT NO.	ANGLES (RADIANS)			
	ϕ	θ	ψ	α
1	-1.5708	1.6057	0.1571	-
2	-1.5708	1.6057	0.1571	-
3	-1.5430	1.7781	0.1604	-
4	-1.5708	1.6057	0.1571	-
5	-1.5402	1.7953	0.1611	-
6	-1.5402	1.7953	0.1611	-
9	-1.6095	1.3644	0.1604	-
10	-1.6095	1.3644	0.1604	-
7	-	-	-	-0.1396
8	-	-	-	-0.1396
11	-	-	-	-0.1047
12	-	-	-	-0.1047

TABLE D-12. IMPACT CONDITIONS, TEST F-7

$$X'_{T1} = -24.0 \text{ in.}$$

$$Y'_{T1} = -12.0 \text{ in.}$$

$$Z'_{T1} = -5.5 \text{ in.}$$

$$\dot{Z}_{T1} = -136.8 \text{ in./sec}$$

SEGMENT NO.	ANGLES (RADIANS)			
	ϕ	θ	ψ	α
1	-2.8461	2.9283	-3.0158	-
2	-2.8461	2.9283	-3.0158	-
3	-2.7266	3.0314	-2.8977	-
4	-2.8461	2.9283	-3.0158	-
5	-2.8967	2.7893	-3.0645	-
6	-2.8968	2.7893	-3.0646	-
9	0.0040	2.9845	-0.1706	-
10	0.0054	2.9845	-0.1692	-
7	-	-	-	-1.5708
8	-	-	-	-1.5708
11	-	-	-	0.0
12	-	-	-	0.0

TABLE D-13. IMPACT CONDITIONS, TEST F-8

$$X'_{T1} = -24.0 \text{ in.}$$

$$Y'_{T1} = -16.0 \text{ in.}$$

$$Z'_{T1} = 17.0 \text{ in.}$$

$$\dot{Z}_{T1} = -136.8 \text{ in./sec}$$

SEGMENT NO.	ANGLES (RADIANS)			
	ϕ	θ	ψ	α
1	-1.5554	1.5562	0.9677	-
2	1.6581	-1.6057	-2.1731	-
3	-1.3386	1.7039	0.9807	-
4	-1.6274	1.5068	0.9705	-
5	-1.4835	1.6057	0.9685	-
6	2.1323	-1.7008	-2.1283	-
9	-0.1478	-0.9221	-1.0000	-
10	-1.5554	1.5562	0.9677	-
7	-	-	-	-1.3963
8	-	-	-	-0.6981
11	-	-	-	1.5708
12	-	-	-	1.2217

TABLE D-14. IMPACT CONDITIONS, TEST M-1

$$X'_{T1} = -18.0 \text{ in.}$$

$$Y'_{T1} = -2.9 \text{ in.}$$

$$Z'_{T1} = 9.0 \text{ in.}$$

$$\dot{Z}'_{T1} = -108.0 \text{ in./sec}$$

SEGMENT NO.	ANGLES (RADIANS)			
	ϕ	θ	ψ	α
1	-1.5708	-15884 ?	0.0545	-
2	-1.5708	1.5884	0.0545	-
3	-1.5634	1.5884	0.0552	-
4	-1.5708	1.5884	0.0545	-
5	-1.5708	1.5884	0.0545 OK	-
6	-1.5708	1.5884	-0.0545 ?	-
9	-1.5708	1.6668	0.0611	-
10	-1.5708	1.6668	0.0611	-
7	-	-	-	-0.2051
8	-	-	-	-0.366
11	-	-	-	0.0698
12	-	-	-	0.20

TABLE D-15. IMPACT CONDITIONS, TEST M-2

$$X'_{T1} = -18.0 \text{ in.}$$

$$Y'_{T1} = -3.9 \text{ in.}$$

$$Z'_{T1} = 8.0 \text{ in.}$$

$$\dot{Z}_{T1} = -108.0 \text{ in./sec}$$

SEGMENT NO.	ANGLES (RADIANs)			
	ϕ	θ	ψ	α
1	-1.5708	1.6145	0.0937	-
2	-1.5725	1.6145	0.0937	-
3	-1.5436	1.8925	0.0987	-
4	-1.5708	1.6145	0.0937	-
5	-1.5533	1.7969	0.0961	-
6	-1.5533	1.7969	0.0961	-
9	-1.5708	1.6319	0.0960	-
10	-1.5708	1.6319	0.0960	-
7	-	-	-	-0.4712
8	-	-	-	-0.7240
11	-	-	-	0.0349
12	-	-	-	0.0349

TABLE D-16. IMPACT CONDITIONS, TEST M-3

$$X'_{T1} = -24.0 \text{ in.}$$

$$Y'_{T1} = -1.9 \text{ in.}$$

$$Z'_{T1} = 8.0 \text{ in.}$$

$$\dot{Z}_{T1} = -182.4 \text{ in./sec}$$

SEGMENT NO.	ANGLES (RADIANs)			
	ϕ	θ	ψ	α
1	-1.6077	1.5552	-1.0128	-
2	-1.6078	1.5552	-1.0128	-
3	-1.5930	1.5460	-1.0131	-
4	-1.6078	1.5552	-1.0128	-
5	-1.8406	1.2033	-0.9676	-
6	-1.5523	1.6440	-1.0112	-
9	-1.5708	1.6144	-1.0123	-
10	-1.5375	1.5936	-1.0112	-
7	-	-	-	0.0
8	-	-	-	-0.0262
11	-	-	-	0.1571
12	-	-	-	0.1265

TABLE D-17. IMPACT CONDITIONS, TEST M-4

$$X'_{T1} = -24.0 \text{ in.}$$

$$Y'_{T1} = -2.0 \text{ in.}$$

$$Z'_{T1} = 27.0 \text{ in.}$$

$$\dot{Z}_{T1} = -217.0 \text{ in./sec}$$

SEGMENT NO.	ANGLES (RADIANS)			
	ϕ	θ	ψ	α
1	-1.5126	1.5506	1.0753	-
2	-1.5126	1.5506	1.0753	-
3	-1.6397	1.4825	1.0822	-
4	-1.5126	1.5506	1.0753	-
5	-1.5624	1.6427	1.0740	-
6	-1.0506	0.8783	0.8999	-
9	-1.5708	1.6581	1.0734	-
10	-1.3917	1.7520	1.0974	-
7	-	-	-	-0.0436
8	-	-	-	-0.0524
11	-	-	-	0.0044
12	-	-	-	0.0131

TABLE D-18. IMPACT CONDITIONS, TEST M-5

$$X'_{T1} = -24.0 \text{ in.}$$

$$Y'_{T1} = -4.9 \text{ in.}$$

$$Z'_{T1} = 9.0 \text{ in.}$$

$$\dot{Z}_{T1} = -123.6 \text{ in./sec}$$

SEGMENT NO.	ANGLES (RADIANs)			
	ϕ	θ	ψ	α
1	-1.5446	1.6371	-0.0506	-
2	-1.5446	1.6371	-0.0506	-
3	-1.5529	1.7975	-0.05417	-
4	-1.5446	1.6371	-0.0506	-
5	-1.9248	1.8786	-0.1725	-
6	-1.1955	1.7380	0.0069	-
9	-1.5357	1.4628	-0.0508	-
10	-1.5357	1.4628	-0.0508	-
7	-	-	-	0.0
8	-	-	-	0.0
11	-	-	-	0.0873
12	-	-	-	0.2618

TABLE D-19. IMPACT CONDITIONS, TEST M-6

$$X'_{T1} = -24.0 \text{ in.}$$

$$Y'_{T1} = -3.9 \text{ in.}$$

$$Z'_{T1} = 8.0 \text{ in.}$$

$$\dot{Z}_{T1} = -123.6 \text{ in./sec}$$

SEGMENT NO.	ANGLES (RADIAN)			
	ϕ	θ	ψ	α
1	-1.5708	1.7104	-0.0349	-
2	-1.5708	1.7104	-0.0349	-
3	-1.5678	1.6232	-0.0393	-
4	-1.5708	1.7104	-0.0349	-
5	-2.0892	1.5534	-0.1172	-
6	-1.0425	1.5880	0.0232	-
9	-1.5641	1.5186	-0.0351	-
10	-1.5641	1.5186	-0.0351	-
7	-	-	-	0.0
8	-	-	-	0.0
11	-	-	-	0.2094
12	-	-	-	0.2094

TABLE D-20. IMPACT CONDITIONS, TEST M-7

$$X'_{T1} = -24.0 \text{ in.}$$

$$Y'_{T1} = -2.5 \text{ in.}$$

$$Z'_{T1} = 7.7 \text{ in.}$$

$$\dot{Z}_{T1} = 192.00 \text{ in./sec}$$

SEGMENT NO.	ANGLES (RADIANs)			
	ϕ	θ	ψ	α
1	-1.8328	1.6057	-0.6451	-
2	-1.8328	1.6057	-0.6451	-
3	-1.8328	1.6057	-0.6451	-
4	-1.8328	1.6057	-0.6451	-
5	-2.1139	1.3972	-0.6254	-
6	-1.3956	1.9078	-0.5621	-
9	-1.5708	1.5533	-0.6109	-
10	-1.5708	1.5533	-0.6109	-
7	-	-	-	0.0
8	-	-	-	0.0
11	-	-	-	0.1745
12	-	-	-	0.1745

TABLE D-21. IMPACT CONDITIONS, TEST M-8

$$X'_{T1} = -24.0 \text{ in.}$$

$$Y'_{T1} = -14.0 \text{ in.}$$

$$Z'_{T1} = 4.5 \text{ in.}$$

$$\dot{Z}_{T1} = -202.8 \text{ in./sec}$$

SEGMENT NO.	ANGLES (RADIANS)			
	ϕ	θ	ψ	α
1	-1.5708	1.4137	3.1416	-
2	-1.5708	1.4137	3.1416	-
3	-1.5708	1.1519	3.1416	-
4	-1.5708	1.4137	3.1416	-
5	1.5708	-1.3617	-0.0701	-
6	1.2990	-1.8389	0.0460	-
9	-1.5708	1.5882	3.1411	-
10	-1.5708	1.5882	3.1411	-
7	-	-	-	0.0
8	-	-	-	0.0
11	-	-	-	0.4363
12	-	-	-	0.4363

TABLE D-22. IMPACT CONDITIONS, TEST M-9

$$X'_{T1} = -24.0 \text{ in.}$$

$$Y'_{T1} = -2.0 \text{ in.}$$

$$Z'_{T1} = 12.0 \text{ in.}$$

$$\dot{Z}_{T1} = -235.2 \text{ in./sec}$$

SEGMENT NO.	ANGLES (RADIANS)			
	ϕ	θ	ψ	α
1	-1.8336	1.6581	-0.7516	-
2	-1.8336	1.6581	-0.7516	-
3	-1.9552	1.7846	-0.7699	-
4	-1.9552	1.7846	-0.7699	-
5	-2.1514	1.6053	-0.7468	-
6	-1.8224	1.8259	-0.7983	-
9	-1.5945	1.4030	-0.7613	-
10	-1.5945	1.4030	-0.7613	-
7	-	-	-	0.0
8	-	-	-	0.0
11	-	-	-	0.0524
12	-	-	-	0.0524

APPENDIX E
ACCELEROMETER DATA

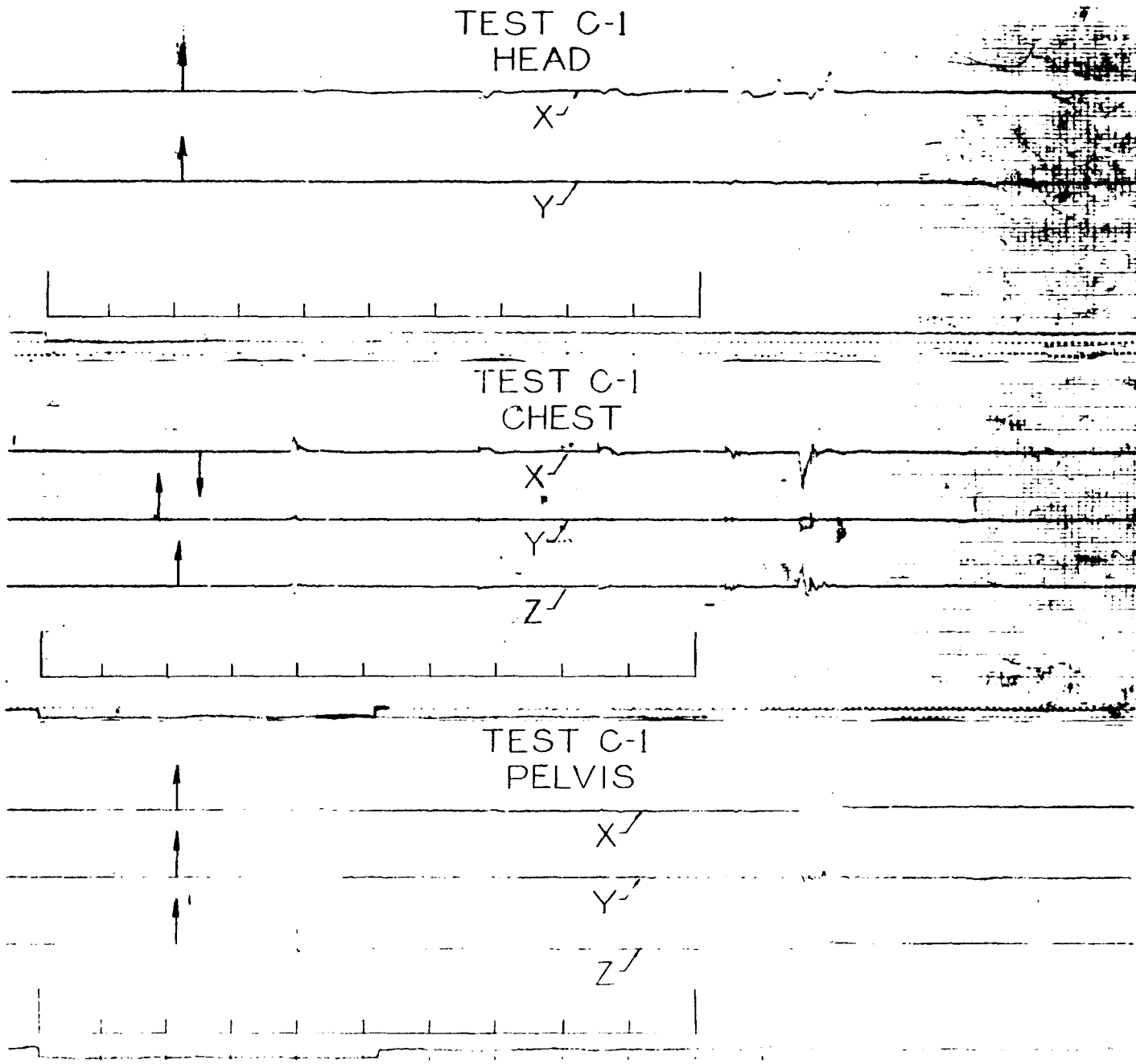


FIGURE E-1. ACCELEROMETER DATA, TEST C-1

TEST C-2
HEAD

X

Y

TEST C-2
CHEST

X

Y

Z

TEST C-2
PELVIS

X

Y

Z

E-2

FIGURE E-2. ACCELEROMETER DATA, TEST C-2

TEST C-3
HEAD

X✓

Y✓

TEST C-3
CHEST

X✓

Y✓

Z✓

TEST C-3
PELVIS

X✓

Y✓

E-3

FIGURE E-3. ACCELEROMETER DATA, TEST C-3

TEST C-4
HEAD

X✓

Y✓

TEST C-4
CHEST

X✓

Y✓

Z✓

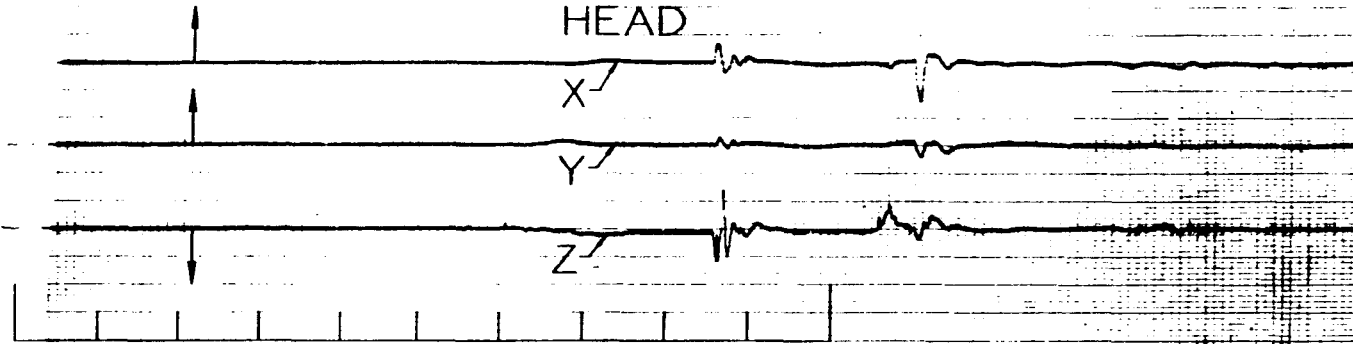
TEST C-4
PELVIS

X✓

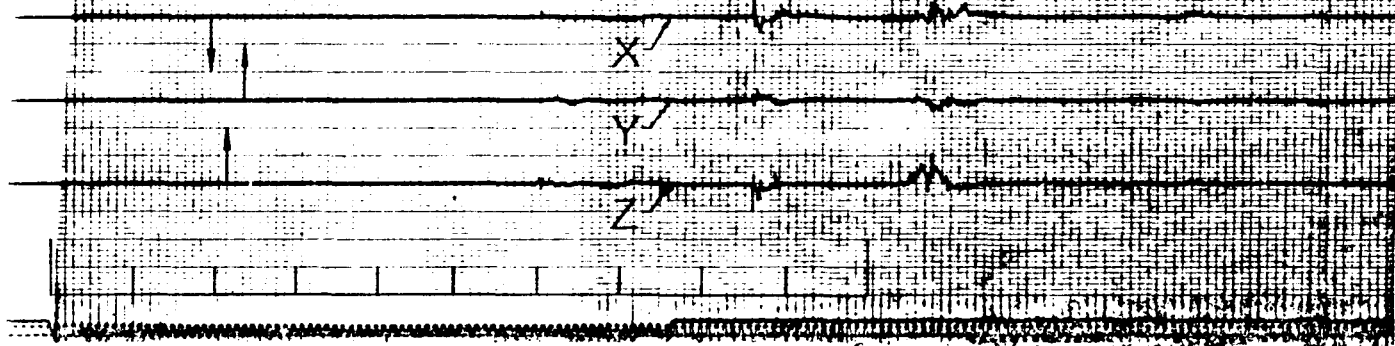
Y✓

FIGURE E-4. ACCELEROMETER DATA, TEST C-4

TEST C-5
HEAD



TEST C-5
CHEST



TEST C-5
PELVIS

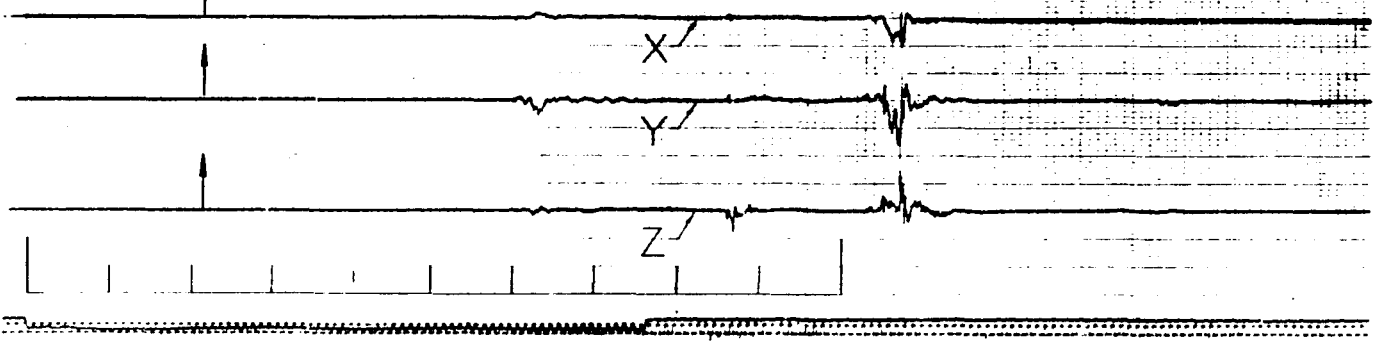
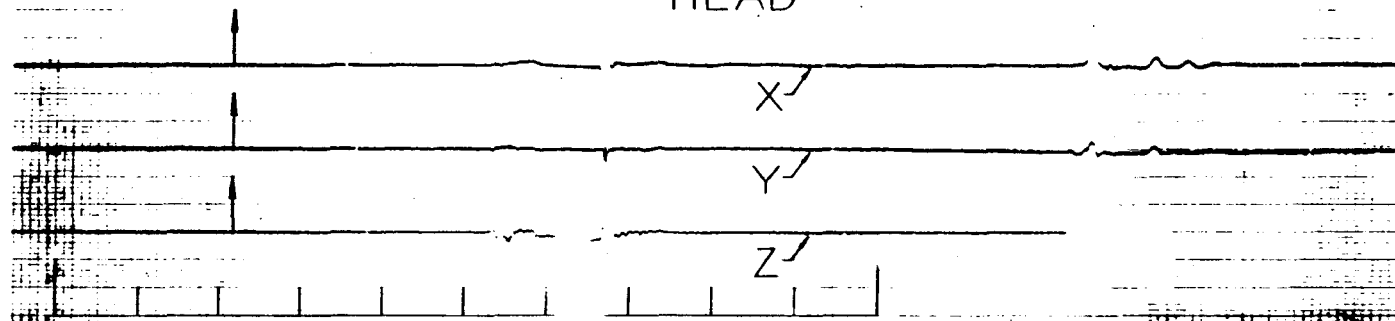


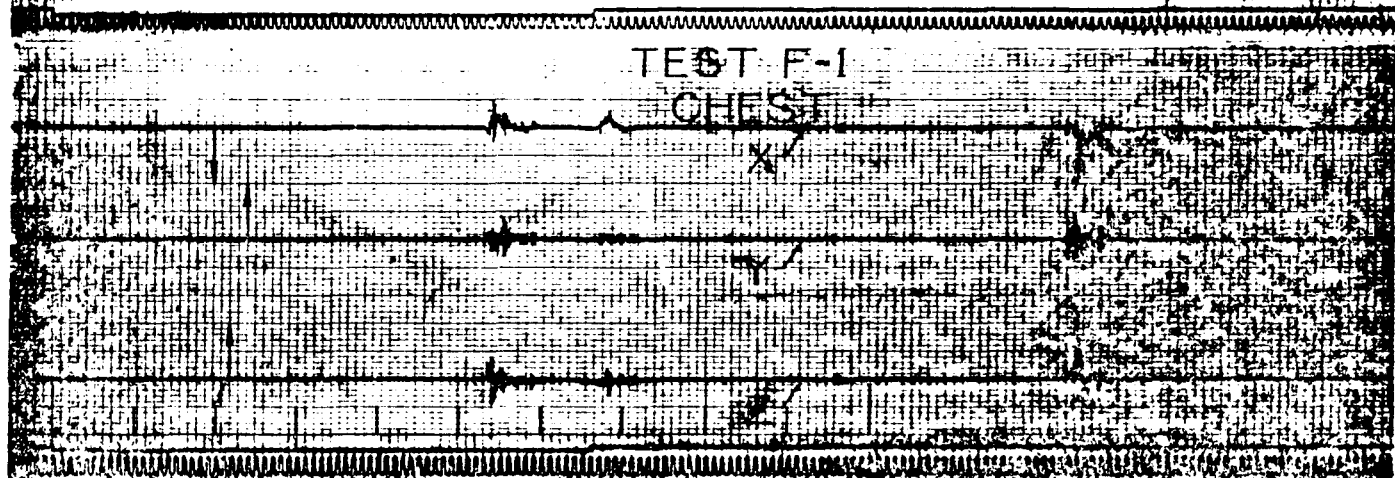
FIGURE E-5. ACCELEROMETER DATA, TEST C-5

E-5

TEST F-1
HEAD



TEST F-1
CHEST



TEST F-1
BELT

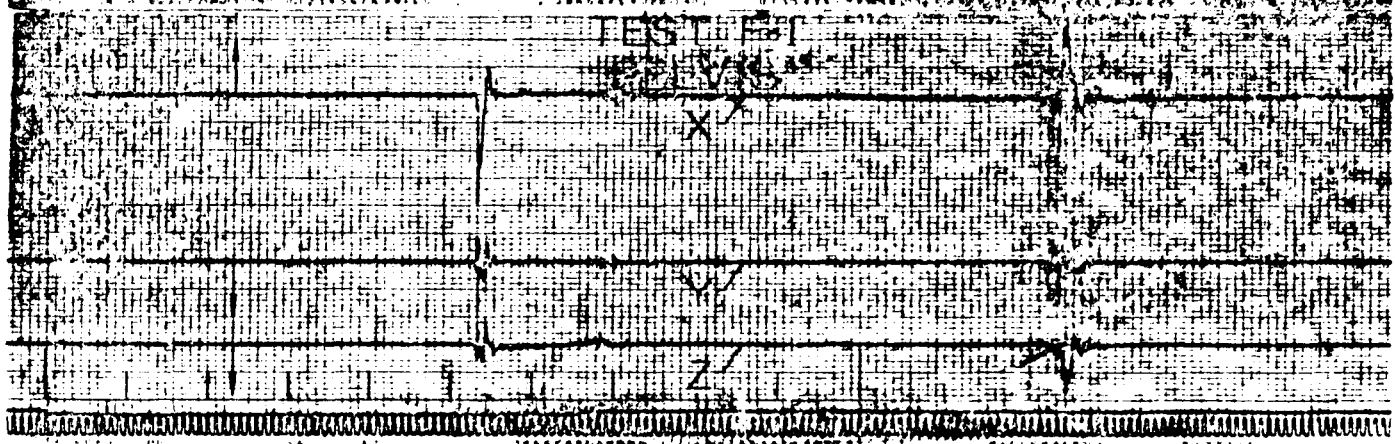


FIGURE E-6. ACCELEROMETER DATA, TEST F-1

E-6

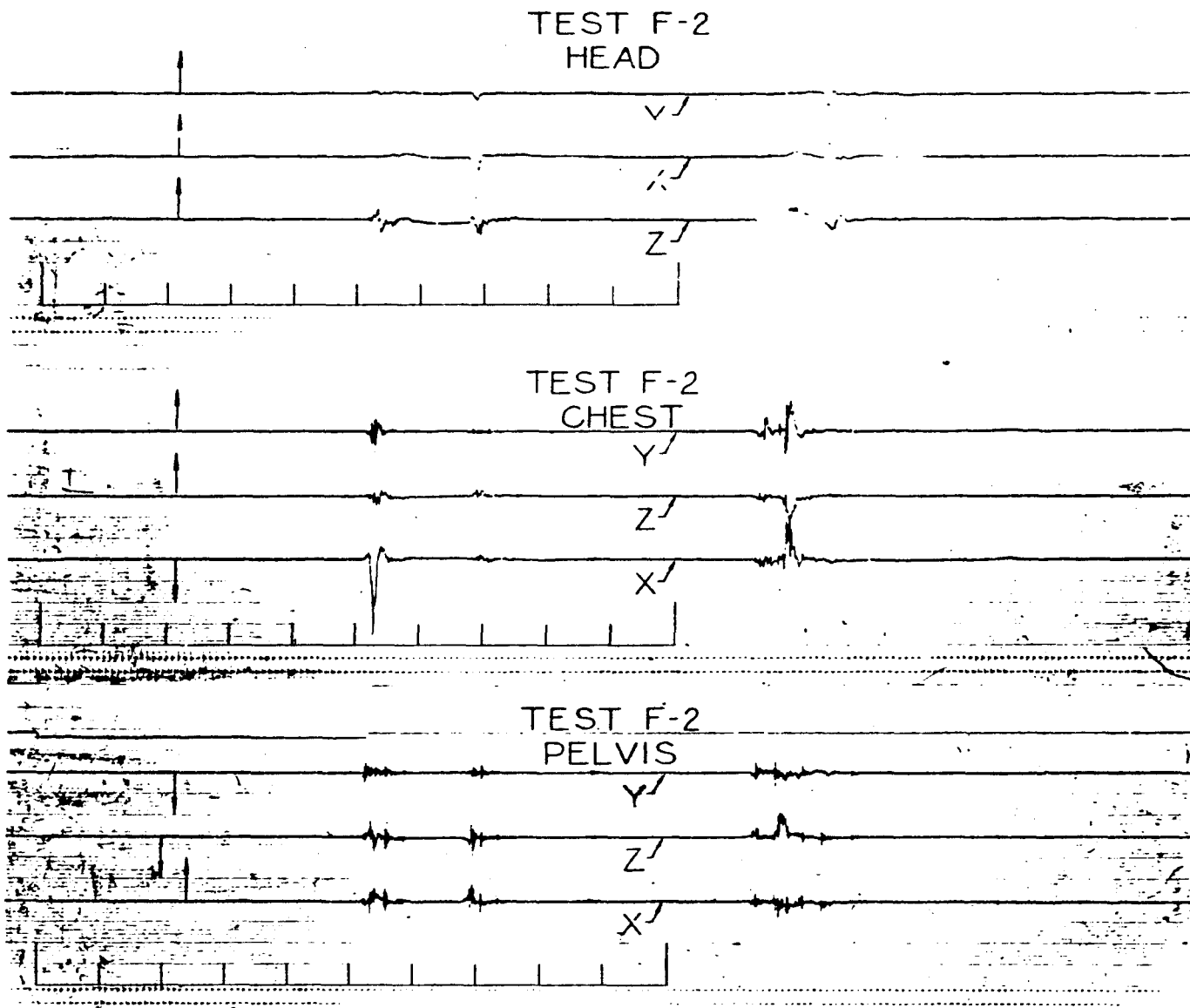
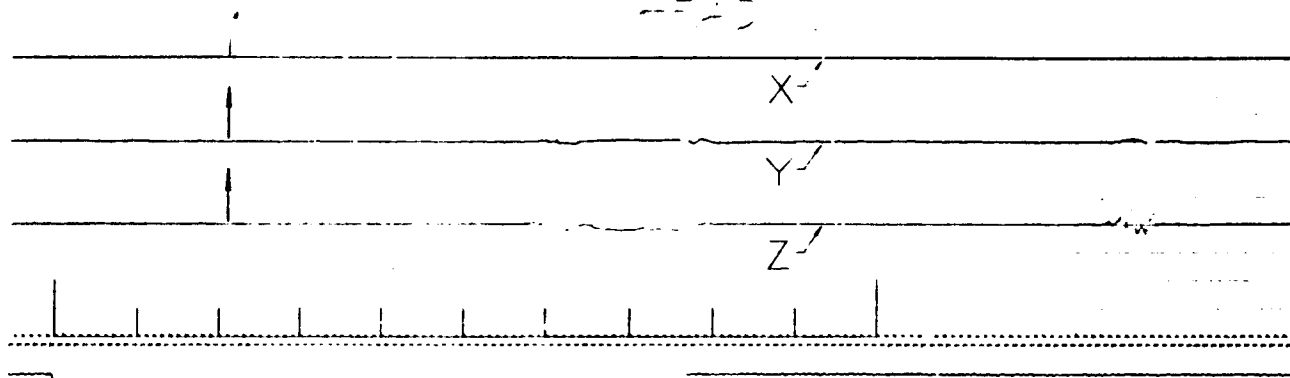


FIGURE E-7. ACCELEROMETER DATA, TEST F-2

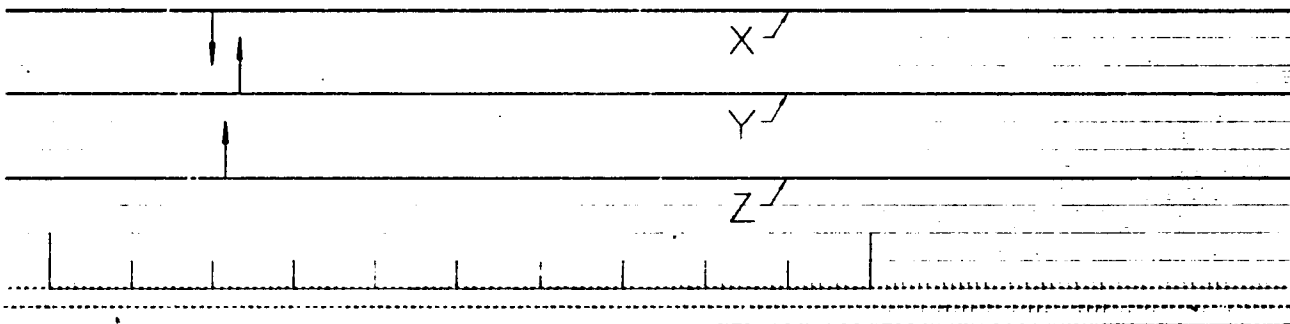
Note: Loss of high-speed film negated results of Test F-3.

FIGURE E-8. ACCELEROMETER DATA, TEST F-3

TEST F-4



TEST F-4
CHEST (not VALID)



TEST F-4
PELVIS

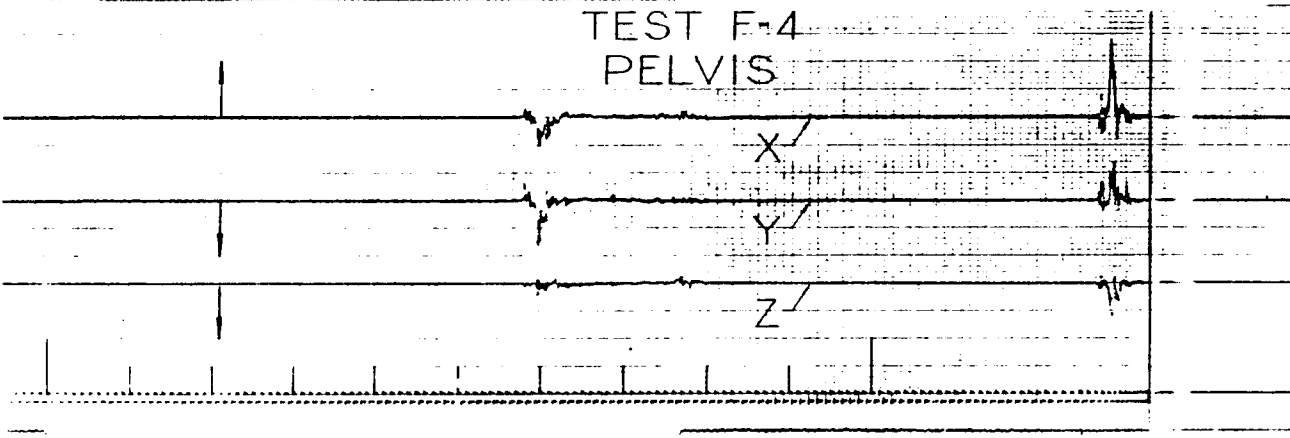


FIGURE E-9. ACCELEROMETER DATA, TEST F-4

TEST F-5
HEAD

X ✓

Y ✓

Z ✓

TEST F-5
CHEST

X ✓

Y ✓

Z ✓

TEST F-5
PELVIS

X ✓

Y ✓

Z ✓

FIGURE E-10. ACCELEROMETER DATA, TEST F-5

E-10

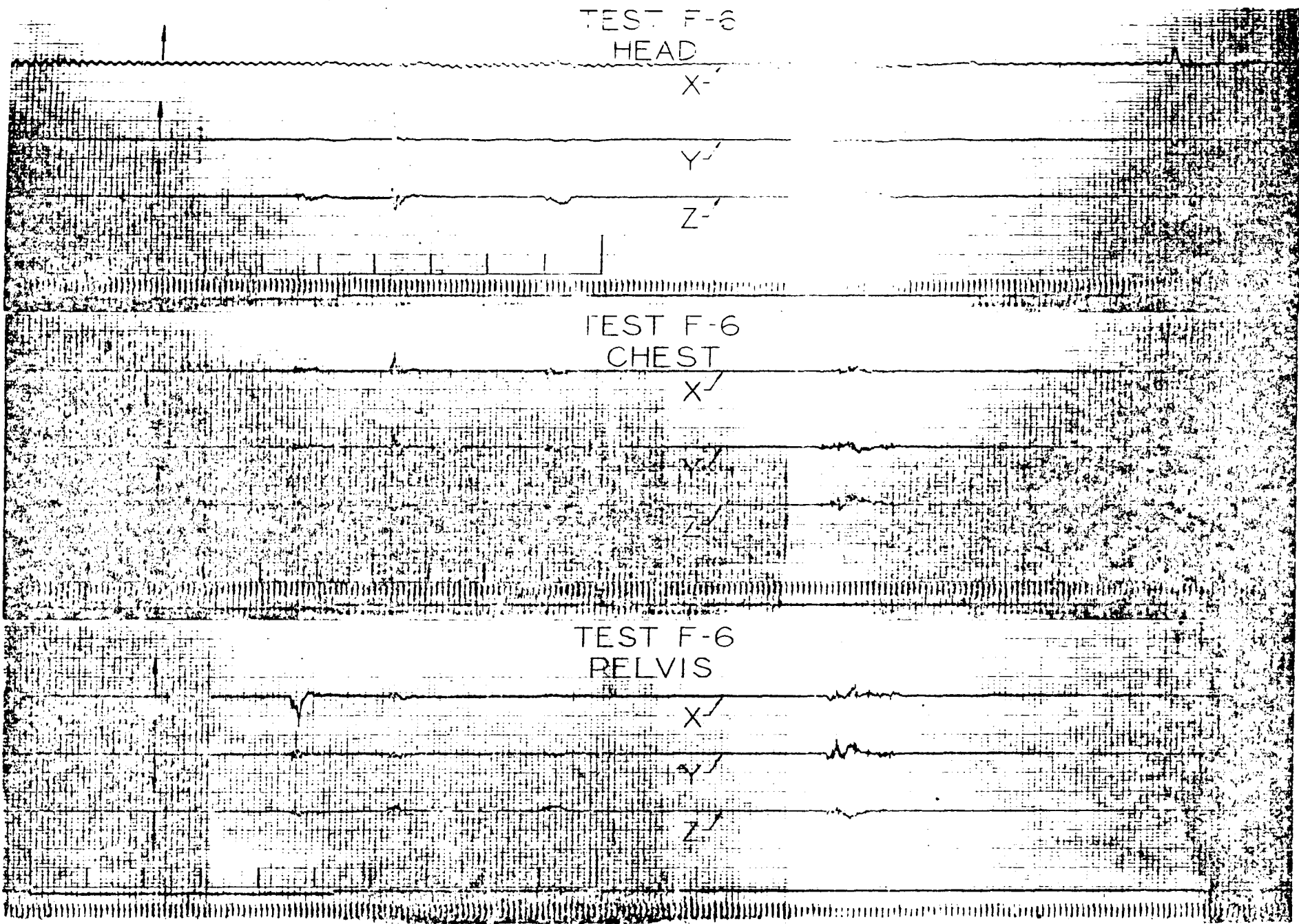
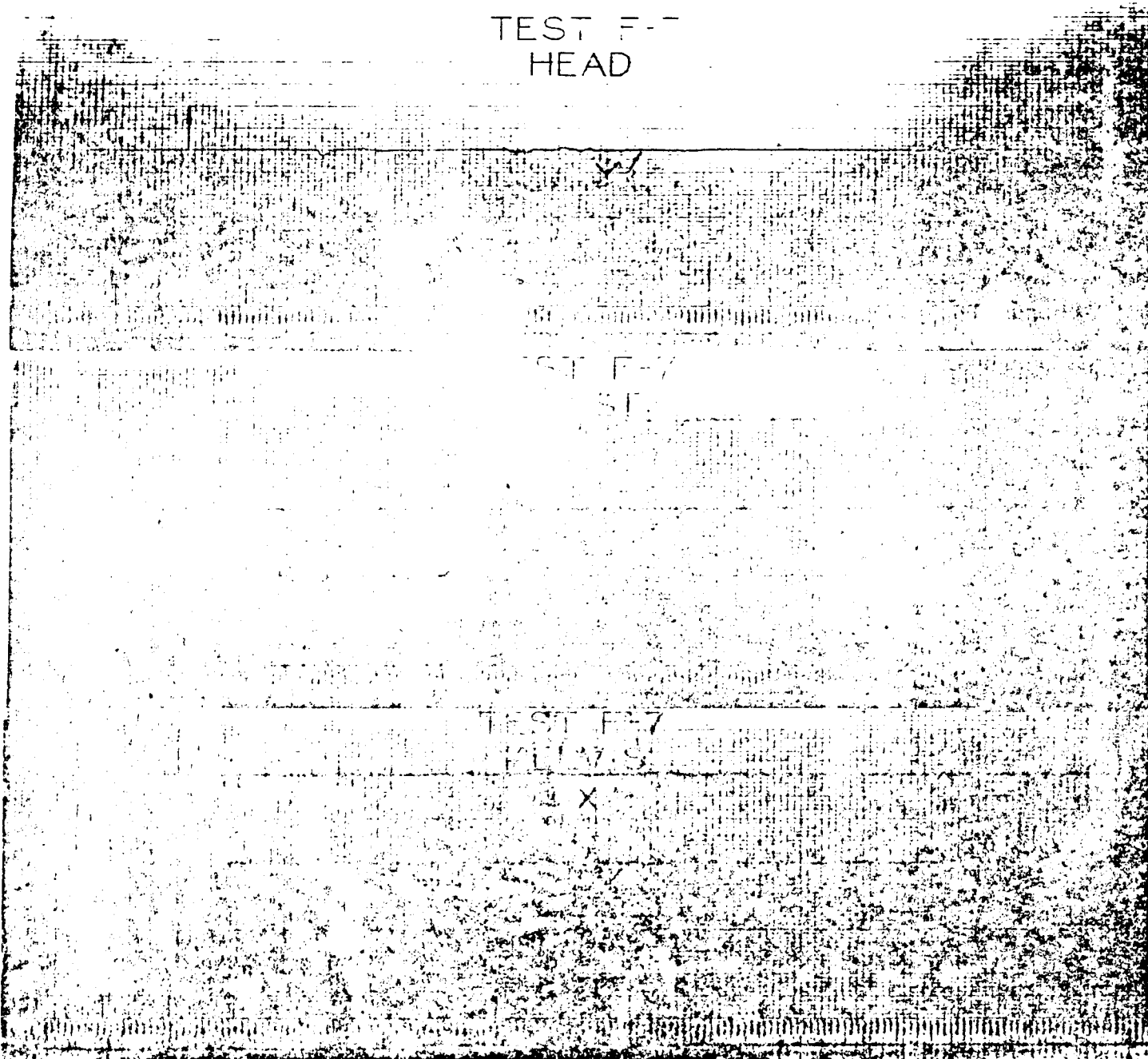


FIGURE E-11. ACCELEROMETER DATA, TEST F-6

TEST F-7
HEAD



E-12

FIGURE E-12. ACCELEROMETER DATA, TEST F-7

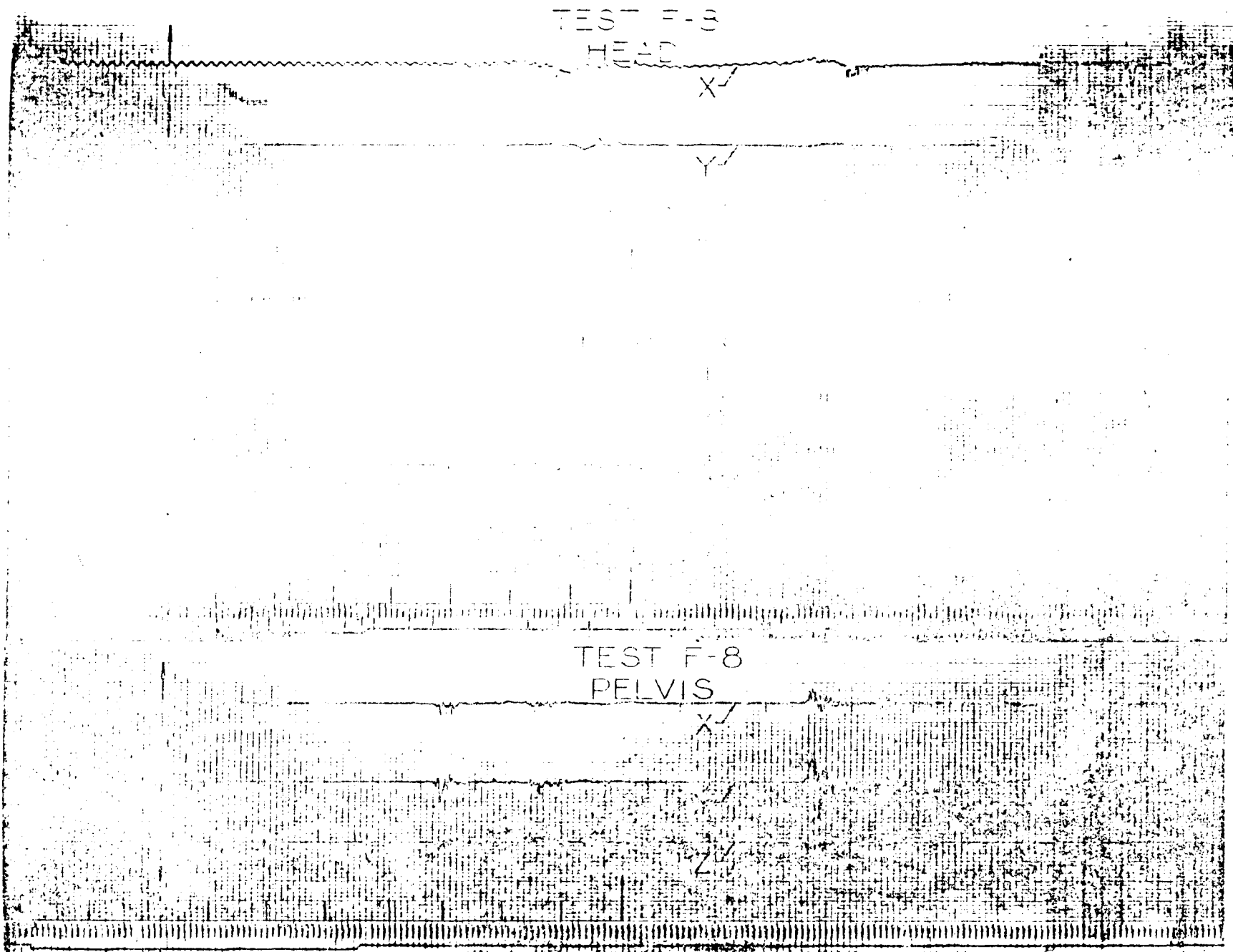


FIGURE E-13. ACCELEROMETER DATA, TEST F-8

TEST M-1
HEAD

X

TEST M-1
PELVIS

FIGURE E-14. ACCELEROMETER DATA, TEST M-1

TEST M-2
HEAD

X-

FIGURE E-15. ACCELEROMETER DATA, TEST M-2

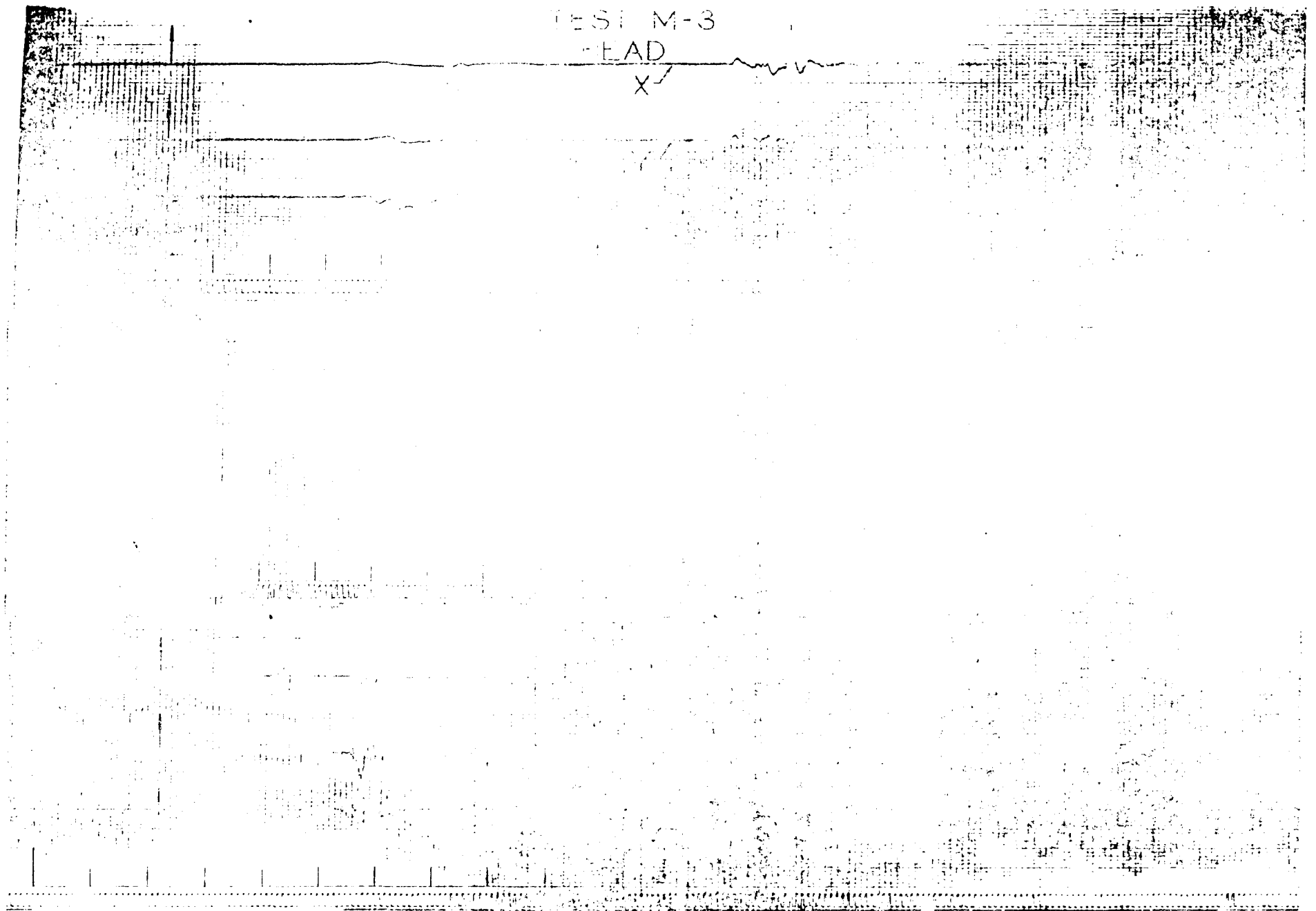


FIGURE E-16. ACCELEROMETER DATA, TEST M-3

TEST M-4

FEA

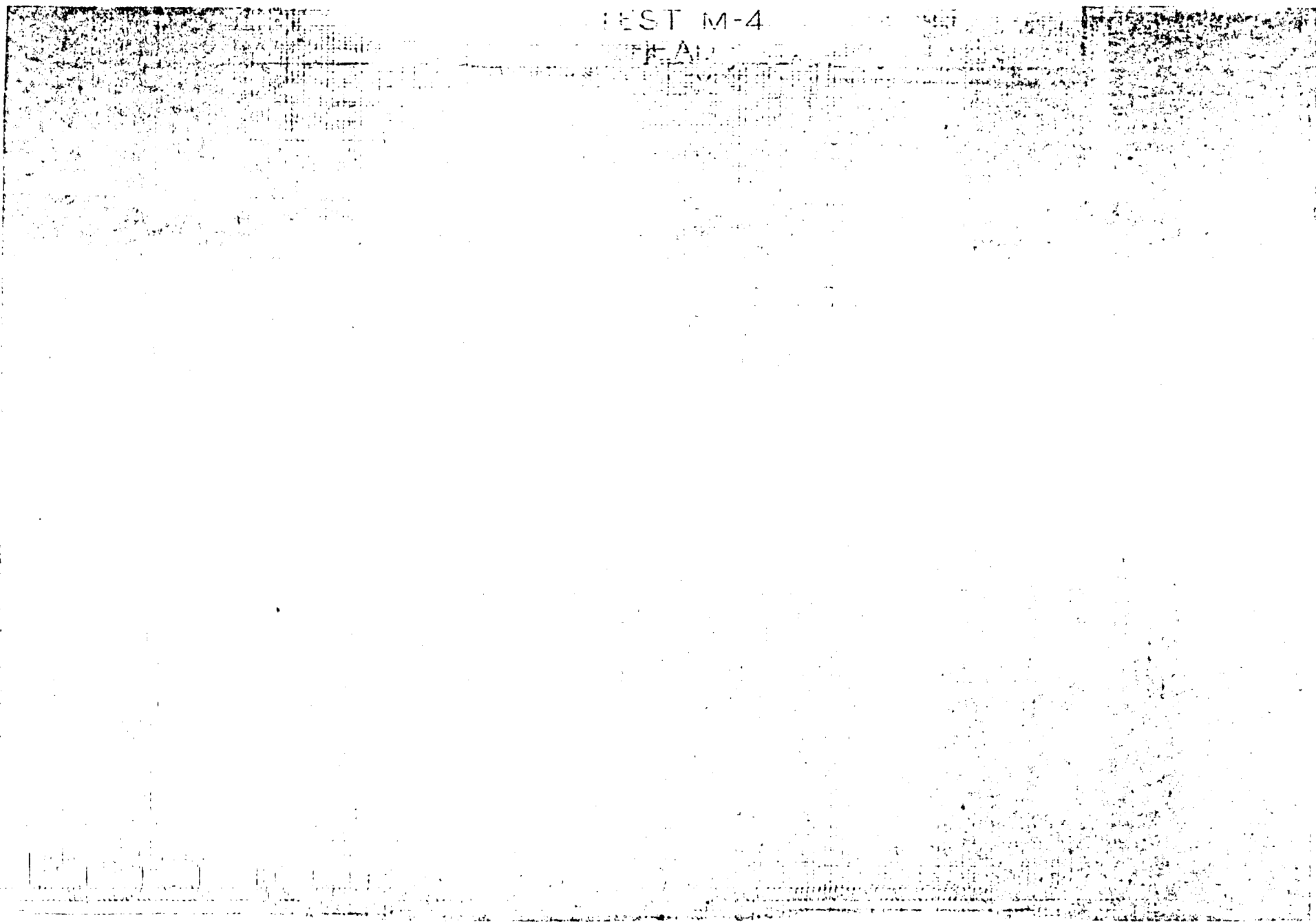


FIGURE E-17. ANOMEROMETER DATA, TEST M-4

TEST M-5
HEAD

X

Y

Z

TEST M-5
PELVIS

X

Y

Z

E-15

FIGURE E-18. ACCELEROMETER DATA, TEST M-5

TEST M-6

HEAD

TEST M-6

CH

TEST M-6

PELVIS

X

Y

Z

E-19

FIGURE E-19. ACCELEROMETER DATA, TEST M-6

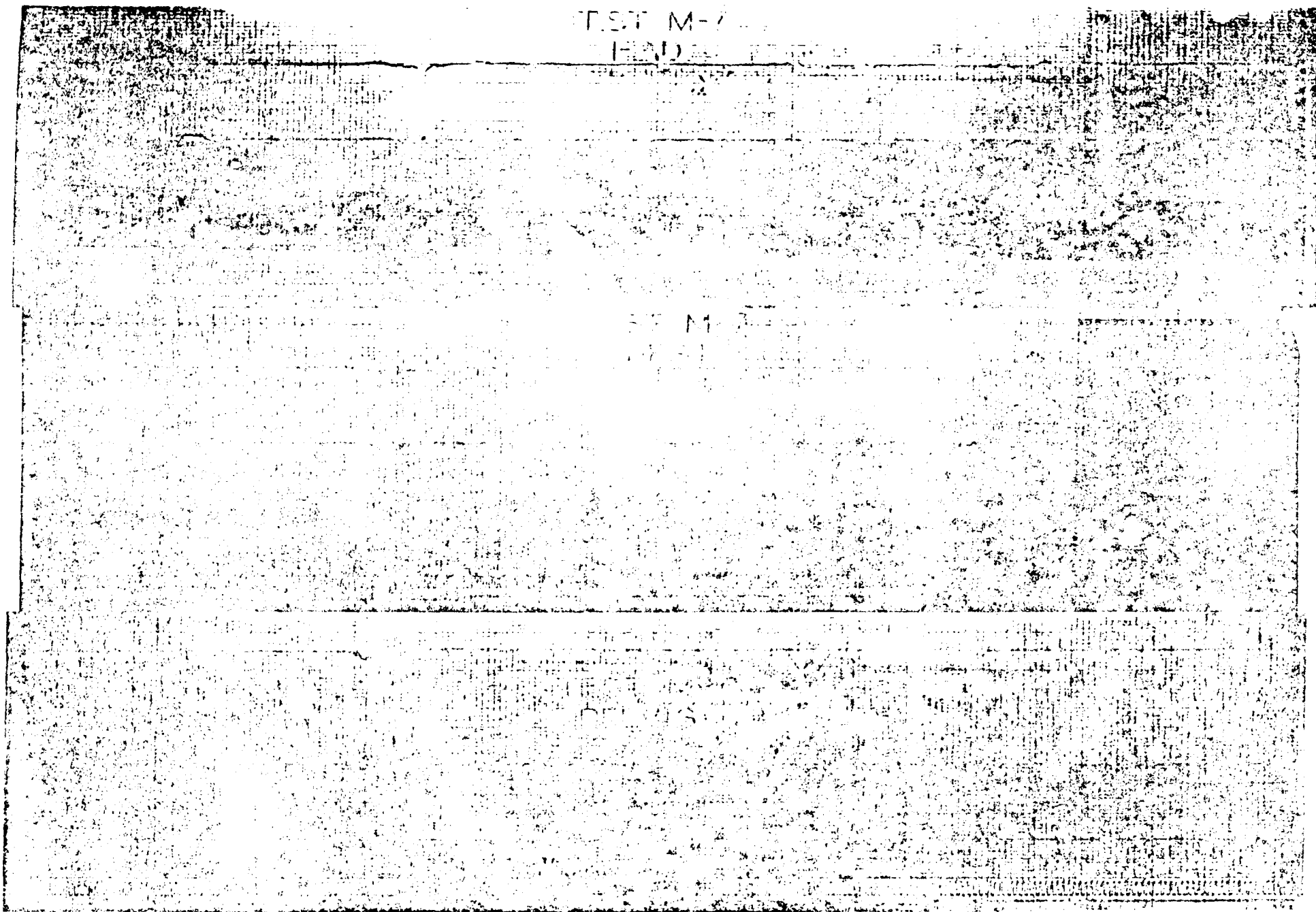


FIGURE F-20. ACCELEROMETER DATA, TEST M-7

TEST M-8
HEAD

TEST M-8
PELVIS

TEST M-8
CHEST

X/

Y/

Z/

20 SEC 12475 20

E-21

FIGURE E-21. ACCELEROMETER DATA, TEST M-8

TEST M-9
HEAD

X

Y

Z

TEST M-9
CHEST

X

Y

Z

TEST M-9
PELVIS

X

Y

Z

E-22

FIGURE E-22. ACCELEROMETER DATA, TEST M-9